ISAS - INTERNATIONAL SCHOOL
FOR ADVANCED STUDIES

Intrinsic variability and short-term changes in synaptic transmission in the rat hippocampal CA3 region

Thesis submitted for the degree of "Doctor Philosophiae"

CANDIDATE
Marco Canepari

SUPERVISOR
Prof. Enrico Cherubini

CO-SUPERVISOR
Dr. Alessandro Treves

Table of contents

ACKNOWLEDGMENTS

NOTE

The work described in this dissertation was carried out at the International School for Advanced Studies, Trieste, Italy, between November 1995 and November 1998. All work reported, with the exception of the experiments performed by Henry Markram at the Weizmann Institute in Israel, arises solely from my own experiments and this thesis has not been submitted in whole or in part to any other University.

Part of the data reported in the present thesis have been published or submitted in the articles listed below.

CANEPARI, M. AND CHERUBINI, E. Dynamics of transmitter release: analysis of synaptic responses in CA3 hippocampal neurons following repetitive stimulation of afferent fibres. *J. Neurophysiol.* 79: 1977-1988, 1998.

CANEPARI, M. AND CHERUBINI, E. Dynamics of neurotransmitter release in CA3 hippocampal neurons. In *Neural Circuits and Networks*, (ed. by V.Torre and J.Nicholls), NATO ASI Series F, Vol. 167, Springer Verlag, Berlin-Heidelberg,1998.

CANEPARI, M. AND MAMMANO, F. Imaging neuronal calcium fluorescence at high spatio-temporal resolution. *J. Neurosci. Meth.*, 87: 1-11, 1999.

MAMMANO, F., CANEPARI, M., CAPELLO, G., IJADUOLA, R. B., CUNEI, A., YING, L., FRATNIK, F. AND COLAVITA, A. An optical recording system based on a fast CCD sensor for biological imaging. *Cell Calcium*, 25: 115-123, 1999.

CANEPARI, M. AND TREVES, A. Characterization of the variability of synaptic responses to presynaptic trains in the hippocampus. Submitted.

CANEPARI, M., KACHALSKY, S. G., RAHAMIMOFF, R., AND CHERUBINI, E. Temperature dependence of GABAergic activity and Giant Depolarizing Potentials (GDPs) in the neonatal rat hippocampus. Submitted.

Abbreviations used in the text

ACh: Acetylcholine

AMPA: (*RS*)-α-amino-3-hydroxy-5-methyl-4-isoxadepropionate

AP5: D(-)2-amino-5-phosphonovalerate

AP7: D(-)2-amino-7-phosphonovalerate

BAPTA: bis-(-*o*-aminophenoxy)ethane-N,N,N',N'-tetraacetic acid

$[B_m]$: mobile exogenous buffer (dye) concentration

$[B_s]$: immobile endogenous buffer concentration

$[Ca^{2+}]_i$: intracellular calcium concentration

$[Ca^{2+}]_o$: extracellular calcium concentration

$[Cl^-]_i$: intracellular chloride concentration

CNQX: 6-cyano-7-nitroquinoxaline-2,3-dione

CNS: central nervous system

CPP: (+)-3-(2-carboxy-piperazin-4-yl)-propyl-1-phosphonic acid

CV: coefficient of variation

D: depression

D-AP5: D(-)-2-amino-5-phosphonopentanoic acid

DCG-IV: 2-(2,3-dicarboxycyclopropyl) glycine

DG: dentate gyrus

DMSO: dimethylsulphoxide

DNQX: 6,7-dinitroquinoxaline-2,3-dione

DQA: dynamic quantal analysis

EGTA: ethylene glycolbis (b-aminoethyl ether) N,N,N',N'-tetraacetic acid

EPP: end plate potential

EPSC: excitatory postsynaptic current

EPSP: excitatory postsynaptic potential

F: facilitation

GABA: γ-aminobutyric acid

GABA$_A$: type A GABA receptor

GABA$_B$: type B GABA receptor

GDPs: Giant Depolarizing Potentials

HEPES: N-2-hydroethylpiperazine-N'-2-ehanesulfonic acid

IPSP: inhibitory postsynaptic potentials

KA: kainate

LTD: long-term potentiation

LTP: long-term potentiation

mGluRs: metabotrobic glutamate receptors

NMDA: N-methyl-D-Aspartate

P: postnatal day

PKA: protein kinase B

PKB: protein kinase B

PKC: protein kinase C

PLC: phospholipase C

PTP: post-tetanic potentiation

QA: quantal analysis

S/N: ratio between signal and noise

TTX: tetrodotoxin

1 ABSTRACT

- The patch clamp technique (whole cell configuration) was used to record excitatory postsynaptic currents (EPSCs) evoked by repetitive stimulation (3-10 pulses at 40-80 ms interval) of afferent fibers in the *Stratum Lucidum-Radiatum*. Different synaptic behaviours (EPSC patterns) were classified in terms of facilitation or depression of the mean amplitude of the second, third and fourth EPSC with respect to the previous one. A large variety of EPSC patterns was observed by stimulating different afferent fibers. Experiments with the mGluR2/mGluR3 agonist DCG-IV (1 μM), a compound that reduces release at mossy but not at associative commisural fibers and therefore allows to identify the origin of synaptic responses, showed that particular EPSC patterns could not be associated to the activation of a specific type of synaptic input. In several experiments the extracellular calcium concentration was varied from 0.8 mM to 4 mM. EPSC patterns dominated by depression, characteristic of high release probability conditions, could be observed in the majority of the cases in the presence of higher calcium concentrations.

- A simple model for the dynamics of transmitter release has been developed. Experimental results have been compared to data computed with the simplest implementation of a model taking into account the probability of release and the time course of reavailability. This comparison indicates that short-term changes of presynaptic conditions occurring during a train of action potential may account for the high variability of EPSC responses.

- In order to further analyse EPSCs elicited by trains of presynaptic action potentials and to characterise their variability, an approach based on stochastic chains has been developed. Excitatory postsynaptic currents have been statistically analysed with simple binomial distributions and with binomial chains. The comparison shows that although both models could give a good description of synaptic responses at the level of single spikes, only stochastic chains could account for the correlation observed within the train.

- This approach has also been applied to analyse excitatory synaptic potentials from paired pyramidal neurons in the neocortex and GABAergic synaptic currents in CA3 pyramidal neurons. This analysis shows that variability and short-term plasticity are intrinsic characteristics of different synaptic systems in the brain. In particular, in comparisons to

other synaptic systems, glutamatergic synaptic responses in the hippocampus are characterised by a larger variability both in amplitude and in short-term plasticity behaviours.

- The statistics of binomial chains, investigated with computer simulations, indicates that different release probabilities may lead to distinct forms of presynaptic short-term plasticity of synaptic responses, that could in principle be discriminated from those due to contributions of postsynaptic mechanisms.

- The analysis of synaptic responses at different frequencies of presynaptic firing allows a measure of transmitted information to be associated to synaptic variability. The type of short term plasticity could be altered from facilitating to depressing by increasing the extracellular calcium concentration, as mentioned above. This resulted in a change in synaptic variability and in a faster time course for the related transmitted information.

- *Appendix.* A considerable part of my PhD work has been devoted to the development of a high space-time resolution imaging system, utilised to investigate the time-course of intracellular calcium concentration ($[Ca^{2+}]_i$) gradients generated by action potentials in CA1-CA3 pyramidal cells within brain slices of the rat hippocampus. The system, based on a fast commercial CCD camera with customised hardware and software partially developed in my PhD work, could acquire hundreds of 128×128 pixel images in sequence, with minimal inter-frame interval of 1.36 ms (735 frames/sec) and 12 bit/pixel accuracy. By synchronising patch clamp recordings with image capture, the timing of transmembrane potential variation, ionic Ca^{2+} current and Ca^{2+} diffusion were resolved at the limit of the relaxation time for the dye-Ca^{2+} binding reaction (approximately 5 ms at room temperature). Numerical simulations were used to relate measured fluorescence transients to the spatio-temporal distribution of intracellular Ca^{2+} gradients. The results obtained indicate that dye reaction-diffusion contributes critically to shaping intracellular ion gradients. The imaging system was used to investigate the role of temperature on depolarising GABAergic activity in the hippocampus of neonatal rats. During the first postnatal week, network activity is characterised by GABA-driven giant depolarising potentials (GDPs). These spontaneous events, which are associated to calcium transients, are strongly temperature-dependent since they are blocked when temperature is lowered from 32 °C to 24 °C. The role of temperature in regulating

GABAergic synaptic transmission and GDPs generation was investigated in the CA3 area of the rat hippocampus during the first postnatal week by combining electrophysiological recordings and high space-time resolution calcium imaging. It was found that GDPs- and GABA-triggered calcium signals spread to neighbouring cells in hundreds of ms and that their propagation is faster and involves a larger number of neurons at higher temperature. At 32 °C, miniature GABAergic currents occurred at higher frequency and showed faster kinetics. Moreover, at this temperature, the depression of synaptic currents evoked by low frequency trains of stimulation was weaker. These results suggest that the temperature-dependent change in network activity, leading to a transition from a non-oscillating to an oscillating state, is due to an increased effectiveness of GABA-mediated intercellular communication. This follows the enhancement of GABA release and the concomitant reduction of the shunting properties associated to the speed up of postsynaptic $GABA_A$ receptor kinetics.

2 INTRODUCTION

The function of the nervous system depends on the signal integration properties of neurons and synapses. Since passive and active signal integration in neurons can be well described by deterministic input-output functions as the Hodgkin and Huxley equations (Hodgkin and Huxley, 1952), it is tempting to investigate the complex behaviours of neural networks simply in terms of chaotic dynamics. However, it turns out that synaptic transmission and therefore the way in which neurons can communicate is rather understood as a stochastic process in which, at the level of single synapses and single synaptic events, the coefficient of variation, associated to synaptic signals, can be higher than 1. In order to investigate the biophysics of synaptic transmission and the way in which synaptic signals can be integrated by nervous systems, it is therefore necessary to characterise synaptic signals and to describe them with models based on the theory of stochastic processes. Particularly, the study of synaptic transmission elicited by repetitive firing of presynaptic neurons is fundamental to understand both the dynamics of synapses and the possibility of time integration of synaptic signals.

In this chapter, the basic concepts of synaptic transmission that I have used are briefly described. The fundamental theory of synaptic transmission is introduced in the first two sections. The third section is a short anatomical and physiological description of the hippocampus. The fourth section is dedicated to the phenomenon of short term plasticity, i.e. to the changes in the conditions of synaptic transmission normally occurring when synapses are repetitively activated within a time interval shorter than one second.

2.1 Chemical synaptic transmission

2.1.1 General theory

Chemical synaptic transmission is one predominant way of communication among nervous cells and the dynamics of synaptic transmission is the fundamental ingredient that determines the functions of neural networks.

Chemical synapses operate through the release of a neurotransmitter from the *presynaptic* neuron that directly changes the membrane conductance of the *postsynaptic* neuron, in the case of *ionotropic* synaptic transmission, or that activates intracellular cascades of processes, in the case of *metabotropic* synaptic transmission. Ionotropic synaptic transmission is responsible for fast communication in the nervous system. Figure 2.1 shows an oversimplified general model of a fast chemical synapse. The process of ionotropic synaptic transmission includes the presynaptic mechanism of neurotransmitter release followed by the postsynaptic mechanism of neurotransmitter-receptor binding.

Neurotransmitter release occurs when an action potential reaches the nerve terminal and activates voltage-dependent calcium channels. These proteins are clustered in the neighbourhood of active zones where synaptic vesicles are docked (Fatt and Katz 1952; Del Castillo and Katz 1954a). The rise in cytosolic calcium concentration $[Ca^{2+}]_i$, following an action potential, triggers a cascade of events leading to fusion, exocytosis of synaptic vesicles and release of transmitter into the synaptic cleft. The synaptic vesicle cycle can be divided in several steps and involves a large number of proteins (Südhof, 1995). Synaptic vesicles filled with neurotransmitter dock at the active zone and become available for fast release after a maturation process (*priming*). These processes are regulated by *trafficking proteins* such as Rab3. Vesicle *fusion* and *exocytosis* involve several vesicle proteins such as *sinaptotagmins* that bind to Ca^{2+} let in by action potentials. After exocytosis, empty vesicle rapidly internalise (*endocytosis*) and translocate into the interior for *recycling*. Vesicles accumulate neurotransmitter by active transport driven by an electrochemical gradient created by a proton pump (*uptake*). Neurotransmitter *transporters* are the proteins involved in the uptake process. Finally synaptic vesicles diffuse again to the active zone ending the vesicle cycle.

At the postsynaptic site, neurotransmitter molecules bind to receptors placed in the postsynaptic membrane. Ionotropic receptors are ionic channels that are normally closed and that open when they are bound by neurotransmitter molecules, allowing the flow of ions within the cell membrane. Ionotropic receptors are selective either to cations or anions. The flow of ions into the postsynaptic neuron changes its membrane potential either in the positive (depolarisation) or negative (hyperpolarisation) direction. In the case of receptors permeable to Ca^{2+}, the flow of this ion can also activate intracellular biochemical processes.
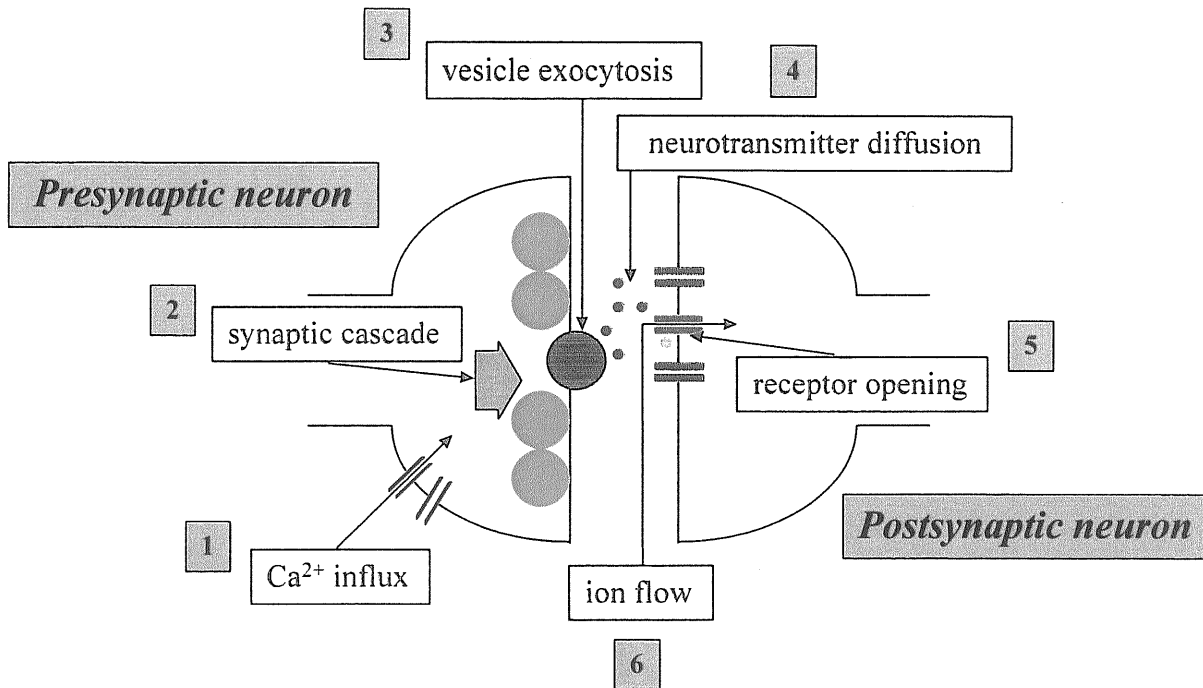
Figure 2.1 Scheme of synaptic transmission. Action potentials in the presynaptic neuron invading synaptic terminals cause Ca^{2+} influx (1). This activates a cascade of intracellular processes (2) leading to fusion and exocytosis of synaptic vesicles (3). Neurotransmitter molecules diffuse in the intersynaptic space (synaptic cleft) (4) and bind to postsynaptic receptors that open (5) and allow cation or anion flow from or to the postsynaptic cytoplasm (6). This flow of current changes the postsynaptic membrane potential.

After opening, postsynaptic receptors normally desensitise, i.e. they remain in an "open state" without allowing ion flow, and they restore their initial condition after recovering from desensitisation.

In the case of metabotropic synaptic transmission, the responses to activation of receptors are mediated by G proteins, so named because they bind guanosine diphosphate and guanosine triphosphate. G proteins modify the activity of other receptor proteins that regulate the synthesis of second messengers. The best understood of the second messenger systems is the type that uses a cyclic nucleotide (most prevalent adenosine 3',5'-cyclic monophosphate) as the intracellular signal molecule. This includes dopamine, serotonin and histamine synaptic systems as well as the cholinergic activity mediated by muscarinic receptors. The inositol triphosphate second messenger pathway is proper of noradrenaline synaptic systems and of glutamate

activity mediated by metabotropic glutamate receptors (mGluR). Intracellular second messenger pathways are basically targeted to ion channels and pumps and they can modulate passive and active membrane properties as well as synaptic transmission itself. (see Shephard, 1994; Nicholls et al.,1992).

2.1.2 Time course of synaptic signals

The time course of fast postsynaptic signals depends on that of transmitter diffusion and receptor binding as well as on the kinetics of desensitisation. The time course of transmitter diffusion depends on several parameters such as the number of vesicles simultaneously released, the concentration of the transmitter in each vesicle, the diffusion coefficient of the transmitter, the geometry of the cleft and other parameters (Clements, 1996). It has been estimated that transmitter concentration during a synaptic event has a peak ranging between 1 mM and 5 mM and decays in a biphasic manner with time constants of approximately 100 μs and 2 ms. The rising phase of postsynaptic signals is determined by the binding process between transmitter molecules and receptors, that depends on the transmitter concentration time course in the synaptic cleft, and by the receptor opening rate. The decay phase of postsynaptic signal is mainly determined by the unbinding process when desensitisation is considerably slow as in the case of nicotinic acetylcholine receptors, or depends also on the kinetics of desensitisation when desensitisation occurs at a time scale comparable to the one of transmitter concentration as in the case of (RS)-α-amino-3-hydroxy-5-methyl-4-isoxadepropionate (AMPA) glutamate receptors (Jones and Westbrook, 1996).

Another important factor that can play a fundamental role in shaping synaptic signals is the *receptor saturation*. This occurs in synapses where all or almost all receptors at the postsynaptic membrane are activated by the released neurotransmitter molecules (Clements, 1996). Receptor saturation prevents the increase of postsynaptic signal amplitudes when a larger number of neurotransmitter molecules is released.

2.1.3 Synaptic transmission in the brain

In the mammalian brain, the principal neurotransmitters operating through ionotropic receptors are glutamate and γ-aminobutyric acid (GABA). Glutamate receptors are cationic channels whereas ionotropic GABA ($GABA_A$) receptors are anionic channels. According to the Goldman

equation, cationic or anionic currents can produce depolarisations or hyperpolarisations depending on the extracellular and intracellular ionic concentrations. Glutamate is always depolarising, while GABA operating through $GABA_A$ receptors is normally hyperpolarizing, and is depolarising in the developing hippocampus where the intracellular Cl^- concentration ($[Cl^-]_i$) is higher (Ben Ari et al., 1989; Cherubini et al., 1991).

Three families of ionotropic glutamate receptors are present in the central nervous system (CNS). The N-methyl-D-Aspartate (NMDA) receptors are channels that are normally blocked at resting membrane potential by Mg^{2+} ions and that can be activated only when the cell is depolarised (Ascher and Novak, 1988). These receptors are highly permeable to Ca^{2+} (Burnashev, 1992), have a slow kinetics and relative synaptic currents last hundreds of ms (Randall and Collingridge, 1992). NMDA receptors can be blocked by MK 801, D(-)2-amino-5-phosphonovalerate (AP5), D(-)2-amino-7-phosphonovalerate (AP7) and (±)3-(2-carboxypiperazin-4-yl)-propyl-1-phosphonic acid (CPP).

AMPA receptors are voltage independent, have a Ca^{2+} permeability depending on the subunit composition and have a much faster kinetics with synaptic currents lasting few ms. The kainate (KA) receptors have kinetics properties similar to those of AMPA receptors and are preferentially activated by KA. Non-NMDA receptors are blocked by 6-cyano-7-nitroquinoxaline-2,3-dione (CNQX), 6-7-dinitroquinoxaline-2,3-dione (DNQX) and by kynurenic acid which also blocks NMDA receptors.

Distinct metabotropic glutamate receptors (mGluR 1-8) are known to be present in the brain. Synaptic responses mediated by mGluR result from blockade of K^+ conductance (Charpak and Gähwiler, 1991); mGluRs differ in their primary sequence and in their signal transduction pathway as well as in their location in distinct neurons (Pin and Bockaert, 1995).

GABA activates two distinct classes of receptors. $GABA_A$ receptors are characterised by their high permeability to anions and their sensitivity to the competitive antagonist bicuculline, to the non-competitive antagonist picrotoxin and to the agonist isoguvacine (Mac Donald and Olsen, 1994). $GABA_B$ receptors are associated to second messenger pathways resulting in an increase in K^+ conductance (Newbarry and Nicoll, 1984) or in a decrease of voltage-dependent Ca^{2+} conductance (Dunlap, 1981).

2.2 The quantal theory of neurotransmitter release

2.2.1 The binomial quantal model of neurotransmitter release

Although the expression *synaptic transmission* is specifically referred to neurons, the understanding of the process of release comes from the early studies of acetylcholine (ACh) release at the neuromuscular junction. In this system, the effect of ACh is to open cationic channels in the endplate membrane and to induce an endplate potential (EPP).

According to the quantal hypothesis, developed at the neuromuscular junction by Del Castillo and Katz (1954a), transmitter is released in packets or *quanta* each of them containing thousands of transmitter molecules. A packet, or quantum, simply represents the smallest unit in which the neurotransmitter is secreted. Quantal release means that only an integer number of quanta is released from the terminals. In general, the number of quanta released from the nerve terminal may vary, but the number of molecules in each quantum is relatively fixed. The early studies on the neuromuscular junction showed that the process of release of acetylcholine *quanta* is not deterministic, but it occurs in a probabilistic manner. Particularly, variability of EPPs reflects the stochastic fluctuations in the number of released quanta (Del Castillo and Katz, 1954a). It has been demonstrated that the amplitudes of end plate potentials evoked by a presynaptic action potential follow a binomial distribution, reflecting the independence of release of each quantum from the others.

Later on the basic concepts of the neurotransmitter process have been extended to the *central* synaptic transmission. Whereas at the neuromuscular junction many quanta are released by a single terminal in response to electrical stimulation of the nerve, activation of single presynaptic fibers in many central synapses usually produces small synaptic responses and *failures* (no response following activation of the presynaptic fiber) (Fesce, 1990).

In a synapse in which N quanta are available for release and the process follows a simple binomial distribution with the same probability p for all the quanta, the probability p(n) that n synaptic quanta are released by one action potential is

$$p(n) = \frac{N!}{n! \cdot (N-n)!} \cdot p^n \cdot (1-p)^{N-n} . \tag{2.1}$$

The mean number of released quanta <n>, its standard deviations σ_n and the probability to have a failure p(0) (release of 0 quanta) are

$$< n > \ = \ p \cdot N \tag{2.2}$$

$$\sigma_n^2 \ = \ N \cdot p \cdot (1-p) \tag{2.3}$$

$$p(0) \ = \ (1-p)^N. \tag{2.4}$$

The compound binomial distribution extends this model to the more general scenario in which the release occurs from $\Re$ releasing sites with a different release probability. In this case, if N_α is the number of available quanta of the αth releasing site and p_α the corresponding release probability, equations 2.2, 2.3 and 2.4 are generalised by

$$< n > \ = \ \sum_{\alpha=1}^{\Re} p_\alpha \cdot N_\alpha \tag{2.5}$$

$$\sigma_n^2 \ = \ \sum_{\alpha=1}^{\Re} p_\alpha \cdot N_\alpha \ - \ \sum_{\alpha=1}^{\Re} [p_\alpha]^2 \cdot N_\alpha \tag{2.6}$$

$$p(0) \ = \ \prod_{\alpha=1}^{\Re} (1-p_\alpha)^{N_\alpha}. \tag{2.7}$$

Two extreme cases of the compound binomial model are the simple binomial model, in the case in which the $\Re$ different releasing sites have the same release probability ($p_\alpha = p \ \forall \alpha$), and the release from releasing sites with a single available quantum, in the case in which $N_\alpha = 1 \ \forall \alpha$. Finally, in the case of very low release probability, the binomial statistics can be approximated by Poisson statistics. The statistics of synaptic responses can be obtained, from equations 2.5-2.7 by accounting for the possible different synaptic responses to a single quantum (quantal amplitudes) at each releasing site. Thus, the term N_α in equations 2.5 and 2.6 must be replaced by $\omega_\alpha \cdot N_\alpha$ where the coefficient ω_α accounts for the different quantal amplitudes and, in the presence of non-negligible variability in the quantal amplitudes, the quantal amplitude variances must be added to the summation in the r.h.s. of equation 2.6.

2.2.2 Quantal analysis of synaptic responses

The use of statistical techniques, based on the assumptions of the quantal theory of neurotransmitter release, to analyse synaptic responses is called *Quantal Analysis* (QA). QA is based on the general assumption, first utilised at the neuromuscular junction, that under the same experimental conditions the postsynaptic effect of a single quantum is rather constant, but

the number of quanta released changes from trial to trial in a stochastic manner (Fatt and Katz 1952; Barrett and Stevens 1972). Thus, fluctuations in amplitude of postsynaptic currents reflect variations in the number of quanta (Voronin 1994) and the postsynaptic current or potential corresponding to the release of a single quantum is called *quantal size*.

QA basically consists in finding the *best fit* of experimental synaptic responses using a particular statistical model (Redman, 1990). For example, in the case of the simple binomial model, QA determines the *best values* for p and N relative to a particular set of experimental synaptic responses. In order to do that, it is first necessary to assign quantitative criteria to determine whether a particular model with a particular set of parameters is statistically significant and to discriminate within different models and/or within different sets of parameters in the same model.

The significance of the agreement between experimental distributions $\Phi^{exp}(n)$ with those predicted by particular models $\Phi^{model}(n)$ can be evaluated with the χ^2 *goodness-of-fit*, i.e. by calculating the quantity

$$\chi^2 = \sum_{n=0}^{N} \frac{\left(\Phi^{exp}(n) - \Phi^{model}(n)\right)^2}{\Phi^{model}(n)}. \tag{2.8}$$

N is the number of states of the model distribution, i.e. the number of bins in which the experimental distribution is divided. The probability of agreement between the two distributions is given by the function

$$P(\chi^2) = 1 - \Gamma_{inc}(\chi^2, N - \eta + 1) \tag{2.9}$$

where Γ_{inc} indicates the incomplete gamma function and η is the number of free parameters of the model (Press et al., 1989).

An alternative way to minimise the discrepancy between the statistics of experimental data and the binomial chain is to use the maximum likelihood L (Kendall and Stuart, 1979) instead of χ^2 which, in the case of a single distribution has advantages in that it allows to determine confidence limits and significance of the model used (Stricker et al., 1994). In this respect, Expectation-Maximization algorithms (Kullmann, 1989), based on the determination of the maximal likelihood, allow to discriminate within different models (Stricker and Redman, 1994). The search of the best discrete distribution can be done for example by running

Montecarlo minimisation algorithms in the space of free parameters of the statistical model used, by deconvolution techniques using information on the noise (Kullmann, 1994a), or in other ways.

Generally speaking, methods using simplified statistical model such as the simple binomial models are defined *basic quantal analysis* whereas the use of more detailed statistical models, such as the compound binomial model, is referred to as *complete quantal analysis* (Voronin, 1994). In the contest of both approaches, information on the quantal parameters can be obtained by indirect methods based on the evaluation of the number of failures (i.e. trials with no detectable response) and/or of the coefficient of variation (CV). These indirect methods, particularly the CV method, have been used with excessive simplification to determine the origin of changes in synaptic efficacy, as pointed out by Korn and Faber, (1991). Any change in the CV has been interpreted as a sign of a presynaptic locus of expression of the synaptic efficacy change. A more accurate evaluation of the CV shows that a change in the CV can be also associated to postsynaptic modifications, and the applicability of a CV method must be based on a more detailed analysis of the statistics of synaptic responses (Faber and Korn, 1991). The search of the mechanisms underlying long-term changes in synaptic efficacy has been the main application of QA. For instance, if the simple binomial QA of synaptic responses before and after a change in the statistics of synaptic responses can be accounted for by a change in p and/or in N, then this is evidence in favour of a presynaptic mechanism. On the other hand, a relevant change in quantal size can be interpreted as an increase or decrease in the postsynaptic membrane conductance and/or in the number of transmitter molecules contained in synaptic vesicles. Long-term changes in synaptic efficacy (*long-term plasticity*) are normally induced at central synapses by the activity of the synapse. The most important example of long-term plasticity is the phenomenon of *Long-Term Potentiation* (LTP), a long lasting increase in synaptic efficacy induced in several in vitro preparations by repetitive activation of presynaptic fibers with high frequency trains of stimulation. LTP, firstly observed in the hippocampus (Bliss and Lømo, 1973), has been considered the first candidate for a synaptic mechanism of rapid learning in mammals as it is similar to the memory mechanism postulated by Hebb, (1949). "When an axon of a cell A is near enough to excite a cell B and repeatedly or persistently takes part in firing it, some growth process of metabolic change take place in one or both cells such as that A's efficiency, as one of the cells firing B, is increased". The strict

definition of hebbian synapse (as proposed by Hebb for a mechanism of associative memory) is a synapse that is strengthened when there is a co-occurrence of presynaptic and postsynaptic activity.

At central synapses, the study of the site of expression of LTP is the most utilised application of QA (Voronin, 1994). LTP has been very well studied in CA1 pyramidal neurons (see section 2.3) where after the initial finding of a presynaptic locus for LTP (Malinow and Tsien, 1990) mainly due to an increase in p, a relevant component due to an increase in quantal size, suggesting a postsynaptic contribution to LTP, has been reported (Foster and McNaugthon, 1991; Larkman et al., 1992).

2.3 The hippocampus

2.3.1 Anatomy of the hippocampus

The brain region hippocampus derives its name from its curving shape, which reminds of that of a sea horse. This part of the brain is one of the first areas of the wall of the forebrain to be differentiated in primitive vertebrates. The hippocampus is one of those regions whose internal circuits are organised in a highly distinctive manner and in which local circuits are used not just to process sensory information, but also to use such information in higher brain functions (Brown and Zador, 1990).

The anatomy and neuronal structure of the hippocampus are shown in Figure 2.2.

The hippocampus *proper* is divided in *stratum oriens* (a), *stratum pyramidale* (b), *stratum radiatum* (c) and *stratum lacunosum-moleculare* (d), The excitatory neurons (pyramidal cells) are located in the stratum pyramidale; this layer is traditionally divided in four regions CA1-CA4, although CA4 can be considered the initial part of CA3 and the small CA2, which is indistinct in some species, can be included in CA1. The dentate gyrus (DG), which is included in the hippocampal region, includes the *stratum granulosum* (d), containing the excitatory neurons (*granule cells*), and the *hilus* (e). The main inputs to the hippocampus come from the entorhinal cortex, from the septum and from the controlateral hippocampus. In the hippocampus there are three main families of excitatory neurons: The granule cells in the DG,

13

the CA3 pyramidal neurons and the CA1 pyramidal neurons. In terms of intrinsic connections, the hippocampus can be considered, as a first approximation, a *trisynaptic* circuit. This idea comes from the fact that three main groups of excitatory fibers contact distinct families of neurons in sequence: DG granule cells receive inputs from the enthorinal cortex (*perforant path*); DG granule cells contact CA3 pyramidal neurons (through *mossy fibers*); CA3 pyramidal neurons contact CA1 pyramidal neurons (through *Schaffer collaterals*). Furthermore commisural associative fibers provide synaptic contacts between CA3 pyramidal neurons and between the two hippocampi.

a: stratum oriens
b: stratum pyramidale
c: stratum radiatum
d: stratum lacunosum-moleculare
e: stratum granulosum
f: hilus
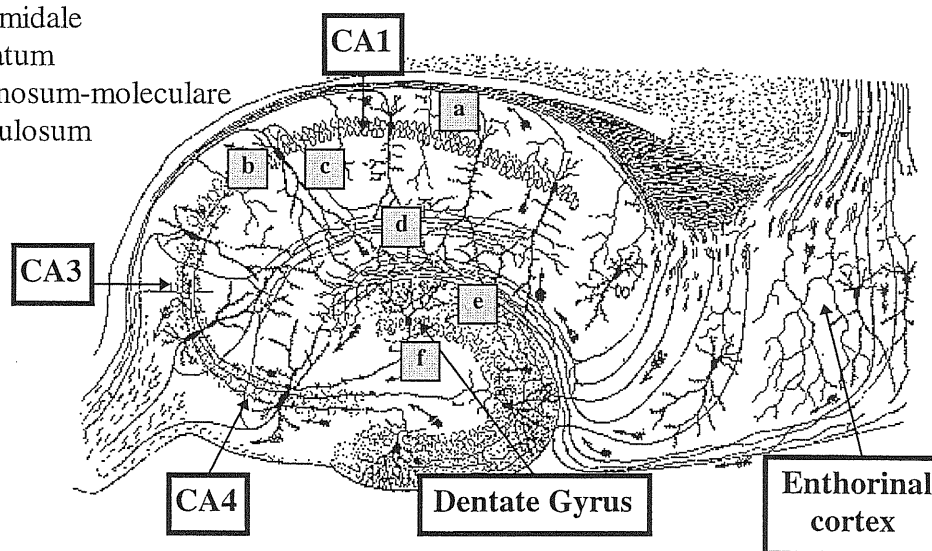
Figure 2.2 Anatomy and neuronal structure of the hippocampus (modified from Ramon y Cajal, 1911).

Output neurons are also controlled by local inhibitory interneurons and a balance is set up between excitation and inhibition. These interneurons are classified in several families

14

according to their morphological characteristics and their specific location in the hippocampus (Ramon y Cajal, 1911; Lorente de No, 1934; Somogyi et al., 1983; Freund and Buzsaki, 1996).

2.3.2 Physiology of hippocampal neurons and synapses

DG granule cells, CA3 pyramidal neurons and CA1 pyramidal neurons are the three families of excitatory cells in the hippocampus. These neurons differ in their passive and active properties. An interesting characteristics of CA3 and CA1 pyramidal neurons is the phenomenon of *accommodation* that eventually limits their maximum frequency of firing. This property distinguishes pyramidal neurons from GABA interneurons that are able to fire up to 400 Hz (Lacaille, 1991).

Firing properties of excitatory neurons are intrinsically related to the way in which they can release neurotransmitter, i.e. to how they can transfer information to postsynaptic targets.

Local excitatory interactions within the hippocampal region are provided by mossy fibers, associative commisural fibers and by Schaffer collaterals. Mossy fibers are the axons of DG granule cells and form synapses with the proximal dendrite of CA3 pyramidal neurons. These fibers are developing in the first two weeks of life in the rat and can be identified by zinc-staining with the method of Timm (Slomianka and Geneser, 1997). Associative commisural fibers within CA3 pyramidal neurons and Schaffer collaterals from CA3 to CA1 pyramidal neurons have an earlier development. Particularly, excitatory postsynaptic currents (EPSCs) or potentials (EPSPs) elicited by mossy fibers stimulation can be distinguished from those evoked by associative commisural fibers stimulation on the basis of the quantal size and of the kinetics of synaptic responses (Henze et al., 1997).

The probability of connectivity of excitatory neurons in the hippocampus is rather low (less than 5% in the adult hippocampus). An hippocampal preparation with a connectivity within pyramidal neurons higher than 50% is the slice organotypic culture after two weeks of development (Gähwiler et al., 1997). This specific preparation is particularly suitable for studies of synaptic transmission.

Single synaptic responses in pyramidal neurons are very variable (Allen and Stevens, 1994) as shown both by using extracellular minimal stimulation (see next chapter) in acute slices and double recordings in slice cultures (Debanne et al., 1996). Interestingly, from the point of view of the quantal theory, the high variability of synaptic responses and the high percentage of

failures suggests that excitatory synapses in the hippocampus have a low release probability and a low number of quanta and/or releasing sites (Jonas et al., 1993).

2.3.3 Long-term plasticity in the hippocampus

An interesting property of excitatory synapses in the hippocampus is that they are highly plastic in the sense that their synaptic efficacy can be strongly modulated by activity. In rats older than two weeks, high frequency trains (100 Hz) induce LTP both in CA3 and in CA1 pyramidal neurons, while low frequency trains normally induce long lasting forms of depression (LTD) (Dudek and Bear, 1992). LTD is more frequent in younger rats where it can be induced also with high frequency stimulation (Battistin and Cherubini, 1994). Since the hippocampus plays a role in certain aspects of learning, although the exact nature of this function at the level of neuronal networks is unclear, LTP and LTD have been proposed to constitute the cellular mechanism underlying fast memory storage (Brown and Zador, 1990).

It turns out that different forms of LTP and LTD exist in hippocampal neurons. LTP types can be roughly divided into two principal categories on the basis of whether or not LTP induction is blocked by antagonists of NMDA glutamate receptors. The induction of LTP in Schaffer collaterals and in associative commisural fibers needs the activation of NMDA receptors allowing Ca^{2+} entry during the train, as LTP is prevented both by addition to the extracellular medium of NMDA receptors blockers and by intracellular perfusion of strong Ca^{2+}chelators such as bis-(-o-aminophenoxy)ethane-N,N,N',N'-tetraacetic acid (BAPTA) (Bliss and Collingridge, 1993). In these types of LTP, Ca^{2+} entry through NMDA receptors triggers cascades of events involving different protein kinases such as Ca^{2+}/phospholipid-dependent kinase, protein kinase C (PKC) and Ca^{2+}/calmodullin-dependent kinase, protein kinase B (PKB) (Bashir and Collingridge, 1992). There is evidence for NMDA dependent types of LTP which are *hebbian*, occurring in synapses in which there is both coincident pre- and post-synaptic activity, and *non-hebbian*, extending to synapses made by concurrently active terminals onto neighbouring cells, whether or not these are active (Bliss and Collingridge, 1993).

In contrast to Schaffer collaterals and associative commisural fibers, LTP is NMDA independent at the mossy fibers (Urban and Barrionuevo, 1996). The site of induction of this type of LTP is controversial; more specifically, it has been shown that both postsynaptic

depolarisation and Ca^{2+} entry are necessary for induction of mossy fiber LTP (Jaffe and Johnston, 1990; Kapur et al., 1998) whereas other results show that this phenomenon is a presynaptic event requiring a rise in presynaptic Ca^{2+} (Zalutsky and Nicoll, 1990; Nicoll and Malenka, 1995). Moreover, it has been shown that the persistent enhancement of glutamate release is dependent on cAMP and protein kinase A (PKA) activation (Weisskopf et al., 1994). Several types of LTD have also been reported. A heterosynaptic form of LTD reported by Lynch et al., (1977) and a homosynaptic form of LTD (Stanton and Sejnowski, 1989) are both present in CA1 pyramidal neurons. The latter form of LTD, also described as associative LTD, has been reported to be sensitive to NMDA (Bear and Malenka, 1994). More recently an NMDA insensitive type of LTD that is blocked by antagonists of mGluRs has been described in the same region (Oliet et al., 1997). Interestingly, in CA3 pyramidal neurons, where the two forms of LTP coexist (Urban and Barrionuevo, 1996), the presence of different types of LTD has been also recently reported during postnatal development (Domenici et al., 1998).

2.4 Short-term plasticity

2.4.1 Short-term plasticity at the neuromuscular junction

Synaptic transmission is not a static process and synaptic responses are generally subject to changes occurring within short time scales when presynaptic fibers are repetitively activated. This phenomenon is called short-term plasticity. Like the general problem of neurotransmitter release, short-term plasticity has been first found and investigated at the neuromuscular junction.

When two action potentials with tens of millisecond interval occur at the nerve terminal, the statistics of synaptic responses evoked by the second action potential is generally changed and the mean response to the nerve terminal stimulation is either increased (*facilitated*) or decreased (*depressed*). The phenomenon of facilitation is thought to be due to an increase in the release probability. The principal hypothesis is that this phenomenon is caused by the presynaptic accumulation of residual calcium $[Ca^{2+}]_i$ after the first action potential (Katz and Miledi 1968; Magleby and Zengel 1982). Because the release probability depends on the intracellular calcium activity in a non-linear manner (Dodge and Rahamimoff, 1967), the effect of a

persisting residual calcium at sites of transmitter release can considerably augment the release probability. As a consequence, the amplitude of the current evoked by the second pulse increases because the probability of release increases (Zucker, 1989). Although the formulation of the residual calcium hypothesis is rather old, the involvement of an accumulation of Ca^{2+} in the phenomenon of facilitation has been more recently demonstrated by using photolabile Ca^{2+} chelators (Kamiya and Zucker, 1994).

Interestingly, at the neuromuscular junction, facilitation is replaced by depression in conditions of increased release probability. This phenomenon of depression is generally believed to be caused by depletion of synaptic vesicles (Betz 1970), i.e. by a decrease in the number of vesicles available for release. Depletion of synaptic vesicles is not the only mechanism underlying short-term depression. For instance it has been shown that receptor desensitisation is the principal source of depression in several preparations such as some types of cholinergic synapses in Aplysia abdominal ganglion motoneurons (Gardner and Kandell, 1977).

A type of plasticity that occurs at a longer time scale and that has been reported at the crustacean neuromuscular junction is the phenomenon of *post-tetanic potentiation* (PTP) (Baxter et al., 1985). PTP is an increase in the efficacy of transmission requiring minutes for its development and decay. As in the case of facilitation, PTP seems to be related to the intracellular Ca^{2+} that triggers neurotransmitter release at the nerve terminal (Erulkar and Rahamimoff, 1978).

In order to account for short-term plasticity phenomena, several extensions of the theory of neurotransmitter release generated by a single spike to the more general case of trains of action potentials, aimed at the release process at the neuromuscular junction, have been proposed (Elmqvist and Quastel, 1965; Mallart and Martin, 1967; Melkonian, 1993; Quastel 1997; Worden et al., 1997). In the case of models accounting for synaptic depression, the characteristics of binomial release have been coupled with changes in N due to depletion-refilling processes. Hence, in these models, N is a random fluctuating variable and does not correspond to the N of binomial release (Vere-Jones, 1966). In the case of facilitation, the increase in the efficacy of transmission has been explained by changes in the binomial release parameters p (Zucker, 1973) and N (Bennett and Florin, 1974).

2.4.2 Short-term plasticity in the mammalian CNS

The phenomena of facilitation and depression are both present in the mammalian CNS. In the hippocampus, excitatory synapses are more likely facilitating both in the CA1 region (Creager et al., 1980) and in the CA3 region (Salin et al., 1996) and experimental evidence indicates that, as in the case of the neuromuscular junction, facilitation has a presynaptic origin.

In the neocortex, synapses between pyramidal neurons are strongly depressing while synapses from pyramidal neurons to inhibitory interneurons are facilitating (Thomson et al., 1993). The analysis of EPSP facilitation in neocortical interneurons shows that this type of facilitation has a strong postsynaptic component due to the progressive depolarisation of the target neuron that increases cationic conductance by activating NMDA glutamate receptors.

Other interesting types of synaptic depression has been reported at the brainstem Calyx synapse (von Gersdorff et al., 1997) and at the climbing fiber to Purkinje cell synapse (Dittman and Regehr, 1998). Depression at the Calyx of held is presynaptically originated with a small contribution of metabotropic glutamate receptors. Interestingly, synaptic responses in these systems are characterised by a very high reproducibility with a CV typically lower than 0.1. A detailed analysis of synaptic responses in Purkinje cells gave an estimate of 400-500 functional releasing sites, the same order of magnitude of the neuromuscular junction (Silver et al., 1998). In cases in which both paired-pulse facilitation and depression are considered to be mainly generated by a change in presynaptic conditions also in CNS excitatory synapses, the statistical analysis of these phenomena, using the framework of the quantal analysis, has been used to test the possible presynaptic site of expression of LTP (McNaughton, 1982; Voronin and Khunt, 1990; Manabe et al., 1993). Indeed it has been suggested that LTP in CA3 pyramidal neurons has a main presynaptic expression only at the mossy fibers and not at the associative commisural fibers because only the former type of LTP is associated to a strong decrease in paired-pulse facilitation (Zalutsky and Nicoll, 1990).

2.4.3 Short-term plasticity and neuronal codes

The problem of short-term plasticity in the brain is strongly related to the ability of neurons to integrate and code input signals. If the conditions of release during a train are not constant, the *significance* of synaptic events, i.e. the information transmitted by presynaptic action potentials, changes with time. This problem has been recently addressed by several neuroscientists.

In neocortical neurons, where at normal conditions pyramid-pyramid connections are characterised by a high probability of release that most likely results in depression of postsynaptic potentials evoked by a second and third presynaptic action potential, Tsodyks and Markram (1997) proposed a simple heuristic model to account for mean EPSPs. This model has been lately extended to account for facilitating afferents to interneurons (Markram et al., 1998). Markram and Tsodyks showed that in a train of more than 10 presynaptic action potentials the first mean EPSPs (3-6) are dominated by depression and the following mean EPSPs reach a stationary value that depends on the firing frequency. The time window of transient synaptic responses depends on the initial release probability, i.e. on the strength of depression. This feature can be modulated by synaptic plasticity that can be obtained by pairing presynaptic trains with postsynaptic depolarisation (Markram and Tsodyks, 1996). Markram and Tsodyks showed that the time window of transient synaptic responses determines the interval in which simultaneous synaptic inputs can summate to generate a *transient* postsynaptic response. Indeed, they proposed that this can be a relevant time scale for understanding neural codes (Tsodyks and Markram, 1997).

In the case of facilitating synapses, the question of the time window for neuronal codes has to deal particularly with the problem of the variability of synaptic responses. Since in these synapses the release probability is typically low, unless the number of quanta is considerably large as in the case of the neuromuscular junction, synaptic responses are very *unreliable*. Nevertheless, as proposed by Lisman (1997), the time integration of facilitating synaptic responses can make synapses which are *unreliable* at the level of a single action potential *reliable* at the level of a burst. This would determine the typical synchronous bursting activity that can be observed in several networks characterised by facilitating synapses. Thus, because of short-term plasticity, the best stimulus to fire a cell is coincident bursts, and this has clear implications on the way information would best be coded.

All these studies bring to a new concept of neural representation and computation: the *dynamic synapse* (Liaw and Berger, 1996). In fact, as the probability of neurotransmitter release turns out to be a function of the temporal pattern of action potential occurrence, synaptic efficacy (that can be modulated by long-term synaptic plasticity) becomes a dynamic property of the synapse that determines synaptic integration and neuronal signalling.

2.5 Aim of the work

The aim of this thesis was to characterise synaptic responses to repetitive stimulation of afferent fibers in CA3 hippocampal neurons and to propose a theoretical framework to analyse and interpret experimental data. This problem is particularly interesting in hippocampal excitatory synapses of 7-10 days old rats where a large variability of short-term plasticity is found.

The question of extending the classical quantal theory to the case of repetitive synaptic transmission implies the introduction of stochastic chains accounting for activity dependent changes of synaptic parameters. Since the quantal parameters during short-term plasticity processes can be generally subject to substantial changes, preventing the success of conventional QA methods (Larkman et. al., 1997), the approach to the problem or repetitive release requires the extension of a traditional quantal theory scheme, founded on *static* probabilistic distributions, to a *Dynamic Quantal Theory* scheme based on the theory of stochastic processes.

In contrast to the analysis of synaptic responses corresponding to each presynaptic action potential, with single probability distributions, stochastic chains contain information on the correlation of synaptic responses within the train. This information can be used to discriminate within different models and to more carefully investigate the dynamics of a synapse. An algorithm to fit the statistics of repetitive synaptic responses with stochastic chains (Dynamic Quantal Analysis) has been used to analyse synaptic responses not only in hippocampal excitatory synapses, but also in GABAergic hippocampal synapses and in pyramid-pyramid connections in the neocortex. Neocortical data have been recorded at the Weizmann Institute of Science, Rehovot, Israel by Henry Markram.

The problem of the variability of synaptic responses evoked by trains of action potential is also particularly relevant to investigate time integration of synaptic signals. As discussed in the introduction, short-term plasticity can determine the time domain for postsynaptic signals integration. Therefore, a quantification of the capability of temporal integration requires a detailed analysis of the variability of synaptic responses. Thus, the characterisation of synaptic responses proposed in this thesis is also used to investigate the synaptic properties of signal integration and coding, by calculating an information quantity that can be transmitted by

synaptic signals, i.e. by evaluating the capability of a synapse to discriminate within different presynaptic inputs.

The analysis of synaptic variability aimed at investigating signal integration and neuronal processing can be extended from single synapses to networks. In order to do that, multisite recording techniques allowing to detect nervous signals from many neurons simultaneously must be used. A considerable part of my PhD work has been devoted to the development of a high space-time resolution imaging system particularly aimed at the recording of calcium signals. This part is reported in the appendix. It is shown that the temporal resolution of calcium signals recorded with this imaging system, which is limited only by the kinetics of the process of Ca^{2+}-dye binding and diffusion, allows the use of these signals to detect firing activity in single cells. Furthermore, it is shown that network activity can be investigated by recording signals from brain slices stained with AM-ester calcium dyes. This final part of the thesis, dedicated to fast calcium imaging, can be considered a possible development of the studies on signal variability at the level of neuronal networks.

3 SHORT-TERM PLASTICITY OF SYNAPTIC RESPONSES IN CA3 HIPPOCAMPAL NEURONS

In this chapter, the phenomenology of short term plasticity due to short trains of presynaptic action potentials is analysed. Postnatal (P) P7-P10 days old rats were used. These experiments were conducted in CA3 hippocampal neurons where two types of excitatory afferent fibers, namely the mossy fibers from DG granule cells and the associative commisural fibers from other CA3 pyramidal neurons are present. Mossy fibers are not completely developed at this age (Slomianka and Geneser, 1997) and can be activated by a stimulating electrode placed within 100 μm from the pyramidal neurons layer in the stratum lucidum-radiatum.

It is shown that very different types of short-term plasticity are present in these synapses and that the type of short-term plasticity depends on the concentration of the extracellular calcium and on the frequency of stimulation.

3.1 Methods

3.1.1 Slice preparation and solutions

For the study of synaptic transmission in the mammalian CNS, the in vitro brain slice preparation presents many advantages. Principally, synaptic connections are maintained almost intact, neurons can be visually identified and the whole cell patch clamp technique can be used. Hippocampal slices were prepared following the methods described by Sciancalepore et al., (1995).

Postnatal (P) days P7-P12 old Wistar rats were decapitated under urethane anaesthesia (0.5 ml ip of a 10% solution) and their brains removed. Transverse hippocampal slices (200 μm thick) were cut with a vibroslicer and placed in a bath containing (in mM): 126 NaCl, 3.5 KCl, 2 $CaCl_2$, 1.2 NaH_2PO_4, 1.3 $MgCl_2$, 14 $NaHCO_3$, 11 glucose, gassed with 95% O_2 and 5% CO_2 at 32 °C (pH 7.3). They were allowed to recover for at least 1 hour before being transferred to the recording chamber in which they were superfused at 3 ml/min. The extracellular solution contained (in mM): 126 NaCl, 3.5 KCl, 2 $CaCl_2$, 1.2 NaH_2PO_4, 1.3 $MgCl_2$, 25 $NaHCO_3$, 11

glucose, gassed with 95% O_2 and 5% CO_2 at room temperature (24°C, pH 7.3). Synaptic currents evoked by afferent stimulation were recorded at -70 mV holding potential. This potential corresponded to the reversal potential for Cl⁻ calculated by the Goldman equation. At this potential, the NMDA component of EPSCs with a slow decay time (>100 ms) was almost absent. The majority of the experiments have been performed in the presence of bicuculline (10 µM, purchased from Sigma) and CPP (20 µM, gift of Dr. Herrling, Novartis, Basel). In these conditions only the fast AMPA component of the glutamatergic current was present. In some experiments, extracellular calcium concentration $[Ca^{2+}]_o$ was varied from 0.8 mM to 4 mM in order to modify the probability of neurotransmitter release.

3.1.2 Patch clamp recordings

Recording pipettes were pulled from 2 mm borosilicate glass and had a resistance of 2-5 MΩ when filled with intracellular solution. Intracellular solution contained (in mM): 120 K-gluconate, 4 $MgCl_2$, 49 N-2-hydroethylpiperazine-N'-2-ehanesulfonic acid (HEPES), 0.6 ethylene glycolbis (b-aminoethyl ether) N,N,N',N'-tetraacetic acid (EGTA), 2 Na_2ATP, 0.2 Na_2GTP, adjusted to pH 7.2 with KOH. EPSCs from CA3 hippocampal neurons were recorded at -70 mV in voltage clamp mode, with a standard patch clamp amplifier (EPC-7 List Medical Instruments) after optimising capacitance and series resistance compensation. Series resistance (typically 10-15 MΩ) was continuously checked for stability during the experiment. The extracellular solution introduced a junction potential of 20-30 mV that was compensated by replacing a resistance in the patch clamp amplifier.

3.1.3 Stimulation

Patch pipettes with a tip of 10-30 µm diameter filled with the extracellular solution were used for stimulation. The stimulating electrode was placed under visual control on the surface of the slice in the *stratum lucidum-radiatum* 50-200 µm above the CA3 pyramidal layer. In this position, either mossy fibers and/or associative commisural fibers could be stimulated. EPSCs were evoked by short trains of pulses at frequencies ranging from 10 to 25 Hz, (each pulse 40 µs duration), repeated every 10 s. Figure 3.1 A shows a picture of the preparation with both the stimulating and the recording electrodes. Figure 3.1 B shows four consecutive recordings of

EPSCs evoked by trains of four pulses of stimulation delivered at 20 Hz. The high *unrealiability* of synaptic responses that can be observed is due to a relatively low probability of neurotransmitter release p combined to a low number of quanta N (see equations 2.1-2.4) (Allen and Stevens, 1994).

To stimulate the minimal number of fibers, the stimulus intensity was adjusted just above threshold to evoke an EPSC. The mean EPSC amplitude, plotted against stimulus intensity, showed an all or none behaviour with an abrupt increase at a given stimulus strength corresponding to threshold and then remained constant when the stimulation intensity was kept within a given range (see also Jonas et al., 1993). A further increase in stimulus strength gave rise to larger EPSC, indicating the involvement of more fibers. Typically the intensity of stimulation to evoke a minimal EPSC ranged from 4 to 10 V. In the representative example illustrated in Figure 3.2 A, the voltage range between 4 and 5.5 V corresponded to the minimal stimulation required to evoke an EPSC. One or more additional fibers were recruited when the stimulation intensity was in the range of 6-7.5 V. From Figure 3.2 B it is clear that short-term plasticity generally changes when additional fiber(s) are recruited whereas it does not change within the same stimulation range. In some cases, discarded from the present results, unclamped antidromic spike could be detected following stimulation pulses.

3.1.3 Data Analysis

The analysis of experimental synaptic responses and the calculation of the relevant statistical quantities have been done using programs developed with Matlab 4.2C for PC (The Math Works, Inc., Natick, USA). Matlab is a high level programming language that allows fast developing and debugging of codes, the use of a very large number of dedicated libraries, the easy setting up of graphical interfaces. Matlab is available for PC, Macintosh or UNIX systems and source codes, that do not require a compilation, can be easily transferred from one system to another. In comparison with C or C++, Matlab programs are considerably slower since all variables are *double* as default. However, by using processors like Pentium 200 or more advanced releases, the speed of the programs is not a limit to use Matlab for many applications of data analysis and computer simulations.

A

Stratum Radiatum

Stimulating Electrode

Recording Electrode

CA3

200 μm

B

25 pA

50 ms

C

10 pA

50 ms
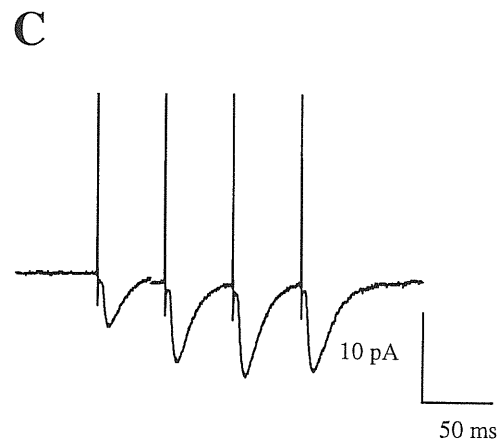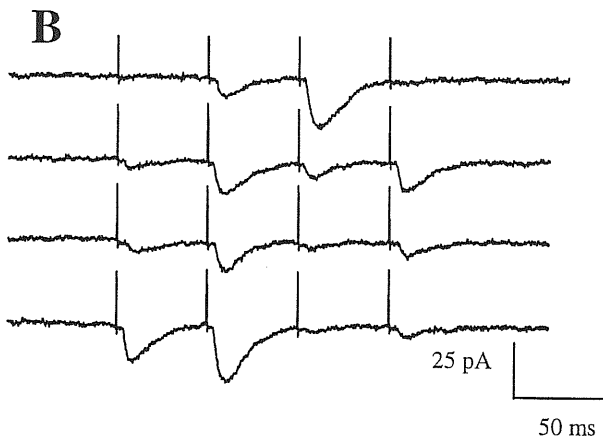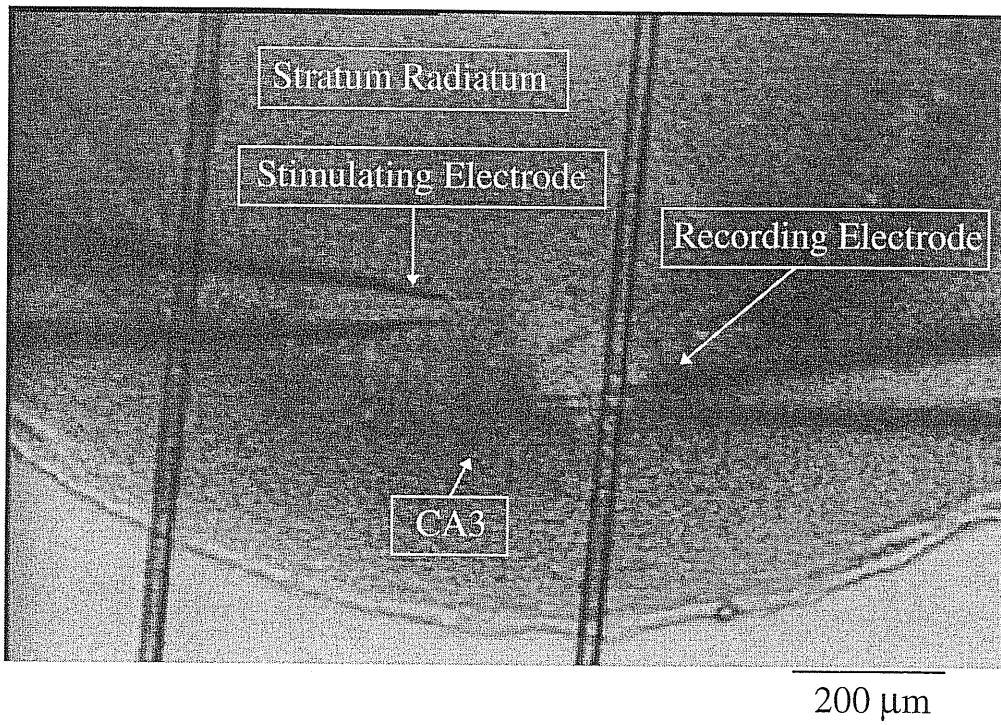
Figure 3.1 Experimental protocol. A. Hippocampal slice obtained from a P9 old rat with a recording electrode positioned in the CA3 pyramidal region and a stimulating electrode placed in the *stratum lucidum-radiatum*. EPSCs (n=100) were evoked by four pulses at 20 Hz. B. Four consecutive recordings. C. Average of the 100 recordings, showing a facilitation of the second EPSC with respect to the first and of the third with respect to the second.

26

A

First mean EPSC amplitude
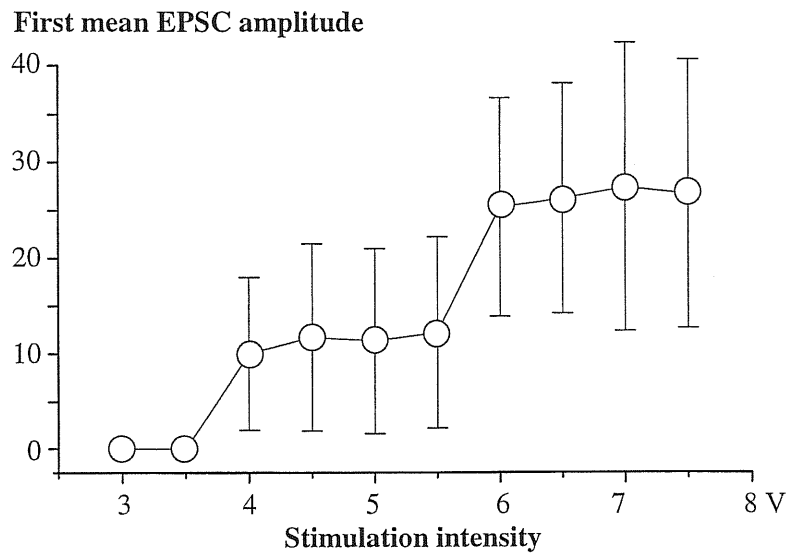
B
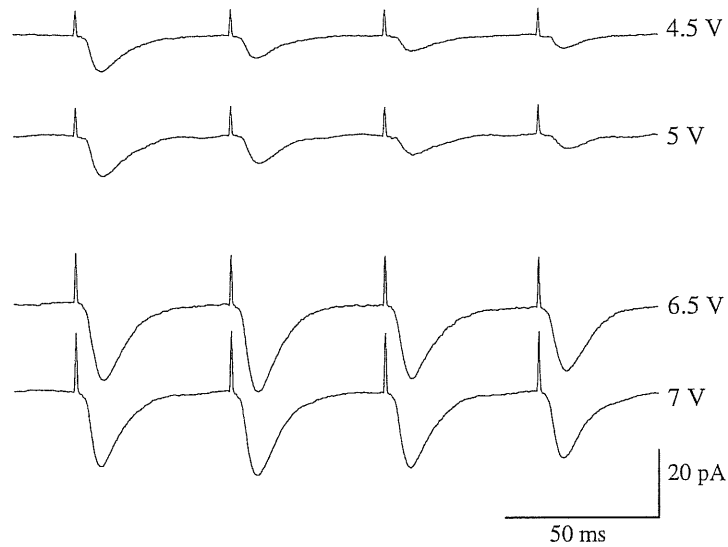
Figure 3.2 EPSCs evoked at different stimulation intensities. A. Plot of mean amplitude of the first EPSC vs. stimulation intensity. Each open symbol represents the mean amplitude of 30 recordings (bars are the standard deviations). In the voltage range between 4 and 5.5 V, corresponding to the minimal stimulation required to evoke a synaptic response, mean EPSC amplitudes did not change. One or more additional fibers were recruited when the stimulation intensity was in the range of 6-7.5 V. B. Four traces representing the average of 30 recordings at different stimulation intensities. Distinct EPSC patterns were observed at different stimulation ranges whereas EPSC patterns did not change within the same stimulation range.

Figure 3.3 shows two parts of a window (graphical interface) of a program used for data analysis. The program is able to read binary files (including the header), to plot experimental samples, and to analyse EPSC amplitudes (see also next chapter). The development of programs for data analysis has been a part of this PhD work.

EPSC amplitudes were measured after the detection of stimulation artefacts. Since in most of the experiments the smallest detectable currents was higher than the background noise, a response having an amplitude three times smaller than the standard deviation of the signal recorded during the 50 ms interval preceding the first stimulus artefact was considered a failure. It must be said that failure detection and, more generally, the appearance of peaks corresponding to quantal currents in the amplitude distributions, could be visually tested when quantal currents were larger than 15-20 pA.

3.2 Results

3.2.1. Different types of short-term plasticity at CA3 hippocampal synapses

In 57 experiments, 40 recordings with four 20 Hz pulses of stimulation have been considered. The sequences of the mean EPSC amplitudes (EPSC patterns) were classified in terms of facilitation (F) or depression (D) of the nth EPSC with respect to the $(n-1)^{th}$. For example, FDD indicates facilitation of the second EPSC with respect to the first one and depression of the third with respect to the second and of the fourth with respect to the third. EPSC patterns could be therefore grouped in eight cases. This classification is only qualitative and is aimed at showing the variability in short-term plasticity behaviours observed in these synaptic responses.

The case with three consecutive facilitations (FFF) was observed only 6 times while the case with three consecutive depressions (DDD) was more common (19 times). Cases FFD and FDD, considered as *intermediate* cases were observed 19 times. All the other cases in which facilitation occurred after a depression were observed 13 times. As shown in Figure 3.4 B, the four normalised averaged EPSCs in the sequence had a similar decay time, suggesting that AMPA receptor desensitisation does not play an important role in determining different EPSC patterns (Jones and Westbrook 1996).
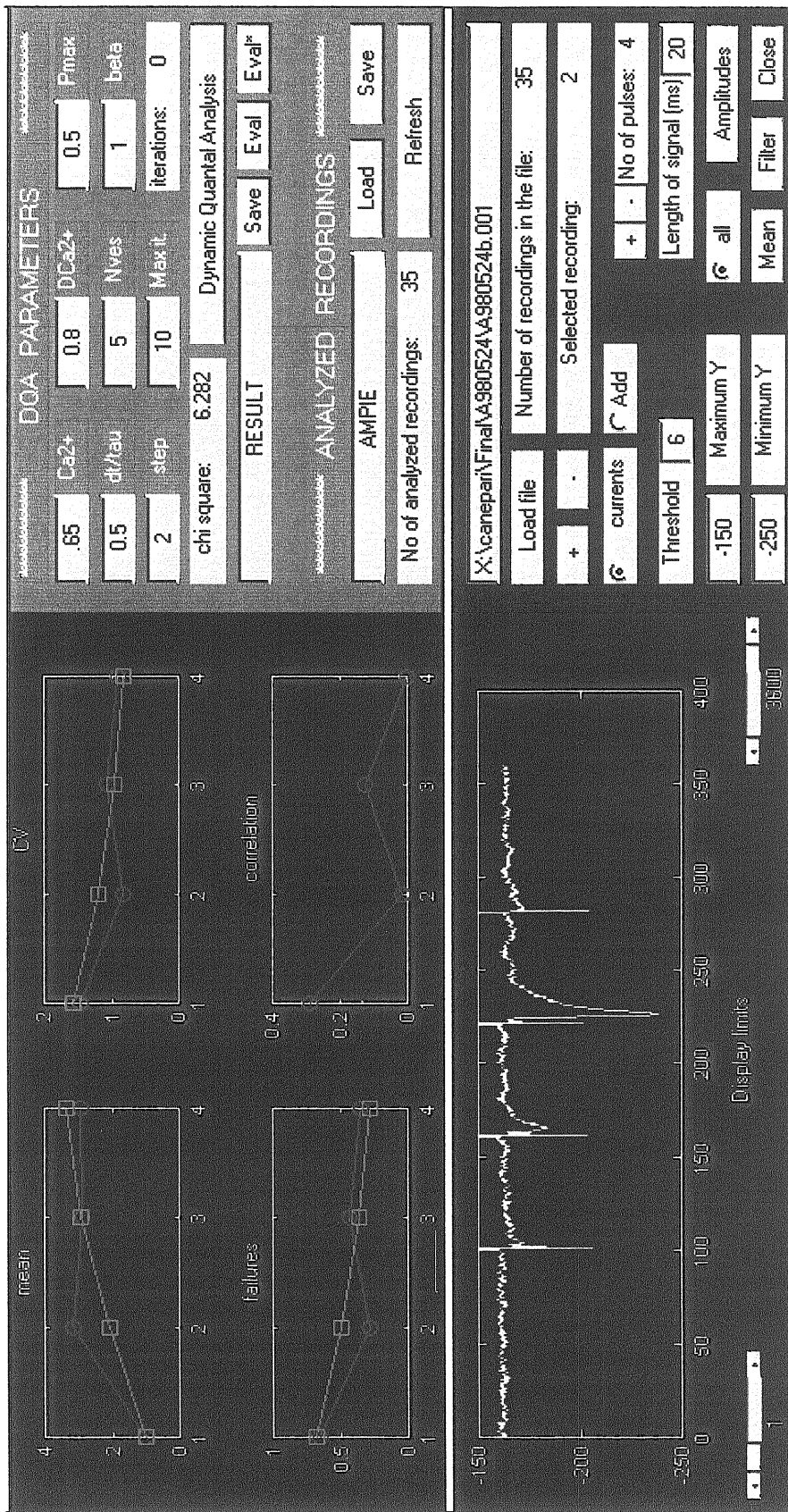
Figure 3.3 Graphical interface of a program used for the analysis of EPSCs. Bottom-left. Plot of a recording. Bottom-right. Commands to select a file containing binary data (upper part), to adjust the scale, to choose the parameters for analysis and to measure EPSC amplitudes. Top-left. Results of data analysis superimposed to a model fitting (see next chapter). Top-right. Commands for model fitting.

In fact, in the case of synaptic responses mediated by AMPA receptors, the decay phase of synaptic currents basically mimics the kinetics of desensitisation and the observation that normalised EPSCs can be superimposed indicates that desensitisation is constant within the stimulation train.

In order to test whether different EPSP patterns could be generated in the same cell by stimulation of other afferent fibers, in additional experiments, the intensity of stimulation was increased and/or the position of the stimulating electrode was changed. As illustrated in Figure 3.2, recruiting additional fibers by increasing stimulus strength changed the EPSC patterns. These results show that, in comparison with neocortical pyramidal neurons (Thomson et al., 1995) a higher variability of synaptic behaviours could be elicited in the developing hippocampus even in the same cell.

3.2.2 Identification of presynaptic fibers responsible for EPSCs

In the adult guinea pig hippocampus, differences in short-term plasticity between synaptic responses evoked by repetitive stimulation of mossy fibers and those elicited by associative commisural fibers have been reported (Salin et al., 1996). In order to see whether the high variability in EPSC patterns observed in the present experiments reflected the activation of different types of synaptic inputs, the mGluR2/mGluR3 specific agonist 2-(2,3-dicarboxycyclopropyl) glycine (DCG-IV, 1 μM) was used. Activation of mGluR2/mGluR3, which are localised on the mossy but not on the associative commisural fibers (Shigemoto et al., 1997), induces a reduction of neurotransmitter release and therefore allows to distinguish between the two different synaptic inputs (Kamiya et al., 1996). In 3 out of 8 cells in which DCG-IV was tested, a reduction of the mean amplitude of the first EPSC (larger than 30%) was observed, whereas in the remaining cases the mean EPSC amplitude was unchanged.

In the presence of DCG-IV, modifications of EPSC patterns occurred as shown in the representative example of Figure 3.5 A, in which a DDD pattern changed to a FDD pattern. All these experiments have been done in the presence of 20 μM CPP since DCG-IV is also an agonist of NMDA glutamate receptors.
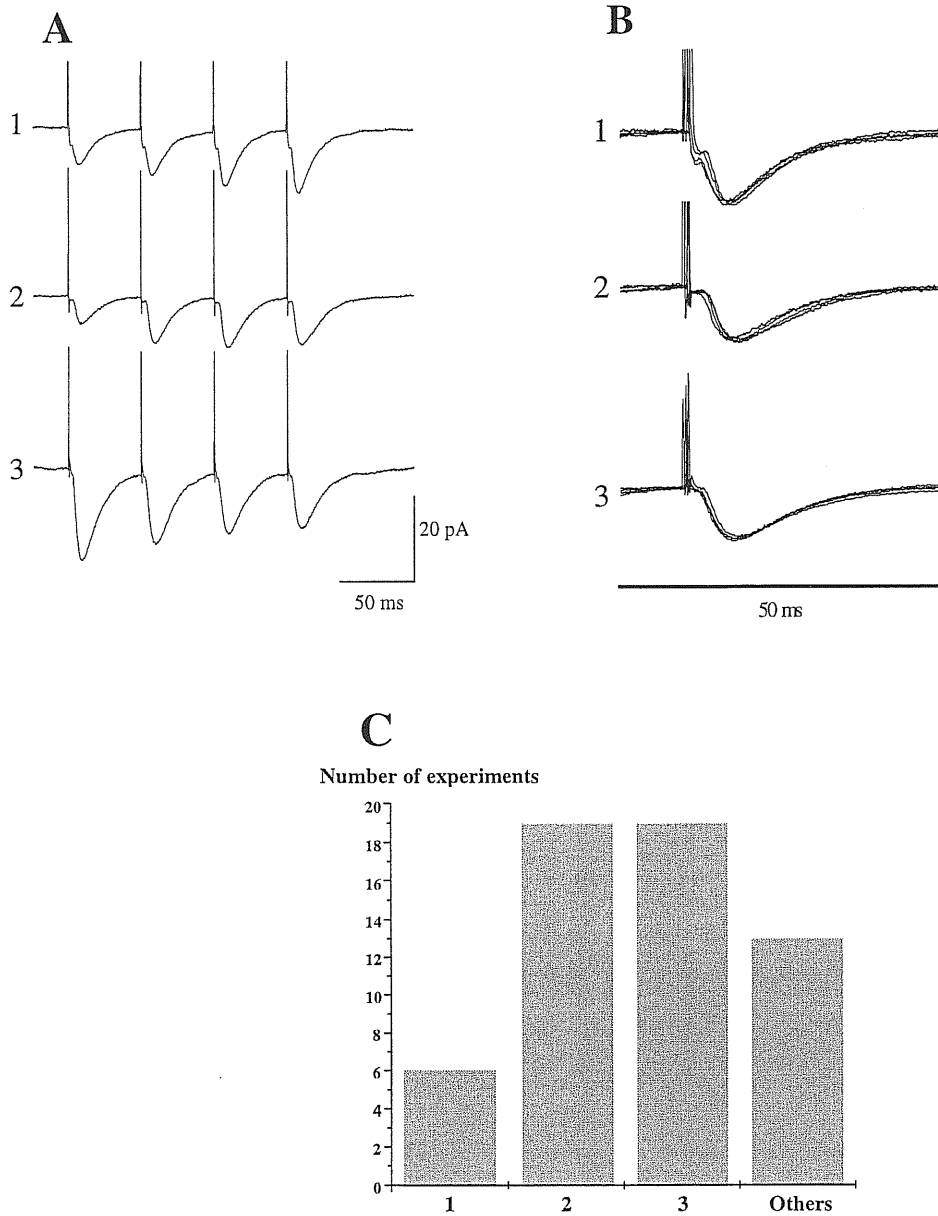
Figure 3.4 Different EPSC patterns evoked by 4 pulses. A. Each trace is the average of 40 recordings obtained from 3 different cells (1-3). A-1 and A-3 show the extreme cases of EPSC patterns in which there is facilitation or depression of the second third and fourth EPSC with respect to the previous one (FFF and DDD). A-2 represents an *intermediate* case in which the fourth EPSC is slightly depressed in comparison to the previous one (FFD). B. The four mean currents in the three cases shown in A were normalised and superimposed (1-3). C. The column diagram summarises the results obtained in 57 experiments. Case 1 and 3 have been observed 6 and 19 times respectively. *Intermediate* cases have been observed 19 times and the other cases (FDF, DFD, DDF and DFF) 13.

Interestingly, in the DCG-IV-sensitive cases the mean amplitude of the first EPSC was larger than 20 pA with a CV higher than 70%, while in the DCG-IV-insensitive responses, the first EPSCs had either a mean amplitude smaller than 20 pA or a CV lower than 50% and almost no failures. These results suggest that EPSCs evoked by the release of a single quantum at mossy fiber synapses are generally larger in amplitude then those at associative commisural fibers as recently demonstrated by Henze et al., (1997). In about 32% of the experiments, EPSCs had characteristics similar to those of the DCG-IV-sensitive cases, suggesting that only in a minority of the cases synaptic responses were elicited by the stimulation of the mossy fibers. A high variability of EPSC patterns has been observed both with large and small mean EPSC amplitudes. It must be said that the specificity of DCG-IV to mossy fibers during the second postnatal week has not been tested. Therefore, the results presented in this section cannot be considered conclusive. Moreover, from these results it appears that a particular EPSC pattern cannot be associated to the activation of a specific synaptic input, since both facilitating and depressing behaviours could be observed by stimulating either mossy fibers of associative commisural fibers.

3.2.3 Effects of changing $[Ca^{2+}]_o$ on EPSC patterns

In order to investigate how EPSC patterns are affected by the probability of release, EPSCs have been recorded in the presence of different $[Ca^{2+}]_o$. Changing $[Ca^{2+}]_o$ from 2 to 4 mM produced not only a significant ($p<0.05$) increase in the mean amplitude of the first EPSC (22 ± 7 pA at 2 mM $[Ca^{2+}]_o$ and 30 ± 10 pA at 4 mM $[Ca^{2+}]_o$, mean $\pm$ SD) and a decrease in the number of failures, but also a change of the EPSC pattern (Figure 3.6 A and B).

Figure 3.6 C summarises the results obtained in six experiments in which $[Ca^{2+}]_o$ was changed from 2 mM to 4 mM. In all the cases, in the presence of 4 mM $[Ca^{2+}]_o$, a decrease in the ratio between the nth EPSC and the first one and an increase of the mean amplitude of the first EPSC were observed. With the higher calcium concentration in 5/6 experiments, DDD patterns were obtained. These results indicate that it is possible to change most of the EPSC patterns to DDD configurations, by increasing the probability of release.

A

Mossy fiber

Control

+1μM DCG-IV

30 pA

50 ms

B

Associative commisural fiber

Control

+1μM DCG-IV

15 pA

50 ms
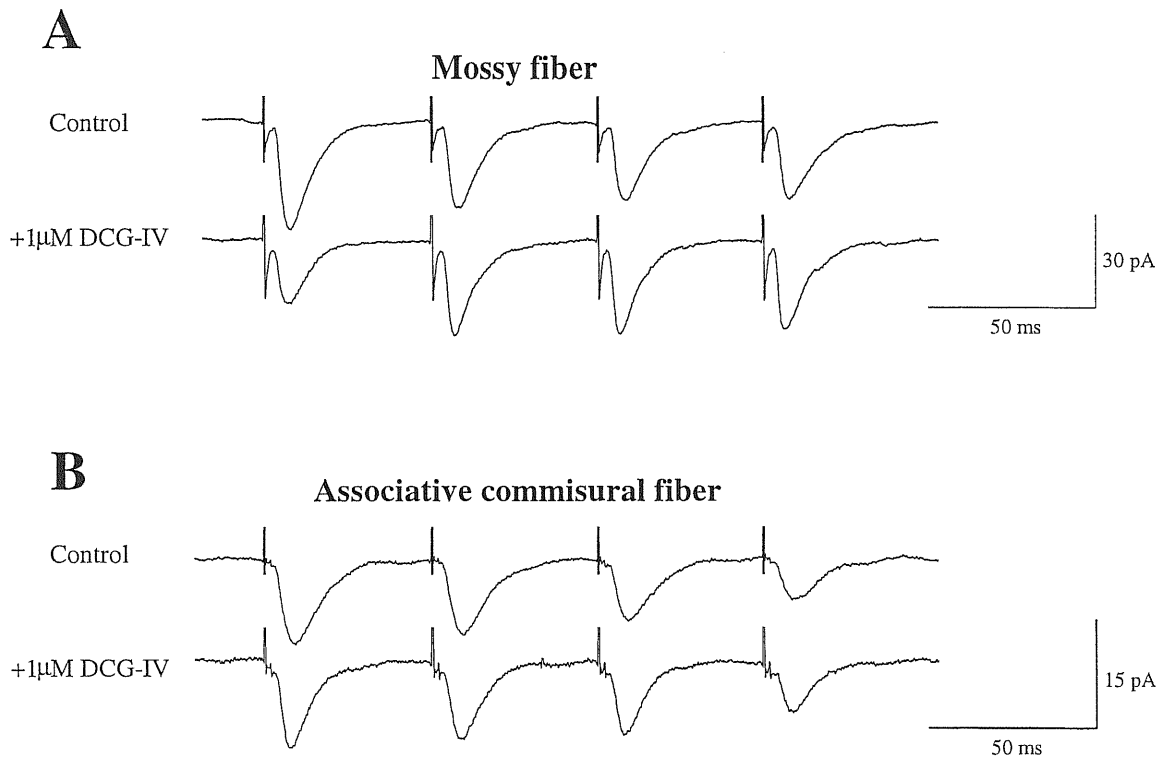
Figure 3.5 Identification of presynaptic fibers responsible for EPSCs. A and B. Traces representing the average of 40 recordings of DCG-IV-sensitive (A) and DCG-IV-insensitive (B) synaptic responses in control condition and in the presence of 1 μM DCG-IV.

3.3 Simple modelling of short term plasticity

3.3.1 A simple theoretical background of transmitter release dynamics

According to the quantal theory, exocytosis of synaptic vesicles occurs in a stochastic manner and different numbers of quanta are released following a discrete probabilistic distribution. In a stochastic process in which N vesicles or quanta have a probability p to be released when the terminal is reached by an action potential, the mean number of released vesicles is given by equation 2.2. The probability p can be expressed by a function of the transient intracellular calcium concentration $[Ca^{2+}]_i$ that triggers transmitter release in presynaptic terminals.
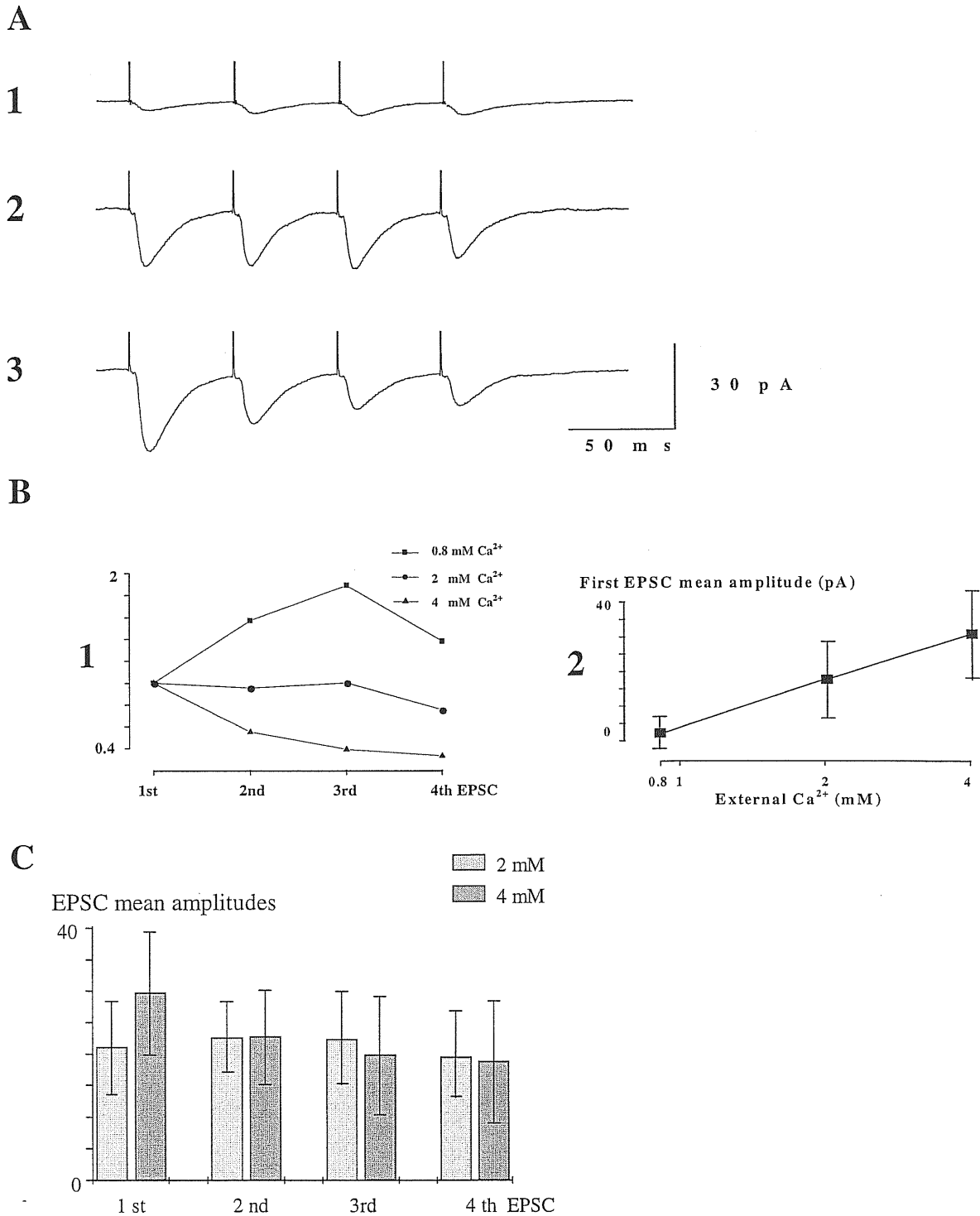
Figure 3.6 EPSC patterns evoked in the presence of different $[Ca^{2+}]_o$. A. Traces representing the average of 40 recordings obtained in the presence of 0.8 mM (1), 2 mM (2) and 4 mM (3) $[Ca^{2+}]_o$. B. The ratios between the four mean EPSC amplitudes and the first one are shown in 1. In 2 each point represents the mean amplitude of the first EPSC evoked in the three different $[Ca^{2+}]_o$. C. Light and dark columns indicate the mean of the mean EPSC amplitudes obtained in six experiments with 2 mM and 4 mM $[Ca^{2+}]_o$ respectively. Error bars are SDs.

A simple expression of the probability function is given by a generalised Dodge-Rahamimoff equation (Dodge and Rahamimoff, 1967; reviewed by Van der Kloot and Molgó, 1994)

$$p([Ca^{2+}]) = \frac{p_{max}}{1 + (K \cdot [Ca^{2+}])^{-4}} \qquad (3.1)$$

where K is a constant and p_{max} is the maximum value of p; $[Ca^{2+}]$ represents the peak concentration of calcium in the terminal.

Short-term variations of synaptic efficacy such as paired-pulse facilitation and paired-pulse depression have been explained with statistical changes of release properties (Del Castillo and Katz, 1954b); when a second action potential reaches the synaptic terminals a short time (< 200 ms) after the first one, the probability of release will be generally increased by residual calcium due to the first action potential, while the number of available transmitter quanta will be decreased by a fraction of the quanta released during the first action potential (depletion). The first mechanism can be responsible for facilitation and the second for depression. These mechanisms can be simply expressed by an equation for the mean number of released vesicles during a second action potential

$$< n_2 > \; = \; p([Ca^{2+}] + \Delta[Ca^{2+}]) \cdot (N - < n_1 > \cdot f(\Delta t)) \qquad (3.2)$$

where f(t) is a function that accounts for reavailability mechanisms of synaptic vesicles and Δt is the time between the two action potentials; f(t) must satisfy the following requirements:

$$f(0)=1 \quad \text{(no reavailability immediately after the first release)} \qquad (3.3a)$$

$$f(t \to \infty) \to 0 \quad \text{(complete reavailability after a long time).} \qquad (3.3b)$$

The simplest way to express the reavailability function is to use a single exponential function $e^{-t/\tau}$ or a sum of several exponential functions indicating different possible time constants.

If j action potentials reach the synaptic terminal with a constant time interval Δt, equation 3.2 can be generalised for the mean number of vesicles released during the jth action potential as

$$< n_j > \; = \; p([Ca^{2+}] + \Delta_{j-1}[Ca^{2+}]) \cdot (N - \sum_{i=1}^{j-1} < n_i > \cdot f((j-i) \cdot \Delta t)) \qquad (3.4)$$

where $\Delta_{j-1}[Ca^{2+}]$ is the change of effective calcium concentration produced by the first j-1 spikes. EPSC amplitudes can be considered approximately proportional, to the first order, to the

number of released vesicles and therefore the mean EPSC amplitude A can be expressed by the relation

$$A = \beta \cdot <n>. \tag{3.5}$$

In general an EPSC can be generated by the release of $\mathfrak{R}$ independent different terminals and/or releasing sites; the mean j^{th} EPSC amplitude recorded during a train of action potentials occurring with a time interval Δt is the weighted sum of the contributions of the single terminals and/or releasing sites

$$A_j^{\mathfrak{R}} = \sum_{h=1}^{\mathfrak{R}} \beta_h \cdot p_h([Ca^{2+}]_h + \Delta_{j-1}[Ca^{2+}]_h) \cdot (N_h - \sum_{i=1}^{j-1} <n_i>_h \cdot f((j-i)\cdot \Delta t)_h). \tag{3.6}$$

In this expression, the possible delay between the release at different terminals and/or releasing sites is neglected. By choosing particular forms of $p([Ca^{2+}])$ and $f(t)$ and by introducing a possible dependence of p_j on the jth action potential, this general model could account not only for calcium dependent exocytosis dynamics, but also for other possible mechanisms of modulation of calcium entry and transmitter release during the activation of the synaptic terminal. A probability function 3.1 in which there is a summation of constant contributions to residual calcium ($\Delta_{j-1}[Ca^{2+}]=(j-1)\cdot\Delta[Ca^{2+}]$) can account for simple mechanisms of facilitation. Each contribution $\Delta[Ca^{2+}]$ depends on Δt, (i.e. on the frequency of presynaptic firing), since the residual calcium decays in time.

It should be stressed that equation 3.6 can also describe postsynaptic mechanisms, leading to a change in the quantal size, if a dependence of β_h on j or on $<n_i>_h$ is introduced. As already mentioned, the kinetics of EPSCs in the sequence did not change suggesting that receptor desensitisation does not play a relevant role in these measurements. Moreover, in contrast to EPSPs recorded from neocortical interneurons (Thomson and Deuchars, 1994), in the present experiments self-facilitation at NMDA-receptor-mediated synapses did not give any contribution since EPSCs were recorded in voltage clamp conditions at -70 mV and in the presence of NMDA blockers. Finally, another possible postsynaptic mechanism that can contribute to different EPSC patterns is AMPA receptor saturation, (see also section 4.2). Recent studies in which single quanta at individual synapses have been studied by using loose-patch recordings have shown that AMPA receptors are not saturated at hippocampal synapses

(Forti et al., 1997). However AMPA receptor saturation has not been tested in the present experiments.

3.3.2 EPSC patterns generated by different parameters

While the synchronous release of neurotransmitter generated by a single action potential in a presynaptic terminal can be described by a simple probabilistic model based on the binomial distribution, release of neurotransmitter triggered by a train of action potentials is a much more complicated stochastic process. However, the discrete dynamic system represented in equation 3.6 can account for the mean EPSC amplitudes elicited by trains of spikes. In order to compare the experimental results with the predictions obtained by equation 3.6 in different conditions, EPSC amplitudes were normalised to the amplitude of the first one. In the case of one terminal, normalised EPSC amplitudes do not depend on the initial number of available vesicles N, while in the case of more than one terminal, the number of terminals and/or releasing sites N_h can be included in the coefficients of the weighted sum by replacing β_h with $\alpha_h=\beta_h \cdot N_h$. This type of analysis implies that: 1) The number of stimulated fibers is constant during the train (assuming that possible phenomena such as an increase in the number of stimulated fibres due to the local accumulation of extracellular potassium, that it is not possible to exclude, are negligible). 2) The quantal amplitude does not vary during the train (i.e. postsynaptic effects are negligible).

In order to reproduce different EPSC amplitude patterns, equation 3.6 has been applied to different conditions of release probability. In the simplest case of one synaptic terminal, FFF cases are generated by a low probability of release produced by calcium entry in the synaptic terminal while the other extreme cases of DDD are the result of a high probability of release. Figure 3.7 A shows three EPSC patterns calculated from equation 3.6 by using a single terminal with the probability function of equation 3.1, a summation of constant contributions to residual calcium and f(t) expressed by a single exponential function; these patterns resemble those shown in Figure 3.4 A and are obtained by varying only the relative calcium concentrations in the probability function.

Other cases can also be obtained with a high probability of release and a relatively fast reavailability time constant (i.e. a DDF case produced by $\Delta t/\tau = 0.25$, $p_{max} = 1$, $[Ca^{2+}] = 2 \cdot K^{-1}$, $\Delta[Ca^{2+}] = 1 \cdot K^{-1}$). However, the contribution of more than one releasing site and/or terminals to the EPSC (see Figure 3.2) or the statistical error deriving from a small number of recordings

may account for the cases in which a facilitation follows a depression. While the probability function prevails in determining the EPSC patterns elicited by the first four pulses, reavailability dynamics plays a fundamental role in shaping EPSCs occurring towards the end of a train of more than four pulses. Figure 3.7 B shows four EPSC patterns generated by equation 3.6 with 10 stimulation pulses in which a single exponential function with four different values for $\Delta t/\tau$ has been used.

The EPSC amplitudes always reach a stationary value which is equal to 0 in the absence of reavailability ($\Delta t/\tau = 0$) while it is proportional to $p_{max} \cdot N$ in the case of a full reavailability ($\Delta t/\tau \rightarrow \infty$). It is finally interesting to predict from the model possible EPSC patterns generated at different frequencies of stimulation; in this case both the consecutive contributions of residual calcium and the timing of reavailability change. Figure 3.7 C and 3.7 D show 100 EPSC patterns generated by simulating an increase in the interval between two presynaptic spikes from 50 ms to 500 ms in the case of a synapse with a low release probability and in the case of a synapse with a high release probability, respectively. These simulations are obtained by progressively reducing both $\Delta[Ca^{2+}]$ and Δt in equation 3.6.

3.3.3 Comparison between experiments and theory

As already shown in the previous paragraph, changes in the mean amplitude of EPSCs evoked by trains of stimuli were obtained by changing $[Ca^{2+}]_o$ or by activating mGluR2/mGluR3 in the case of mossy fibers. In terms of parameters of equation 3.6, an increase in $[Ca^{2+}]_o$ leads to an increase of both $[Ca^{2+}]$ and $\Delta[Ca^{2+}]$. In order to compare experimental data with those generated by the model, sets of parameters were chosen by using a semiautomatic procedure in order to reproduce experimental patterns in control conditions (2 mM $[Ca^{2+}]_o$). This procedure was based on the random generation of parameter sets within a given range until a good fit of the experimental patterns was obtained. Once the control condition was reproduced, the higher $[Ca^{2+}]_o$ condition was mimicked by changing $[Ca^{2+}]$ and $\Delta[Ca^{2+}]$ (Figure 3.8). A very good agreement was found between all the experimental data in which $[Ca^{2+}]_o$ was changed and those generated by the model. In the same way, in order to reproduce the EPSC pattern recorded in the presence of DCG-IV (and shown in Figure 3.6 A), the possible reduction in calcium entry following inhibition of voltage-dependent calcium channels by activation of mGluR2/mGluR3

(Takahashi et al., 1996) was simulated with a decrease of both $[Ca^{2+}]$ and $\Delta[Ca^{2+}]$ (Figure 3.9 A). Furthermore, in order to see how changes in the frequency of presynaptic spikes could affect EPSC patterns in our system, ten pulses at 10-20 Hz were delivered to afferent fibers.
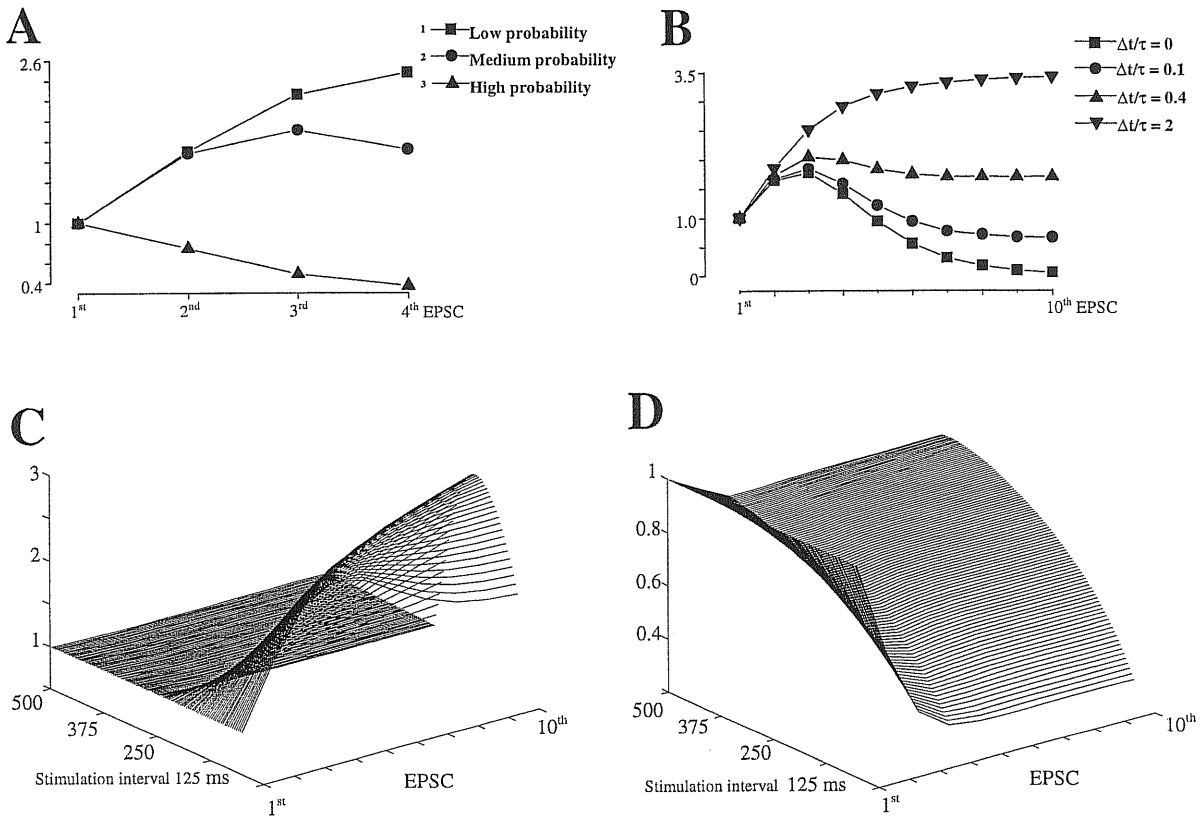
Figure 3.7 Different EPSC patterns calculated from equation 3.6. A and B. Ratios between the nth mean EPSC amplitude and the first one calculated from equation 3.6. In both cases a single negative exponential function with time constant τ was used as reavailability function and equation 3.1 with a summation of constant contributions to residual calcium was used as probability function. In A, only the probability function parameters were varied. The set of parameters was $\Delta t/\tau = 0.2$, $p_{max} = 0.5$, $[Ca^{2+}] = .66 \cdot K^{-1}$ (1), $.76 \cdot K^{-1}$ (2) and $1.45 \cdot K^{-1}$ (3), $\Delta[Ca^{2+}] = .14 \cdot K^{-1}$ (1), $.21 \cdot K^{-1}$ (2) and $0.4 \cdot K^{-1}$ (3). In B, only the reavailability exponential function was changed, while the other parameters were the ones used in A(2) (values of $\Delta t/\tau$ are indicated in the figure). 100 ratios between the nth mean EPSC amplitude and the first one calculated from equation 3.6 by simulating a progressive change in the interval between two presynaptic spikes from 50 ms to 500 ms. In C the set of parameters of A(1) was used to produce the values at 50 ms stimulation interval; the contribution to residual calcium was linearly reduced and reached zero at 300 ms. In D the set of parameters at 50 ms stimulation interval was $\Delta t/\tau = 0.2$, $p_{max} = 0.5$, $[Ca^{2+}] = 2 \cdot K^{-1}$, $\Delta[Ca^{2+}] = 0.4 \cdot K^{-1}$; the contribution to residual calcium was linearly reduced and reached zero at 500 ms. EPSC patterns represented in B, C and D are calculated for 10 pulses of stimulation.

In these experiments, EPSC patterns were reproduced by increasing $\Delta t/\tau$ and sometimes decreasing $\Delta(K \cdot [Ca^{2+}])$ at the lower stimulation frequency (Figure 3.9 B). In this case, f(t) was a weighted sum of a fast ($\tau \sim 50$ ms) and a slow ($\tau \sim 500$ ms) exponential function.
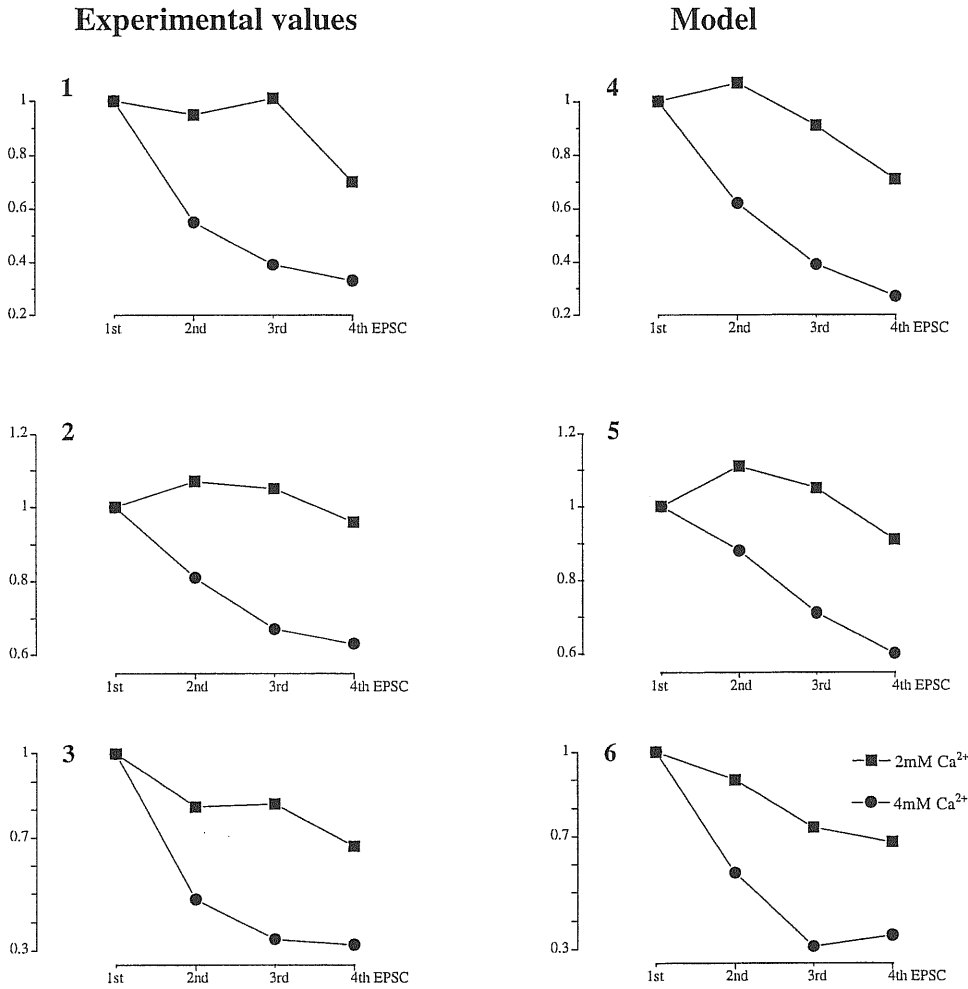
Figure 3.8 Comparison between experimental and computed data (different [Ca^{2+}]$_o$). Ratios between the nth mean EPSC amplitude and the first one obtained in some experiments (left column) in comparison to patterns calculated from equation 3.6 (right column). In these three experiments 2 mM and 4 mM. [Ca^{2+}]$_o$ were used. In patterns computed from the model only the parameters in the probability function (equation 3.1 with a summation of constant contributions to residual calcium) were changed in order to reproduce variations in [Ca^{2+}]$_o$. A single exponential function with $\Delta t/\tau = 0.1$ (4), 0.2 (5) and 0.5 (6) was used as reavailability function, while the other fixed parameter p_{max} was 0.45 (4), 0.32 (5) and 0.78 (6). [Ca^{2+}] was varied from $1 \cdot K^{-1}$ to $2 \cdot K^{-1}$ (4), from $1 \cdot K^{-1}$ to $1.4 \cdot K^{-1}$ (5) and from $1 \cdot K^{-1}$ to $2 \cdot K^{-1}$ (6), while $\Delta[Ca^{2+}]$ was varied from $0.2 \cdot K^{-1}$ to $0.25 \cdot K^{-1}$ (4), from $0.13 \cdot K^{-1}$ to $0.25 \cdot K^{-1}$ (5) and from $0.1 \cdot K^{-1}$ to $0.2 \cdot K^{-1}$ (6).

A
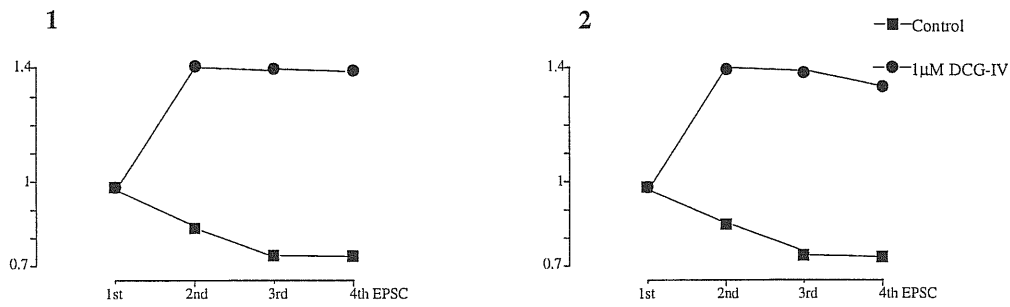
B
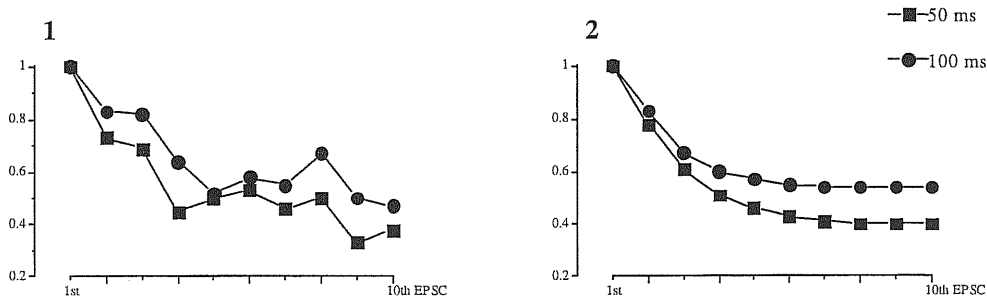
Figure 3.9 Comparison between experimental and computed data (activation of glutamate metabotropic receptors and different frequencies of stimulation). Ratios between the nth mean EPSC amplitude and the first one obtained in some experiments (left column) in comparison to patterns calculated from equation 3.6 (right column). In A, ratios obtained from data shown in Figure 3.6A were compared to those obtained with the model. The experimental condition in which $1\mu M$ DCG-IV was added to the external solution was simulated by decreasing both $[Ca^{2+}]$ and $\Delta[Ca^{2+}]$. The timing of the re-availability function was $\Delta t/\tau = 0.8$, while the other fixed parameter p_{max} was 0.3. $[Ca^{2+}]$ was varied from $3 \cdot K^{-1}$ to $1.05 \cdot K^{-1}$, while $\Delta[Ca^{2+}]$ was varied from $2 \cdot K^{-1}$ to $0.45 \cdot K^{-1}$. In B, ratios obtained from one experiment in which EPSCs were evoked by 10 pulses of stimulation at 50 ms and 100 ms stimulation interval were compared to those computed with equation 3.6. The reavailability function was $\beta_1 exp(\Delta t/\tau_1)+\beta_2 exp(\Delta t/\tau_2)$. Δt was changed from 50 ms to 100 ms in order to reproduce the modifications in the frequency of stimulation. The fixed parameters were $p_{max} = 0.35$, $[Ca^{2+}] = 2 \cdot K^{-1}$, $\Delta[Ca^{2+}] = 0.5 \cdot K^{-1}$, $\tau_1 = 500$ ms, τ_2 $= 50$ ms, $\beta_1 = 0.45$, $\beta_2 = 0.55$.

4 STATISTICAL ANALYSIS OF SYNAPTIC VARIABILITY AND SHORT-TERM PLASTICITY

In this chapter, a new approach to analyse and interpret synaptic responses is presented. This approach combines the statistical analysis of single synaptic responses to short trains of presynaptic action potentials, which extends the classical quantal analysis, with the analysis of the cumulative responses, containing the temporal correlation within the train. It is shown that the latter type of analysis allows to investigate how synapses can integrate synaptic signals in time.

4.1 The dynamic quantal approach to analyse synaptic responses

4.1.1 Statistical models and correlation detection

In the contest of the binomial quantal theory, each synapse is characterised by the release probability p, by the number of quanta available for release N, and by the quantal size (i.e. by the amount of synaptic response corresponding to a single quantum) q. In the most general hypothesis, each quantum of the synapse has distinct release probability and quantal size. This synapse will be then characterised by 2N+1 free parameters. The number of free parameters becomes independent on N and is reduced to 3 in the particular case of the simple binomial model in which p and q are uniform. By analysing sets of 100 EPSCs in CA3 pyramidal neurons with the statistical procedure of QA described in section 4.1.3, it has been found that the fit of experimental data with the simple binomial model was in general acceptable. Since with this procedure the quantal size q was directly calculated as the ratio between the mean EPSC and the mean number of released quanta in the model, the number of free parameters was also reduced to 2.

Assuming that the simple binomial model is sufficient to account for the variability of synaptic responses at the level of a single action potential, several hypothesis on the evolution of the quantal parameters during a train of presynaptic action potentials can be tested. Each model with particular sets of quantal parameters may in general produce similar series of distributions,

corresponding to the single action potentials in the train, that adequately fit experimental distributions. However, distinct hypothesis generate different dynamics of synaptic transmission leading to differences in the correlations within synaptic responses in the train. On this basis, correlation detection in synaptic responses to short trains of presynaptic action potentials, can discriminate among different binomial chains, i.e. among different hypothesis on the activity dependent changes of quantal parameters, although all of them are associated to similar distributions that fit experimental data. Thus, the dynamic quantal approach developed in this thesis work consists of two steps: 1) Fitting of the experimental data histograms (as described in section 4.1.3) to select the values of quantal parameters in the framework of a particular hypothesis. 2) Comparison between correlation in experimental data and those expected from each model (i.e. from each dynamic hypothesis on quantal parameters).

Different hypothesis have been divided in three groups corresponding to three levels of approximation. At the first level, the fitting was done with binomial chains in which changes in p and N are independent from previous synaptic events (model 0), corresponding to a classical quantal approach where experimental distributions are associated to simple, and *uncorrelated*, binomial distributions. At the second level (model 1), the parameter N depended on the number of quanta released previously, and thus evolved in a stochastic manner, whereas the parameter p evolved in a simple deterministic manner. Finally, at the third level (model 2), the fitting was done with binomial chains in which both N and p were stochastic variables, dependent on previous release. The latter two approaches are referred to as *dynamic quantal approaches*.

Each model is defined by the evolution of the release probabilities p_j and of the numbers of available quanta N_j at the jth action potential of the train. Previous studies have shown that the balance between the effect of residual calcium accumulation and the depletion of vesicles can account for the facilitating and depressing behaviours in the synaptic responses to a train of action potentials in CA3 hippocampal pyramidal neurons (Miles and Wong 1986). In keeping with this, the investigation was limited to binomial chains (models 1 and 2) in which the parameter N_j was changed by the phenomenon of depletion. Namely, at each action potential, N_j was decreased by the n_j released quanta and, before the next action potential, increased by the number of previously released quanta that were made *reavailable* for the $(j+1)^{th}$ release. Then, the number of quanta N_j available for release at the jth action potential of the train was N

decreased by the number of quanta $v_1,...,v_{j-1}$ that have been released after the previous j-1 action potentials and that were not yet *reavailable* for further release.

$$N_j = N - \sum_{k=1}^{j-1} v_k .$$ (4.1)

The simple deterministic approximation of the process of reavailability, which would in general be itself stochastic (Melkonian 1993; Quastel 1997), has been used here. In this approximation, the number of available quanta N_j was a time function of the previously released quanta

$$N_j = N - \sum_{k=1}^{j-1} v_k(t_j - t_k) .$$ (4.2)

$v_k(t)$ can be expressed as the integer number closer to the product $f(t) \cdot n_k$, where $f(t)$ is a time function such that $f(0)=1$ (no reavailability *immediately* after the release) and $f(t \rightarrow \infty)=0$ (complete reavailability *after a long time*). For synaptic release at a constant frequency of presynaptic firing $1/\Delta t$, the reavailability has been simulated with a negative exponential behaviour $f(t_j - t_{j-k}) = f(k \cdot \Delta t) = e^{-k \cdot \Delta t / \tau}$, where τ is the time constant of the deterministic approximation to reavailability.

At the level of model 1, the release probability varied with a purely deterministic evolution, and was defined by a set of release probabilities p_j at each spike j. In order to constrain the otherwise large number of parameters p_j, particularly when describing processes with several presynaptic action potentials, one may introduce simple rules that determine the probabilities p_j in terms of a minimal number of free parameters. A reasonable minimum is 3, since one parameter is needed for the initial p value, one for its change after the first action potential, and one for its asymptotic value after many action potentials. A simple 3-parameter rule, that was used as a crude model of the p_j series, is the equation 3.1. This equation allowed to reduce the number of free parameters to three (p_{max}, $[Ca^{2+}]$ and $\Delta[Ca^{2+}]$) when the number of action potentials was higher than 3.

At the level of model 2, the deterministic approximation for the evolution of the release probability must be replaced by a more general Markovian one in which also the change in the release probability depends on the previous release event. The simplest model that does not introduce further parameters and in which the application of the $\Delta[Ca^{2+}]$ change in equation 3.1

is made conditional on the immediately preceding event not having been a failure, i.e. on its having been a genuine release, has been used. Such a model is a simple and extreme implementation of the hypothesis that failures may not be just *normal* presynaptic events followed by release of zero quanta, but may include failures in the cascade of events underlying quanta exocytosis. A scheme of the three models is shown in Fig. 4.1.

The statistics of cumulative responses A_j after j spikes

$$A_j = \sum_{k=1}^{j} n_k .\qquad(4.3)$$

has been used to detect correlations within the train. The stochastic distribution of cumulative responses to a given train is affected by correlation, because negative correlations will tend to make the distribution narrower, while positive correlations, enhancing the probability of strings of consistently higher-than-average or lower-than-average responses, will tend to make it wider. Denoting with $P^*(A_j)$ the distribution that would be observed if successive events were uncorrelated, a useful method to capture these effects is to plot $P(A_j)-P^*(A_j)$, (in the cases reported in this article j=4), which is the probability of each value of the cumulative response after j spikes minus the mean probability of obtaining any given value of A_j after randomly reshuffling responses across trains. In this case, this was done by averaging over 500 *randomly reshuffled* cumulative responses and by choosing, as the bin for experimental data, the quantal current obtained by quantal analysis of the first distribution. The reshuffling is a standard bootstrap operation (Efron 1982) that combines the response to the first action potential from a train to that to the second spike from another train in a random way and so on. Reshuffling is also a convenient way to measure from the experiment $P^*(A_j)$, (the probability of cumulative responses if uncorrelated), since strictly uncorrelated responses are obviously not available. The comparison between $P(A_j)-P^*(A_j)$ obtained from experimental data and that expected from each model is the crucial point of the dynamic quantal approach that allows to discriminate among different models (hypotheses). At the level of the simplified hypotheses proposed in this thesis, the very different $P(A_j)-P^*(A_j)$ obtained with the three models permit a model discrimination by quantifying the discrepancy between the experimental and the theoretical $P(A_j)-P^*(A_j)$ curves (see section 4.1.2).
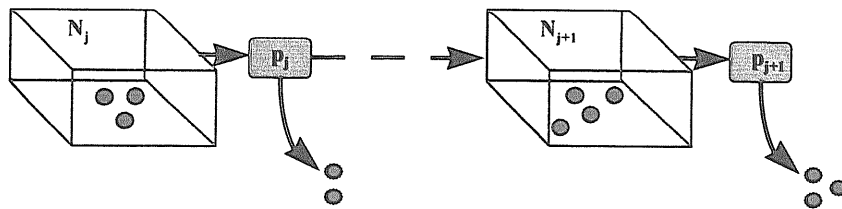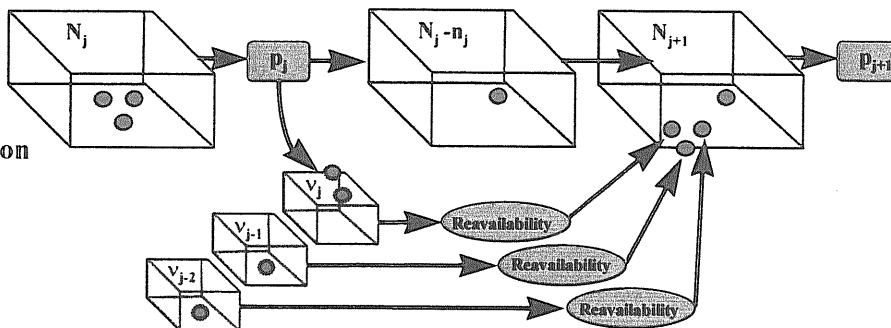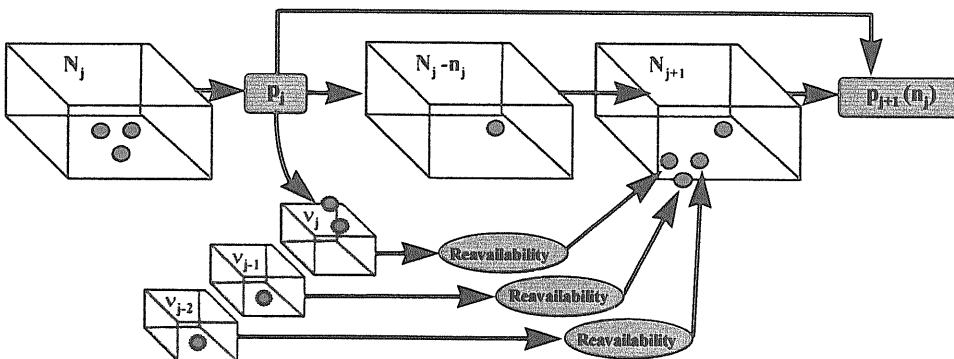
Figure 4.1 Example of stochastic chains representing possible scenarios of neurotransmitter release. Model 0: For successive presynaptic action potentials, the release probability p and the number of available quanta N change in an independent (non-correlated) manner. Therefore each release event correspond to an independent binomial distribution. Model 1: N is a stochastic variable changing in a manner which is dependent on the previous release events. At each interval between two pulses N is decreased by the released quanta and re-increased by the reavailable quanta. The number of released and not yet reavailable quanta is expressed by $v_k(t)$. This model is negatively correlated because the probability to have a high number of released quanta decreases following high previous release events. Model 2: p is also a stochastic variable that depends on previous release events and can introduce to the model a positive contribution to correlation. P_{j+i} is generally different from P_j in all the models.

4.1.2 Discrimination among different hypotheses on the basis of correlation

A set of experiments in which groups of 100 EPSCs were recorded in CA3 pyramidal neurons following trains of 4 action potentials have been analysed both with a classical and a dynamic quantal approach. In these experiments, EPSCs were stable and there was no evidence for a tendency to *run down* or *wind up*. For model 0, experimental distributions have been associated to simple binomial distributions with a different p and N for each action potential of the train. For models 1 and 2, the statistics of experimental data have been associated to that of stochastic processes in which p and N were varying on the basis of previous release events (binomial chains). In model 1, correlations among successive release events are entirely due to the variability in the number of released quanta and are negative, in the evident sense that higher release is more likely following a string of previous low release events, since a higher number of quanta is then available.

At this stage, the ability of three successive simple approximations to describe experimental data has been compared (model 0: independent binomial distributions, no correlation; model 1: stochastic release chain with predetermined changes in p, negative correlation; model 2: stochasticity also affecting changes in p, potential for positive correlation). Figure 4.2 shows six consecutive recordings with EPSCs evoked by four pulses of stimulation at 60 ms interspike interval. Figure 4.2 B shows the average of 100 recordings including those of A; short-term plasticity was dominated by facilitation.

Figure 4.2 C shows the histograms of EPSC amplitudes relative to the four action potentials (including the failures) (left column) and the distributions obtained by running 10,000 computer simulations for each of the three models with sets of parameters giving a good fit (always $P_j(\chi^2) > 10\%$ $\forall j$) of experimental distribution. The distributions obtained with the three models are very similar at the level of single spikes and all of them fitted experimental data. This is also true at the level of the time courses of the mean normalised to the mean of the first synaptic response (Figure 4.3 A(1)), of CV (Figure 4.3 A(2)) and of the percentage of failures (Figure 4.3 A(3)) relative to the experimental EPSCs and to the three models, as shown in Figure 4.2 A.

Turning now to correlations among successive spikes, many possible measures that are sensitive to correlation can be used. A particularly meaningful one is the cumulative response after j spikes (equation 4.3).
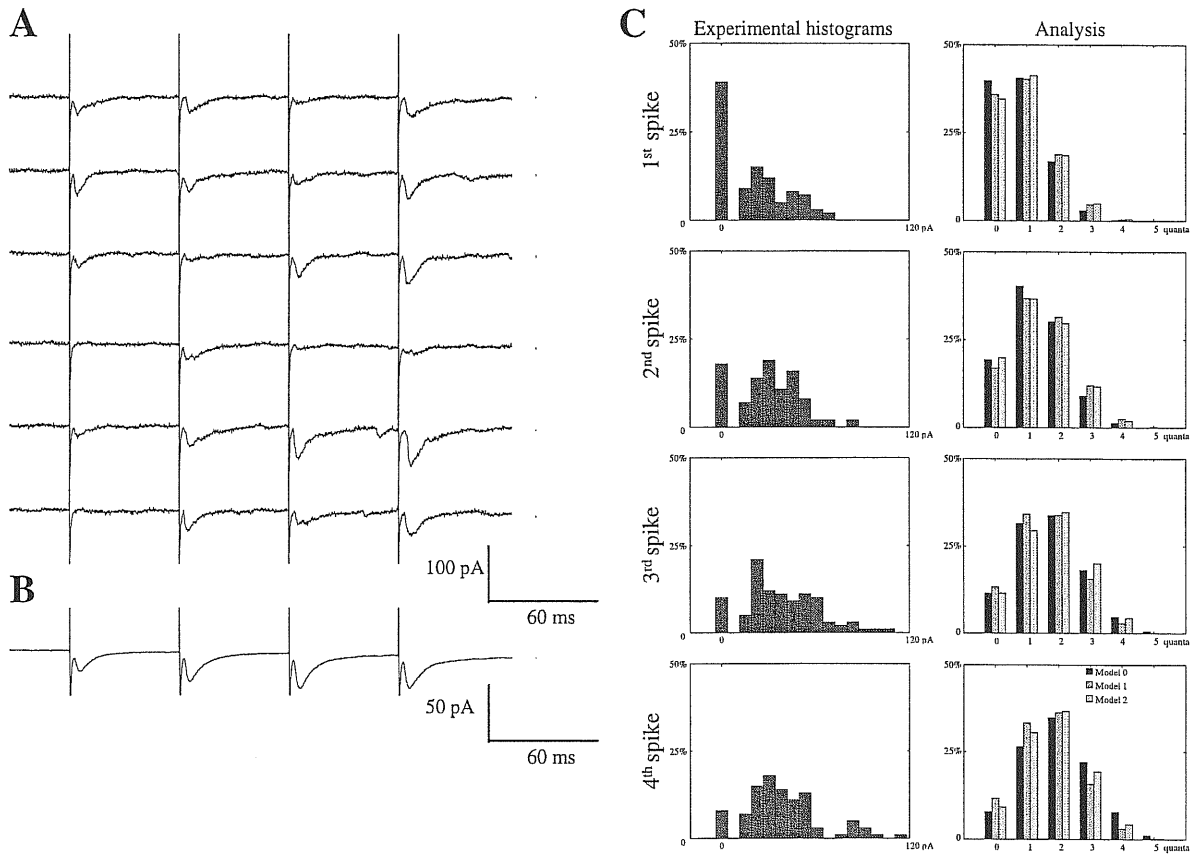
Figure 4.2 Analysis of EPSCs with the classical and the dynamic quantal approach. A. 10 recordings of EPSC from a CA3 pyramidal neuron elicited by a train of 4 pulses with 60 ms interspike interval. B. Average of 100 recordings including those shown in A. C. Left column. Histograms of the EPSC amplitude distributions relative to the four pulses. Right column. Corresponding distributions with sets of parameters giving a statistically significant fit of experimental data, obtained with single binomial models for the four synaptic events (no correlation), with a binomial chain with deterministic release probability evolution (negative correlation) and with a binomial chain with a Markovian release probability evolution (positive correlation). The distributions corresponding to each action potential are very similar.
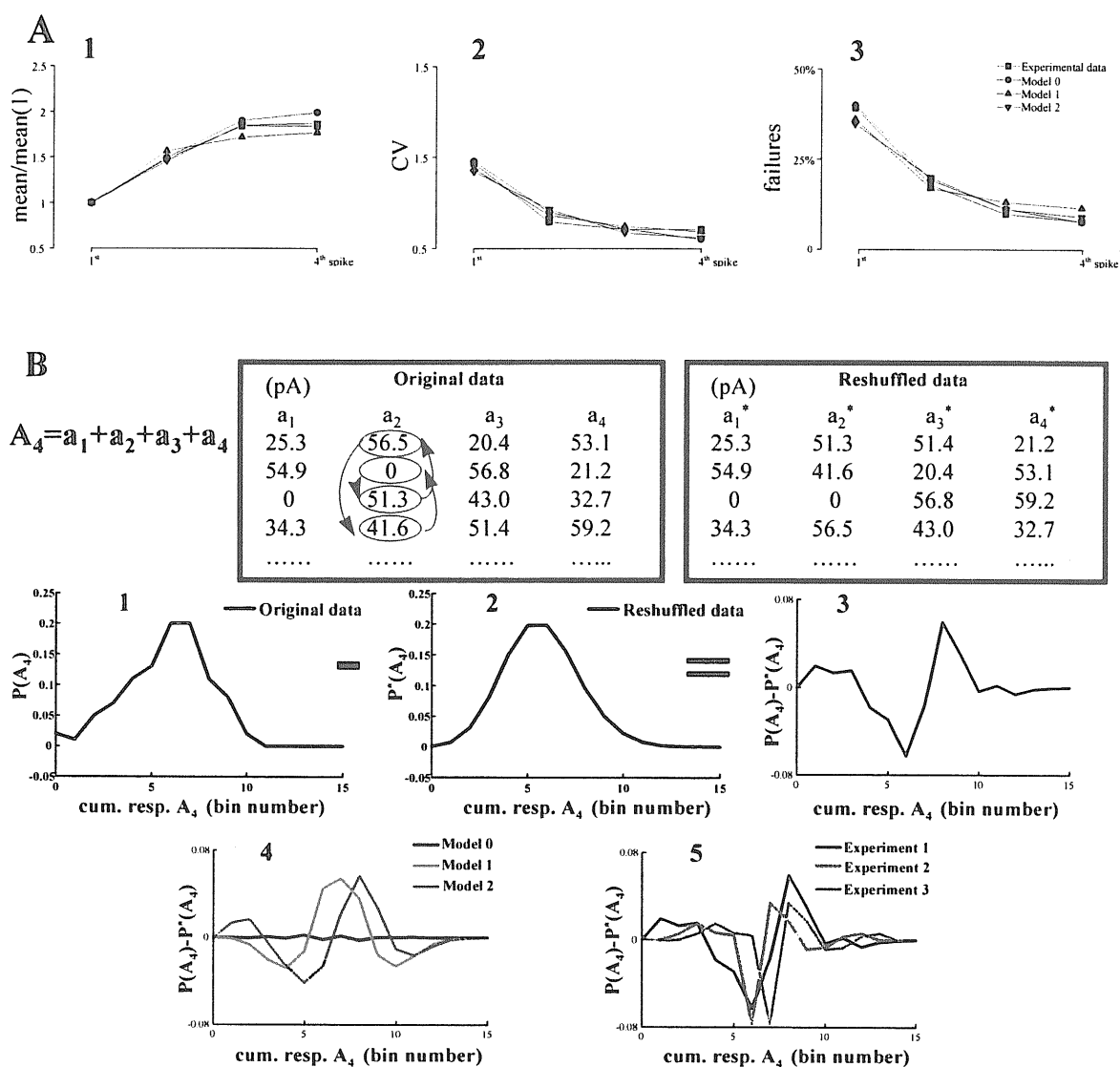
Figure 4.3 Comparison between the classical and the dynamic quantal approach. A. mean/mean(1st) (1), CV (2) and percentage of failures (3) of the experimental EPSCs and of the three models shown in Figure 4.2. B. Correlation distributions obtained by reshuffling data as described in the text and schematically shown in the upper part of B. 1. and 2. Cumulative response amplitude distributions for original data (1) and reshuffled data (1). 3. Difference between 1 and 2 (correlation distribution). 4. Same as (3) but for sets of 10,000 computer simulations obtained with the parameters of the three models of figure 2. 5. Same as (1) with data from two other experiments with a similar statistics of synaptic responses.

In the limit in which successive spikes in the train occur very close to each other, the cumulative (or integrated) response is the most relevant postsynaptic measure. The stochastic distribution of cumulative responses to a given train is affected by correlation, because negative correlations will tend to make the distribution narrower, while positive correlations, enhancing the probability of strings of consistently higher-than-average or lower-than-average responses, will tend to make it wider. A useful method to capture these effects is to plot $P(A_j)-P^*(A_j)$, (in this case j=4), which is the probability of each value of the cumulative response after j spikes minus the mean probability of obtaining any given value of A_j after randomly reshuffling responses across trains (see section 4.1.1). For uncorrelated chains, (model 0), the difference $P(A_j)-P^*(A_j)$ is close to zero at each bin used to measure A_4, (not precisely zero because of finite sampling effects). For model 1, the negative correlations generate a narrower distribution for A_4, which results in the expected central peak in the plot with two negative almost symmetrical flanks (Figure 4.3 B(4)). Positive correlations would result in a wider distribution and in a plot with an opposite shape. Model 2 embodies a mixture of positive and negative correlations; the result is a $P(A_4)-P^*(A_4)$ with an intermediate trend as shown in figure 4.3 B(2). This trend is the same of that of experimental data (Figure 4.3 B(3)). Figure 4.3 B(5) shows the difference $P(A_4)-P^*(A_4)$ in two other experiments with synaptic responses having a statistical behaviour similar to that of the experiment shown in Figure 4.2. Again, as A_4 increases, first a positive difference, then a large negative one, are followed by a large positive one as predicted by model 2. A more quantitative criterion to evaluate the discrepancy between the $P(A_4)-P^*(A_4)$ curves obtained from experimental data and that obtained with each model is to compute the integral of the absolute value of the difference of the two curves and to compare the result with the statistics obtained by running sets of computer simulations with the corresponding model parameters and with the number of simulations in each set equal to the number of experimental recordings. In this way, a model can be rejected on the basis of the value of the integral, i.e. whether and by how many SDs this value exceeds the mean of the distribution of the values obtained by running 100 sets of computer simulations. In the case of the experiment reported in figures 4.2 and 4.3, for model 0, model 1 and model 2 the statistics of the values obtained with the computer simulations were 0.20 ± 0.06, 0.18 ± 0.05 and 0.18 ± 0.06 and the values of the integral were 0.29, 0.37 and 0.16 respectively. Thus, in this case, it was possible to reject models 0 and 1 ($p<0.05$) but not model 2 ($p>0.5$). These results demonstrate that a dynamic quantal approach is

the necessary extension of the classical quantal approach, in order to analyse synaptic responses evoked by trains of presynaptic action potentials, also in term of correlations.

4.1.3 Dynamic quantal analysis of synaptic responses

A *Dynamic Quantal Analysis* (DQA) framework, based on the exact calculation of the release probabilities, has been developed. At the first action potential, the probability $p_1(n)$ that n out of N quanta are released is given by equation 2.1. At the second action potential, the release probabilities $p_2(n)$, n=1,...,N are determined by

$$p_2(n) = \sum_{N_2=0}^{N} p(n/N_2) \cdot P_2(N_2) \qquad (4.4)$$

where $p(n/N_2)$ is the probability that n out of N_2 are released according to the rule for the evolution of p, and the probability $P_2(N_2)$ that N_2 are available at the second action potential is given by

$$P_2(N_2) = \sum_{n_S} p_1(n_S) \qquad \left\{ n_S: N - int(f(\Delta t) \cdot n_S) = N_2 \right\} \qquad (4.5)$$

where N is the initial number of available quanta and n_S are all the possible numbers of released quanta at the first action potential such that the resulting number of available quanta at the second action potential is N_2. At the jth spike, the probability $P_j(N_j)$ that N_j quanta are available is obtained by summing over all possible combinations $C = \{n_1, n_2,..., n_{j-1}\}$ that lead to N_j available quanta. In practice, it is sufficient to iterate

$$P_j(N_j) = \sum_{n_{j-1}} p_{j-1}(n_{j-1}) \qquad (4.6)$$

since $p_{j-1}(n_{j-1})$ is itself determined by the recursive equation

$$p_j(n) = \sum_{N_j=0}^{N} p(n/N_j) \cdot P_j(N_j). \qquad (4.7)$$

It must be said that the evaluation of the j terms $P_j(N_j)$ implies the calculation of $(N+1)^{j-1}$ terms for the summation over all combinations. This means that the calculation of the release probabilities at the 10th action potential for a synapse with 5 initial available quanta requires the computation of $6^9 \sim 10^7$ products. Therefore, when the number of spikes in the train and/or the

number of available quanta is relatively high, the estimation of the release probabilities by using computer simulations becomes convenient.

The evaluation of the agreement between the experimental and the theoretical distributions has been given in terms of the mean probability $P(\chi^2)$. The significance of the agreement between the distributions of EPSCs with those predicted by a model can be evaluated by using the quantity

$$\chi^2 = \sum_{j=1}^{Q} \sum_{n=0}^{N} \frac{\left(\left|\Phi_j^{exp}(n) - \Phi_j^{model}(n)\right| - 1/2\right)^2}{\Phi_j^{model}(n)} . \tag{4.8}$$

Q is the number of spikes in the train and N is the number of available quanta in the binomial chain. $\Phi_j^{model}(n)$ is the predicted number of events with n released quanta calculated as the probability $p_j(n)$ to have n released quanta at the jth action potential times the number of experimental recordings. In the case of binomial chains (models 1 and 2), the first mean number of released quanta $<n_1>$ and the first mean EPSC amplitude $<A_1>$ are used to normalise the two distributions and to calculate the observed frequency of events $\Phi_j^{exp}(n)$, while in the case of simple binomial distributions (model 0) each distribution is normalised separately by using the ratio $<A>/<n>$. Namely the ratio $<A>/<n>$ ($<A_1>/<n_1>$ for binomial chains) is utilised as a bin for the experimental distribution to evaluate $\Phi_j^{exp}(n)$.

$$\Phi_j^{exp}(n) = \begin{cases} \text{number of failures} & \text{for } n = 0 \\[2mm] \text{number of events} > 0 \text{ and } < 1.5 \cdot \dfrac{<A>}{<n>} & \text{for } n = 1 \\[2mm] \text{number of events} > (n-0.5) \cdot \dfrac{<A>}{<n>} \quad \text{and} < (n+0.5) \cdot \dfrac{<A>}{<n>} & \text{for } 1 < n < N \\[2mm] \text{number of events} > (N-0.5) \cdot \dfrac{<A>}{<n>} & \text{for } n = N \end{cases} \tag{4.9}$$

Finally the term 1/2 in equation 4.8 is the Yates correction to take into account the fact that $\Phi_j^{exp}(n)$ takes only integer values, and bins with $\Phi_j^{model}(n) < 1$ have been grouped together.

An alternative way to minimise the discrepancy between the statistics of experimental data and

the binomial chain is to use the maximum likelihood L (Kendall et al., 1979) instead of χ^2 which, in the case of a single distribution has advantages in that it allows to determine confidence limits and significance of the model used (Stricker et al., 1994). For *nested* models, which means that one model is a sub-hypothesis of the other, the method based on the maximum likelihood provides a more useful test for rejecting an alternative model than does the χ^2 goodness-of-fit. However, since the significance of statistical models is evaluated for groups of distributions and at the level of single distribution the different chains cannot be considered nested models, the method based on L appears to have no advantages with respect to that based of χ^2.

The significance of a model for each distribution j is given by the probability of χ^2

$$P_j(\chi^2) = 1 - \Gamma_{inc}(\chi^2, \mu - \eta + 1) \qquad (4.10)$$

where Γ_{inc} is the incomplete gamma function, μ is the number of utilised bins and η is the number of free parameters, which is 2 in the case of model 0 and is effectively 5/Q in the case of models 1 and 2. Finally the mean probability of χ^2 is calculated as

$$P(\chi^2) = e^{\sum_j (\log(P_j(\chi^2))) / Q} \qquad . \qquad (4.11)$$

The $P(\chi^2)$ has no direct statistical meaning because the distributions for each j are not independent, but is still useful to quantify the significance of a model for the whole train. For a model to be in agreement with experimental data, the individual $P_j(\chi^2)$ should be higher than a preset criterion, say 10%.

To perform a DQA of synaptic responses (i.e. to automatically find the best binomial chain that accounts for the variability of EPSCs), the following algorithm has been used. The maximisation of $P(\chi^2)$ in the space of the parameters $[Ca^{2+}]$, $\Delta[Ca^{2+}]$, p_{max} and τ at fixed N is performed through a Montecarlo Metropolis algorithm (Metropolis et al., 1953) in which $P(\chi^2)$ is considered the *energy of the system*. Briefly, the algorithm consists in an iteration in which each parameter is alternatively changed by a random value (dependent on $P(\chi^2)$) and

the new set of parameters is always accepted if the new value of $P(\chi^2)$ is bigger than the older one or accepted with a probability $e^{-\beta \cdot P(\chi^2)}$ otherwise. β is a parameter (representing the *inverse temperature of the system*) to be chosen at the beginning of each iteration. The iteration is stopped when $P(\chi^2)$ fails to increase further over many ($\sim$100) parameter changes. With 4 parameters, the use of a simple Montecarlo algorithm was found to be more efficient than direct minimisation programs such as AMOEBA (Press et al., 1989), to search for a maximum of $P(\chi^2)$. The best value of N is chosen by direct comparison of the minima found with different values of N.

The DQA has been applied to analyse EPSCs recorded in CA3 and elicited by stimulation of synaptic fibers in the Stratum Lucidum-Radiatum with trains of 3-6 pulses at 12.5-25 Hz (see chapter 3). These synaptic responses are characterised by high unreliability within single recordings and by the presence of failures (Allen and Stevens, 1994). Furthermore, very different facilitating or depressing behaviours (EPSC patterns) of mean EPSCs (n≥30) can be observed by stimulating different synaptic fibers or even the same fiber at different $[Ca]_o$. For all data analysed, the correlations were detected as described in section 4.1.2 and, on this basis, in most of the experiments, models 0 and 1 led to lower p values than model 2. In particular, in 14 out of 18 experiments in which 100 (stable) responses have been analysed, $P(\chi^2)$ was never below 0.1 for any of the three models. In all these 14 cases, models 0 and 1 led to higher discrepancy in the $P(A_4)-P^*(A_4)$ function. However, models 0 and 1 could be rejected with p<0.1 only in 7 cases for model 0 and in 4 cases for model 1.

- *Facilitating behaviours.* Most EPSC patterns observed in the presence of 2 mM $[Ca]_o$ are distinguished by the facilitation of the second mean EPSC and, in about 10% of the cases, also by the facilitation of third and fourth mean EPSC when stimulated with 4 pulses at 20 Hz. Figure 4.4 A shows ten representative recordings of EPSCs elicited by the stimulation of a presynaptic fiber characterised by the facilitation of the second, third and fourth mean EPSCs (Figure 4.4 B). These recordings are dominated by a large number of failures and by a high variability (unreliability). As shown in Figure 4.4 C, the time courses of the CV and of the percentage of failures obtained by analysing 100 recordings (including those shown in Figure 4.4 A) indicate a typical behaviour of facilitation due to an increasing release

probability. The difference $P(A_j)-P^*(A_j)$ relative to synaptic responses was also well fitted by model 2.

- *Depressing behaviours.* About 25% at 2 mM $[Ca]_o$ and more than 80% at 4 mM $[Ca]_o$ of the EPSC patterns in CA3 pyramidal neurons are dominated by the depression of the second, third and fourth mean EPSC when stimulated with 4 pulse at 20 Hz. Figure 4.5 A shows ten representative recordings of EPSC elicited by the stimulation of a synaptic fiber characterised by a depressing behaviour (Figure 4.5 B).

As shown in Figure 4.5 C, the time courses of the CV and the percentage of failures obtained by analysing 100 recordings (including those shown in Figure 4.5 A) are very different from those obtained in the cases of facilitating behaviour.

The correlation quantified by the difference $P(A_j)-P^*(A_j)$ relative to synaptic responses was slightly negative, in this case, as predicted by model 2.

The DQA also allows to estimate the quantal current (18±15 pA, n=14). Variations in the quantal current observed in different experiments can reflect the type of synaptic input stimulated. In fact, synaptic responses corresponding to a single quantum from mossy fibers are generally larger in amplitude then those from associative commisural fibers (Henze et. al., 1997).

4.1.4 Dynamic quantal analysis of EPSPs in double recordings from the neocortex

The dynamic approach has been also used to analyse EPSPs in double recordings from interconnected neocortical pyramidal neurons. These data have been provided by Henry Markram from the Weizmann Institute, Israel. EPSPs were recorded from neocortical pyramidal neurons (layer 5) in 300 μm sagittal slices at 30-32 °C. Presynaptic action potentials were elicited by current injection (pulses of 2nA amplitude and 5 ms duration) in neurons of the same type. The interval between two consecutive trains was 20 s in order to guarantee the complete restoring of initial conditions (Markram and Tsodyks, 1996). EPSPs evoked by trains of 16 action potentials at 20 Hz in this preparation show always a strong depression of synaptic responses.

With respect to hippocampal recordings, obtained with the extracellular stimulation technique described in the previous chapter, double recordings allow to monitor the occurrence of presynaptic spikes, although the invasion of action potentials into the terminal cannot still be

tested. As shown in Figure 4.6, synaptic responses are generally less variable with respect to the case of the hippocampus and failures can be seldom observed.
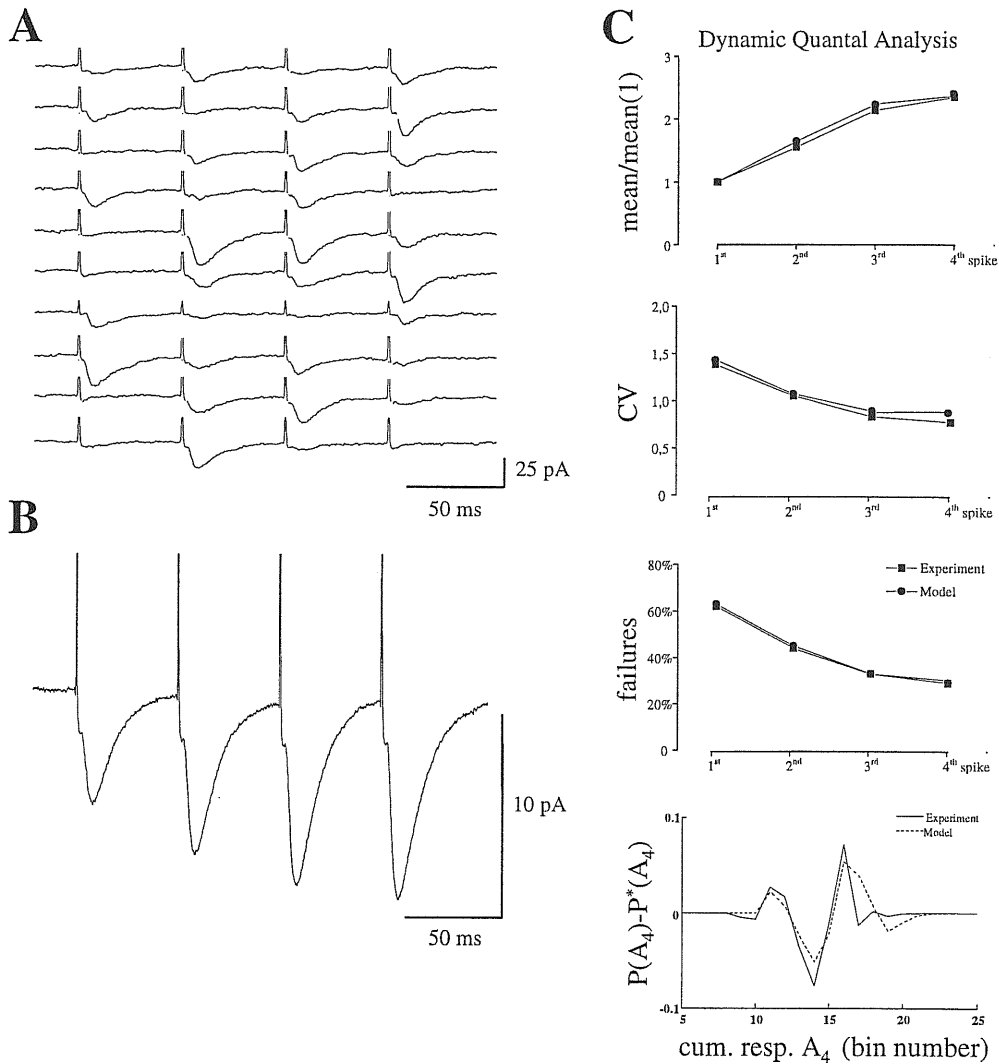
Figure 4.4 Dynamic Quantal Analysis (DQA) of synaptic responses: facilitating behaviour. A. 10 typical recordings of EPSC from a CA3 pyramidal neuron elicited by stimulation of a synaptic fiber with a facilitating behaviour. B. Average of 100 recordings including those shown in A. C. Comparison of the statistics (mean/mean(1st), CV, percentage of failures, difference between the distribution of the total cumulative current and that obtained by reshuffling data as described in the text.) of the 100 synaptic responses used for the average shown in B with that obtained by maximising the mean probability $P(\chi^2)$.
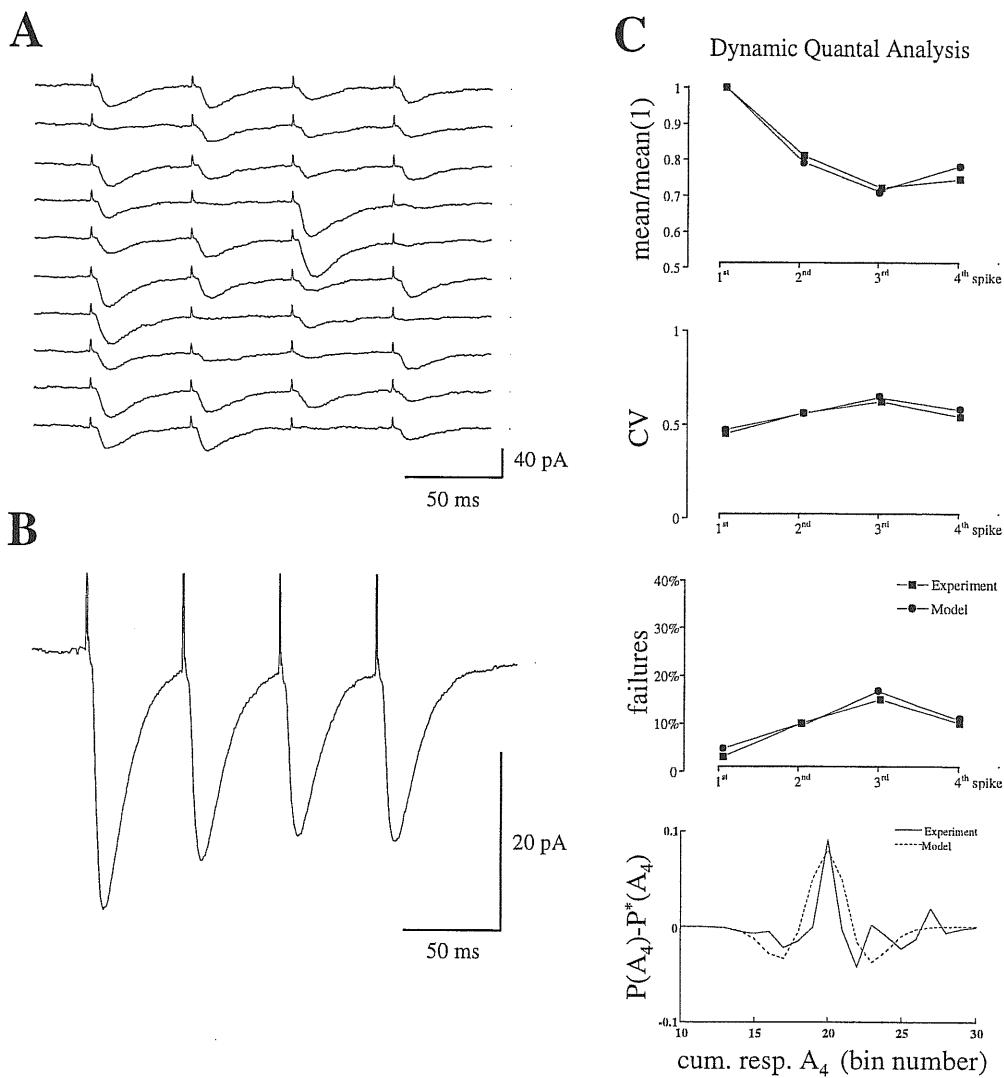
Figure 4.5 Dynamic Quantal Analysis (DQA) of synaptic responses: depressing behaviour. A. 10 typical recordings of EPSC from a CA3 pyramidal neuron elicited by stimulating a synaptic fiber with a depressing behaviour. B. Average of 100 recordings including those shown in A. C. Comparison of the statistics (mean/mean(1st), CV, percentage of failures, difference between the distribution of the total cumulative current and that obtained by reshuffling data as described in the text) of the 100 synaptic responses used for the average shown in B with that obtained by maximising the mean probability $P(\chi^2)$.

A dynamic analysis of the EPSPs showed a high number of total available quanta N (N=35 in the case of data of Figure 4.6) and a longer time constant for reavailability (τ=500 ms).

As in the case of the hippocampus, changes in the $[Ca^{2+}]_o$ could modify the release probability and therefore the short term plasticity. Particularly a decrease in the $[Ca^{2+}]_o$ from 2 mM to 1.5 mM reduced the initial release probability p and, as a consequence, the strength of synaptic depression. This phenomenon could be very well described by a dynamical quantal analysis although the lower variability of synaptic responses did not allow to extract a significant correlation quantified by the difference $P(A_j)-P^*(A_j)$.

4.1.5 Dynamic quantal analysis of GABAergic evoked currents in CA3 pyramidal neurons

The dynamic approach has been finally used to analyse GABAergic synaptic responses in CA3 pyramidal neurons in the hippocampus. These types of synaptic signals are hyperpolarising in the adult brain and depolarising in the developing hippocampus (Cherubini et al., 1991). This is ultimately due to the flux direction of Cl⁻ which is inward in the adult hippocampus and outward in the developing hippocampus. Several types of GABAergic interneurons are present in the hippocampus (Freund and Buzsaki, 1996) and GABAergic responses with different characteristics can be observed by recording postsynaptic responses from DG granule cells (Edwards et al., 1990), from CA3 pyramidal neurons (Miles and Wong, 1983; Lambert and Wilson, 1993) and from CA1 pyramidal neurons (Pierce, 1993). In CA1 pyramidal neurons, synaptic responses to stimulation of the stratum lacunosum-moleculare are slow (mediated by $GABA_{A,slow}$ receptors) with decay time constants of the order of hundreds milliseconds, whereas synaptic responses to stimulation of stratum pyramidale or of stratum radiatum are fast (mediated by $GABA_{A,fast}$ receptors) with time constants of the order of tens of milliseconds (Pierce, 1993). In comparison to glutamatergic synaptic responses, large GABAergic synaptic responses with no failures can be observed in CA3 pyramidal neurons either with a minimal stimulation protocol (Lambert and Wilson, 1993) or by evoking action potentials in impaled presynaptic interneurons (Miles, 1990). The detailed analysis of TTX-resistant miniature synaptic responses and minimally evoked synaptic responses performed by Lambert and Wilson (1993) suggests that the low variability of synaptic responses is due to the relatively high number (tens) of released quanta following a presynaptic action potential.

A

2 mM Ca²⁺

1.5 mM Ca²⁺

2 mV

200 ms

2 mV

200 ms

Averages

2 mV

200 ms

2 mV

200 ms

B

1

0.5

0

1st 16st EPSP

C

—■—2mM calcium simulation
—●—2mM calcium experimental
—▲—1.5mM calcium simulation
—▼—1.5mM calcium experimental

1

0.5

0

1st 16th EPSP
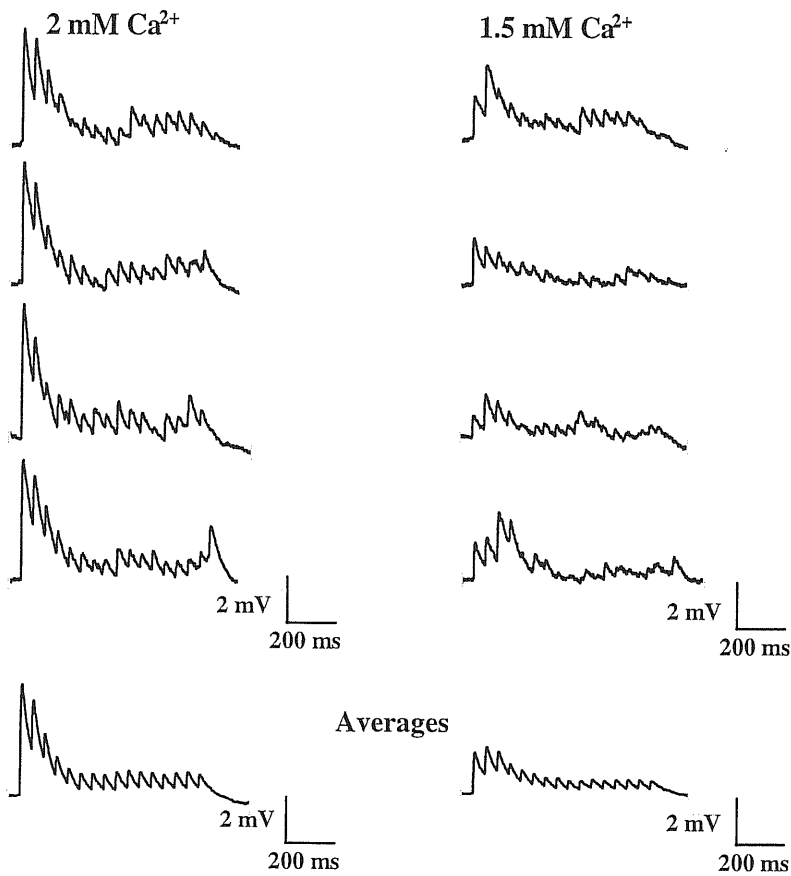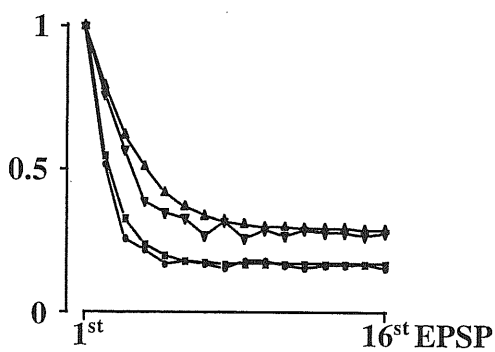
Figure 4.6 Dynamic Quantal Analysis (DQA) of EPSPs in neocortical pyramidal neurons. A. 4 typical recordings of EPSPs elicited by trains of 16 action potentials in a presynaptic pyramidal neuron and the average of 50 recordings at 2 mM and 1.5 mM $[Ca^{2+}]_o$. B and C. Comparison of the mean/mean(1st) (B) and of the CV (C) of the EPSPs of A with that obtained by maximising the mean probability $P(\chi^2)$.

In CA1 pyramidal neurons, synaptic responses evoked by low frequency stimulation (5-25 Hz) of presynaptic afferent fibers typically show a depressing behaviour, which is frequency dependent (Pierce et al., 1995). At 20-25 Hz, there is evidence that this depression which has a postsynaptic component due to the lack of recovery from desensitisation at the highest frequency. In the case of slow GABAergic responses, depression is strongly presynaptically mediated by the activation of $GABA_B$ receptors at the lowest frequencies (5-10 Hz)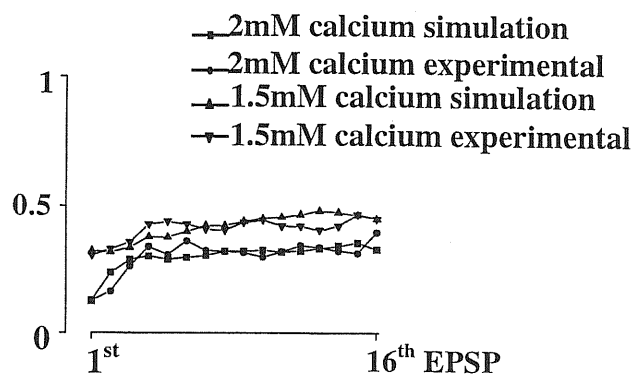, since it is enhanced by the $GABA_B$ receptor agonist baclofen and reduced by the $GABA_B$ receptor antagonist CGP35348.

In the present work, synaptic currents in CA3 pyramidal neurons evoked by the stimulation of the stratum radiatum with trains of 6 pulses at 160 ms interpulse interval were analysed. Experiments were performed in slices taken from P3-P5 rats, by using an intracellular solution containing (in mM) 140 KCl, 1 $MgCl_2$, 5 HEPES, 1 EGTA, 10 Sucrose, 2 Na_2ATP adjusted to pH 7.2 with KOH. The high intracellular chloride concentration used could amplify the synaptic currents acquired at -70 mV holding potential by increasing the driving force for Cl^-. Recordings were done in the presence of 1 mM kynurenic acid in order to block ionotropic glutamatergic synaptic activity. 10 nM tetrodotoxin (TTX) was also routinely added to the external solution in order to reduce spontaneous activity. This set of experiments was done in order to investigate the role of the temperature in the recovery of synaptic responses from depression, a problem which is related to the transitions in the network activity caused by changes in the temperature that can be observed in hippocampal slices at this age (see the appendix).

GABAergic currents were highly reliable (Figure 4.7 A), but reliability decreases within the train (Figure 4.7 B). A DQA of these currents showed a quite high number of total available quanta N (N=30 in the case of data of Figure 4.7) and time constants for reavailability ranging between 150 and 300 ms (228 ms in the case of data of Figure 4.7 at 24 ^{o}C). The increase in CV corresponded to the decrease of the mean suggesting that this type of depression was at least partially mediated by presynaptic mechanisms (see next paragraph). Furthermore, the relatively high EGTA concentration present in the pipette should guarantee a fast recovery from receptor desensitisation (Mozrzymas and Cherubini, 1998). As in the case of glutamatergic synapses, synaptic depletion is a strong candidate for mediating low-frequency synaptic depression.

The increase in temperature always produced an increase in the mean stationary value of synaptic responses after 3-4 synaptic events, that, in terms of DQA, could be explained by a

decrease of the time constant for reavailability (177 ms in the case of data of Figure 4.7 at 32 °C). This result suggests that the highest efficiency of GABAergic synapses that is observed at physiological temperature (see the appendix) is at least partially due to the highest speed of the neurotransmitter release machinery.
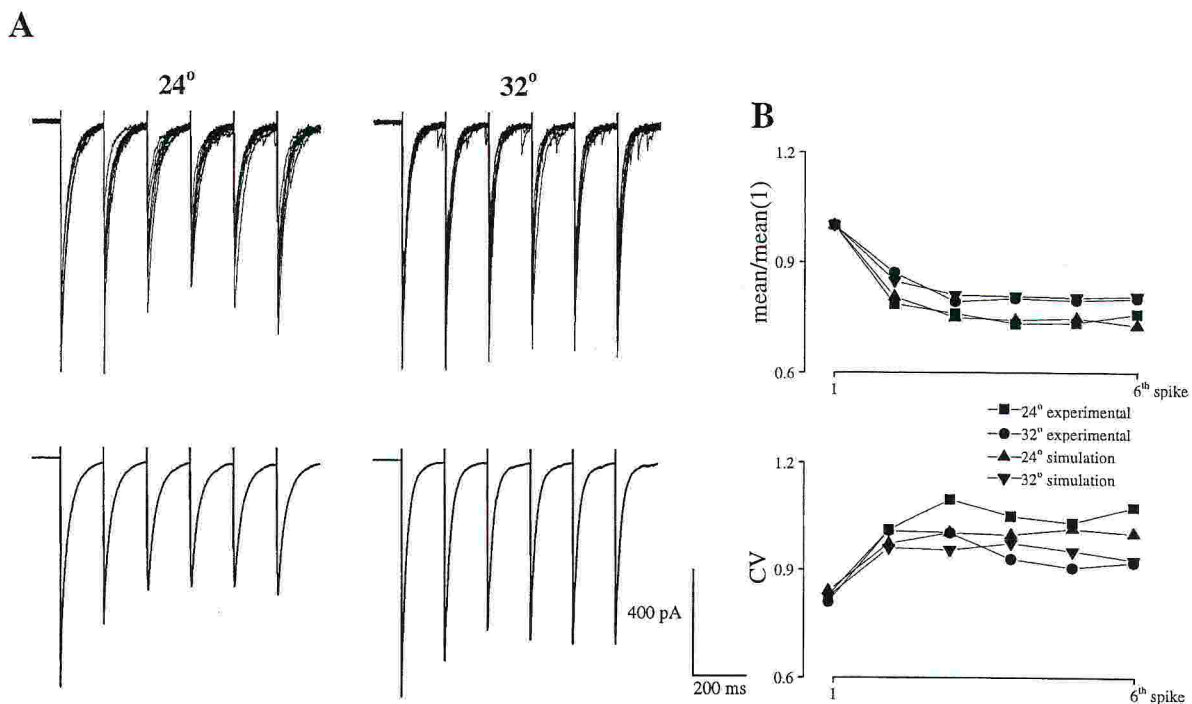
Figure 4.7 Dynamic Quantal Analysis (DQA) of GABAergic currents evoked by short trains of stimulating pulses at 160 ms interpulse interval. A. Top. 10 consecutive recordings of currents evoked by 6 pulses of stimulation at 160 ms interpulse interval at 24 °C (left) and at 32 °C (right). Bottom. Averages of 50 recordings at the two different temperatures including those shown on the top. B. Top and bottom. Comparison between time course of the mean current amplitudes normalised to the first ones (top) and of the amplitude CVs (bottom) relative to the experiment reported in A and the ones obtained by performing a DQA of these data.

4.2 Analysis of the statistics of binomial chains

4.2.1 Statistics of presynaptic release

In all the models described in the previous paragraph, short term plasticity is presynaptic, in that it is due to changes in the parameters of quantal release. In order to investigate whether presynaptic plasticity has a characteristic statistical signature, distinct from that of postsynaptic plasticity, the statistics of binomial chains has been investigated by running computer simulations of the stochastic process. More precisely, a presynaptic short-term plasticity can be always related to changes in the release probability or in the number of available quanta, while postsynaptic short-term plasticity, that can be due to phenomena such as receptor desensitisation, is generally related to changes in the relationship between released quanta and postsynaptic responses, i.e. to changes in the quantal size.

The exact calculation of the probabilities $p_j(n)$ at each action potential is convenient only in the case of short trains with relatively few available quanta. Therefore computer simulations can be used to analyse situations with more available quanta and longer trains.

Sets of 10,000 computer simulations of model 2, each with different parameters, have been run in order to explore distinct statistics of release. Figure 4.8 (first column) shows the time course of the mean number of released quanta normalised to the initial number of available quanta N obtained by running computer simulations (n=10,000) with the different sets of parameters reported in Table 1.

In the four graphs shown in Figure 4.8 A(1) (Table 1 a, b, c, and d), the release probability can increase from 0.1, 0.2, 0.3 and 0.4 to about 0.5 within 10 spikes (N=5 and τ=0.5).

Simulation results can be classified in terms of increase or decrease (facilitation or depression) of the mean number of released quanta during the train. Facilitation characterises stochastic chains with a low initial release probability that increases during the train. In contrast, in stochastic chains in which the initial release probability is high, close to a saturating value (p_{max} in equation 3.1), or decreasing, the time course of the mean number of released quanta is dominated by depression. The balance between facilitation and depression determines, after a few action potentials, an almost stationary condition of release which is strongly dependent on the speed of reavailability as shown in data reported in Figure 4.8 B(1) (parameter sets reported in Table 1 b, e, f, and g). The time course of the mean number of released quanta can reach a

minimum and then increases to the stationary value in the case of relatively slow reavailability, corresponding to fast presynaptic firing.

TABLE 1   Parameter sets used for computer simulations

	$[Ca^{2+}]$	$\Delta[Ca^{2+}]$	N	$\Delta t/\tau$
a	0.715	0.25	5	0.5
b	0.905	0.31	5	0.5
c	1.105	0.35	5	0.5
d	1.415	0.45	5	0.5
e	0.905	0.31	5	0.1
f	0.905	0.31	5	0.25
g	0.905	0.31	5	1
h	0.905	0.31	10	0.5
i	0.905	0.31	20	0.5
l	0.905	0.31	40	0.5

$$p_{max} = 0.5$$

Table 1. Each row (a-l) represents a set of parameters used for computer simulations of stochastic chains as described in the text.

Finally graphs of figure C are relative to stochastic processes with different numbers of available quanta. While small numbers of available (and released) quanta (N<10) characterise synaptic transmission in the hippocampus (Murthy et al., 1997), the typical example of large numbers of quanta available for release (N>100) is the neuromuscular junction (Fesce, 1990). Particular behaviours of the CV (Figure 4.8 second column) can be associated to different stochastic chains. Since the CV is reduced by a larger release probability and augmented by a reduction in the number of available quanta, facilitating and depressing synapses are typically associated to decreasing and increasing trends of the CV, respectively (Figure 4.8 A(2)). Interestingly, the behaviour of the percentage of *failures* or events with release of zero quanta (Figure 4 third column) reflects that of the CV. This is ultimately due to the fact, evident from equations 2.3 and 2.4, but true also for their more complicated extensions, that both CV and failures are monotonically decreasing functions of $<p_j \cdot N_j> = <n_j>$, with only milder

dependence on p_j and N_j alone. In particular, the percentage of failures is purely given by the release process although the statistics of postsynaptic responses can be modulated by possible postsynaptic mechanisms. Thus, the analysis of the percentage of failures that has been used as an indirect method of QA (see the Introduction), can be extended in the context of a more general DQA framework.
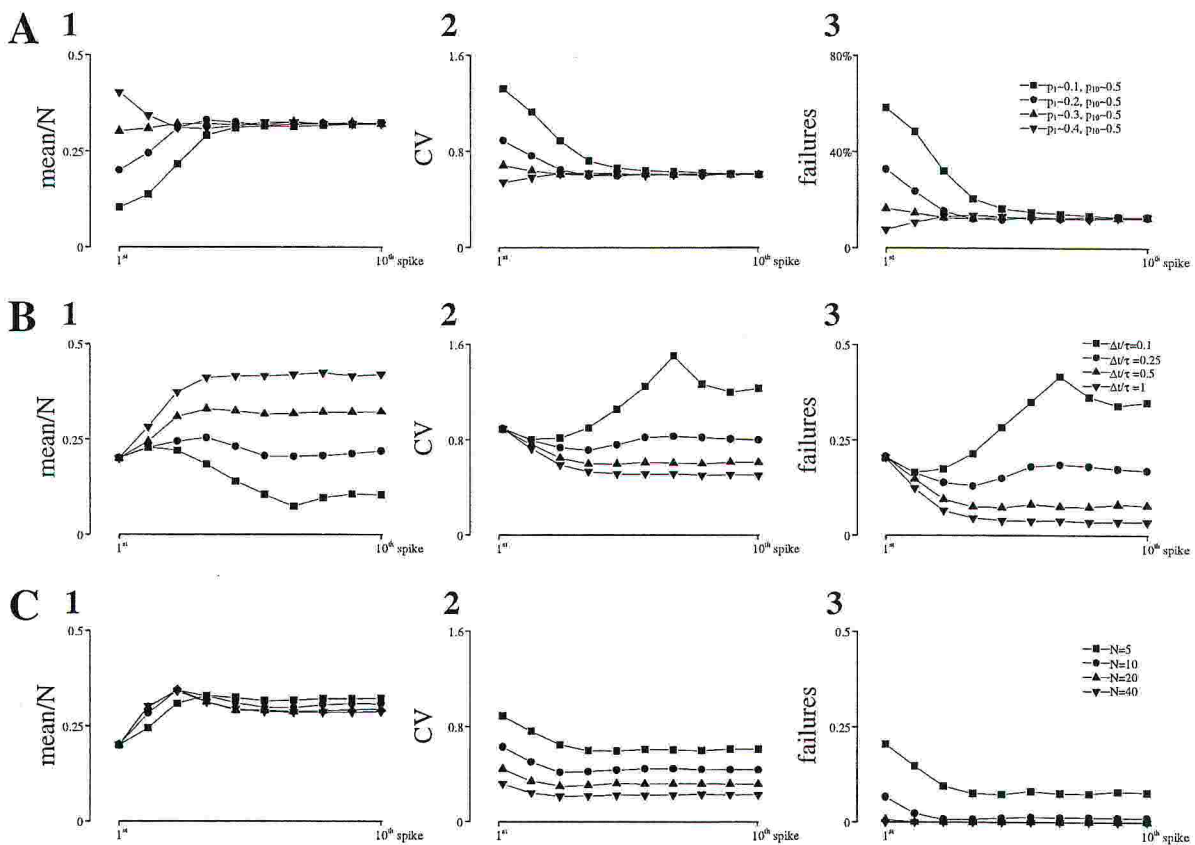
Figure 4.8 Mean, CV and percentage of failures in positively correlated stochastic chains with different sets of parameters. A. Time courses of the mean normalised to the number of available quanta (1), of the CV (2) and of the percentage of failures (3) obtained with 10,000 computer simulations of stochastic processes with the sets of parameters indicated in table 1 a, b, c and d (initial release probability variable). B and C. Same as A but with the sets of parameters of table 1 b, e, f and g (B, reavailability timing variable) and b, h, i and l (C, number of available quanta variable).

4.2.2 Postsynaptic contributions to short term plasticity

Since the statistics of binomial chains can be related to purely presynaptic changes in p and N, it is interesting to investigate the modifications to the presynaptic statistics introduced by possible postsynaptic mechanisms such as receptor saturation (Clements, 1996), receptor desensitisation (Jones and Westbrook, 1996) and activity-dependent enhancing of synaptic responses (Thomson 1993), that can substantially contribute to short-term plasticity. Therefore, the results of computer simulations have been filtered and expressed as $\tilde{n}_j$.

The following *filters* applied to the number of released quanta n_j have been used in the simulations to investigate how distinct postsynaptic mechanisms may contribute to the statistics of synaptic transmission.

- *Receptor saturation.* This mechanism may occur in synapses where the number of receptors at the postsynaptic membrane is saturated by an amount of neurotransmitter molecules contained in a number of quanta n_{max} which is less than the total number of available quanta (Clements, 1996), although this seems not to be the case of AMPA mediated glutamatergic activity (Forti et al., 1997). In this case $\tilde{n}_j$ can be expressed, within the simplest model, by

$$
\tilde{n}_j = \begin{cases} n_j & \text{if } n_j \leq n_{max} \\ n_{max} & \text{if } n_j \geq n_{max} \end{cases}
\tag{4.12}
$$

- *Receptor desensitisation.* As desensitisation is a typical property of neurotransmitter receptors (Jones and Westbrook, 1996), it may modify significantly the statistics of release if the time of recovery from the desensitised state (Khiroug et al., 1998) is not considerably shorter than the times between consecutive action potentials. In this case, the number of receptors activated by a single quantum decreases. This decrease depends on the number of quanta released by the previous action potentials. Let us suppose that ϑ is the fraction of available receptors that are activated by a single quantum of neurotransmitter at the first release event. If τ_d is the mean time of recovery from desensitisation, the number of receptors available for the second release event, if n_1 is the first number of quanta released, will be decreased by a factor $1 - \vartheta \cdot n_1 \cdot e^{-\Delta t/\tau_d}$. In the case of more release events, $\tilde{n}_j$, which is proportional to the number of receptors available at the jth release events, can therefore be expressed by

$$\tilde{n}_j = n_j \cdot \left[1 - \vartheta \cdot \sum_{k=1}^{j-1} \tilde{n}_k \cdot e^{(k-j) \cdot \Delta t / \tau_d} \right] \qquad (4.13)$$

where $\tilde{n}_1 = n_1$.

- *Activity dependent enhancing of synaptic responses.* If the number or the conductance of activated receptors depends on the membrane potential or generally on the *recent* synaptic activity, this can produce an activity-dependent enhancing of the synaptic responses. For instance, in the case of glutamate-mediated synaptic transmission, synaptic responses can be considerably higher at more depolarised membrane potentials because voltage dependent NMDA-receptors are activated (Thomson et al., 1993). The modification introduced by this mechanism depends on the number of quanta released at the previous action potentials. In an oversimplifying theoretical scheme in which activity dependent enhancing of synaptic responses is considered linear, if ϑ is now the fractional enhancement in the overall conductance produced by a single quantum of neurotransmitter and τ_e is the mean time for deactivation of this enhancement, the *effective* number of receptors available for the second release event will be increased by a factor $1 + \vartheta \cdot n_j \cdot e^{-\Delta t / \tau_e}$. In the case of more release events, $\tilde{n}_j$, which is proportional to the number of receptors available at the jth release, can be expressed in the same form as in equation 4.13, with a change in sign, as

$$\tilde{n}_j = n_j \cdot \left[1 + \vartheta \cdot \sum_{k=1}^{j-1} \tilde{n}_k \cdot e^{(k-j) \cdot \Delta t / \tau_e} \right] \qquad (4.14)$$

where $\tilde{n}_1 = n_1$. Although the linear approximation is far from being realistic in describing phenomena such as the involvement of NMDA receptors in glutamatergic synaptic transmission, equation 4.14 can still qualitatively capture the time course of the changes in the statistics of signals due to the activity dependent enhancing of synaptic responses.

Figure 4.9 shows the modifications introduced to the statistics of three different binomial chains in three extreme cases of receptor saturation, receptor desensitisation and activity dependent enhancing of synaptic responses.

In a non-correlated chain based on simple binomial distributions with p=0.5 and N=5 (data of Figure 4.9 A), receptor saturation simply reduces the mean (Figure 4.9 A(1)) and the CV (Figure 4.9 A(2)) of synaptic responses. In contrast, receptor desensitisation (or vice versa activity-dependent enhancing of synaptic responses) can induce a depressing (facilitating) behaviour in

the time course of the mean $\tilde{n}_j$. When applied to computer simulations associated to the chains with the parameter set of Table 1a (Figure 4.9 B, facilitating behaviour) and of Table 1d (Figure 4.9 C, depressing behaviour), the postsynaptic filters can drastically change the type of short-term plasticity (Figure 4.9 first column). However, the alteration of the time course of the CV is much weaker (Figure 4.9 second column) even in the case of strong activity dependent enhancing of synaptic responses that transforms a depressing synapse into a facilitating one (Figure 4.9 C(1)). In the case of a relatively small number of available quanta, since the number of failures is not affected by possible postsynaptic mechanisms, a qualitative evaluation of the presence of postsynaptic contributions can be obtained by comparing the time course of the CV and that of the percentage of failures (Figure 4.9 third column) which are similar for pure (presynaptic) binomial chains. Thus, while different types of binomial chains can generate distinct statistics, at least one criterion can be used, although not quantitatively, to evaluate the presence of superimposed postsynaptic effects.

4.3 Transmitted information in synaptic signals

The stochasticity characterising synaptic events affects the fidelity by which synapses can transmit the occurrence of presynaptic action potentials. For example, a presynaptic high frequency train might be confused postsynaptically with one of lower frequency, because of failures in the transmission of individual spikes. Obviously, the discrimination between the two frequencies will be increasingly reliable with time, as successive spikes in the train arrive at the synapse and are integrated in the cumulative synaptic response A_j. One direct way to quantify this reliability is to measure the trans-information, i.e. the mutual information that the cumulative response at time t, A(t), conveys about a presynaptic variable such as the frequency of presynaptic firing. The trans-information I(t) for $\wp$ given different inputs (frequencies) occurring with the same probability can be defined as

$$I(t) = \sum_{h=1}^{\wp} \sum_{k=0}^{N \cdot t \cdot v_h} P_t(k,h) \cdot \log_2 \frac{\wp \cdot P_t(k,h)}{\sum_{l=1}^{\wp} P_t(k,l)} \qquad (4.15)$$

where $P_t(k,h)$ is the joint probability that a total number of k quanta are released by time t and that the input h is activated and v_h is the frequency of input h.
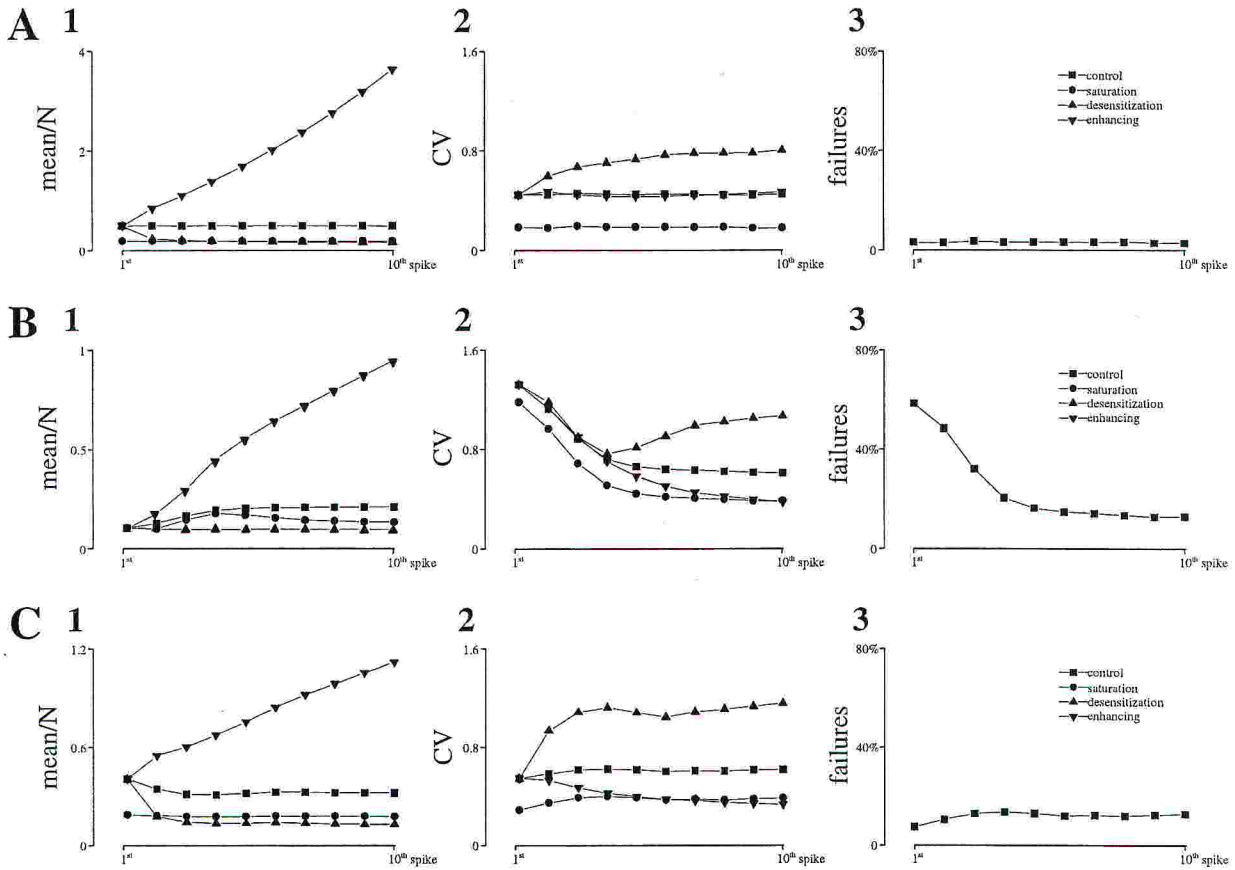
Figure 4.9 Modifications of the statistics of release introduced by postsynaptic mechanisms. A. Time courses of the mean synaptic response normalised to the number of available quanta (1), of the CV (2) and of the percentage of failures (3) quanta obtained with 10,000 computer simulations of a stochastic process in which both the release probability and the number of available quanta are constant (p_j=p=0.5, N_j=N=5). Squares represent the values of the original stochastic process while the other symbols are associated to the same statistics modified by different *postsynaptic* mechanisms (receptor saturation with n_{max}=1, receptor desensitisation with ϑ =0.75 and t/τ_d=0.25 or activity-dependent enhancing of synaptic responses with ϑ =0.75 and t/τ_e=0.25) as described in the text. B and C. Same as A but for computer simulations with the parameter sets of table 1a (B, facilitating behaviour) and of table 1d (C, depressing behaviour).

An important question to be answered is whether and how I(t) is affected by short-term plasticity and by the correlation of synaptic responses. As an example, I(t) has been explicitly computed from experimental data in which two frequencies (12.5 Hz and 25 Hz) were applied. The cumulative responses were evaluated at 80 ms (A_1 and A_2 respectively), 160 ms (A_2 and A_4) and 240 ms (A_3 and A_6). The joint probability $P_t(k,h)$ (h=1,2) was computed as the probability that the cumulative EPSCs occupies the bin k of the quantal distribution given by the QA of synaptic responses of the first pulse at the frequency h, times 0.5 which is the probability of each frequency.

Figure 4.10 A shows the averages of 100 recordings from three different experiments. Mean EPSCs shown in Figure 4.10A(1) are dominated by a strong facilitation at both frequencies, while facilitation is weaker in the mean EPSCs shown in Figure 4.10 A(2) and 4.10 A(3) (Figure 4.10 B(1) and 4.10 B(2)). The time course of I(t) depends on short term plasticity (Figure 4.10 B(3)). In the case of strong facilitation, I(t) has a rather slow onset at the beginning (80 ms) that accelerates at 160 ms; in contrast I(t) has the largest increase already at 80 ms for less facilitating behaviours; in the case shown in Figure 4.10 A(3), where EPSCs are almost depressing at 25 Hz stimulation, I(t) is only very slightly increasing after 80 ms.

This is evidence that the time scale for integrating reliable synaptic signals increases with facilitation, as expected. This result does not depend on the bin used to calculate $P_t(k,h)$. Interestingly, it turns out not to depend much, either, on the correlation in the data, as similar results have been obtained by running computer simulations with the three different models (data not shown). Furthermore the qualitative behaviour of I(t) does not change when the number of inputs (frequencies) is increased.

Since short-term plasticity is not an invariant property of synapses, but can be modulated by activity (e.g. via long-term plasticity) or by changing the composition of extracellular solution, in another series of experiments I(t) has been calculated at two different $[Ca]_o$ (2 mM and 4 mM) in the same cell. Figure 4.11 shows the result of a typical experiment in which the first response was potentiated by increasing $[Ca]_o$. With this protocol, facilitation was reversed to depression for stimulations at 25 Hz (Figure 4.11 A and B). In the presence of 4 mM $[Ca]_o$, I(t) reaches its maximum already at 80 ms, while at 2 mM $[Ca]_o$ it has a longer lasting increase, up to about 1 bit (fully reliable discrimination) after 240 ms (Figure 4.11 C). This result suggests

that the time scale at which synapses can integrate and transmit reliable information is itself not constant, but may be modulated by external agents.
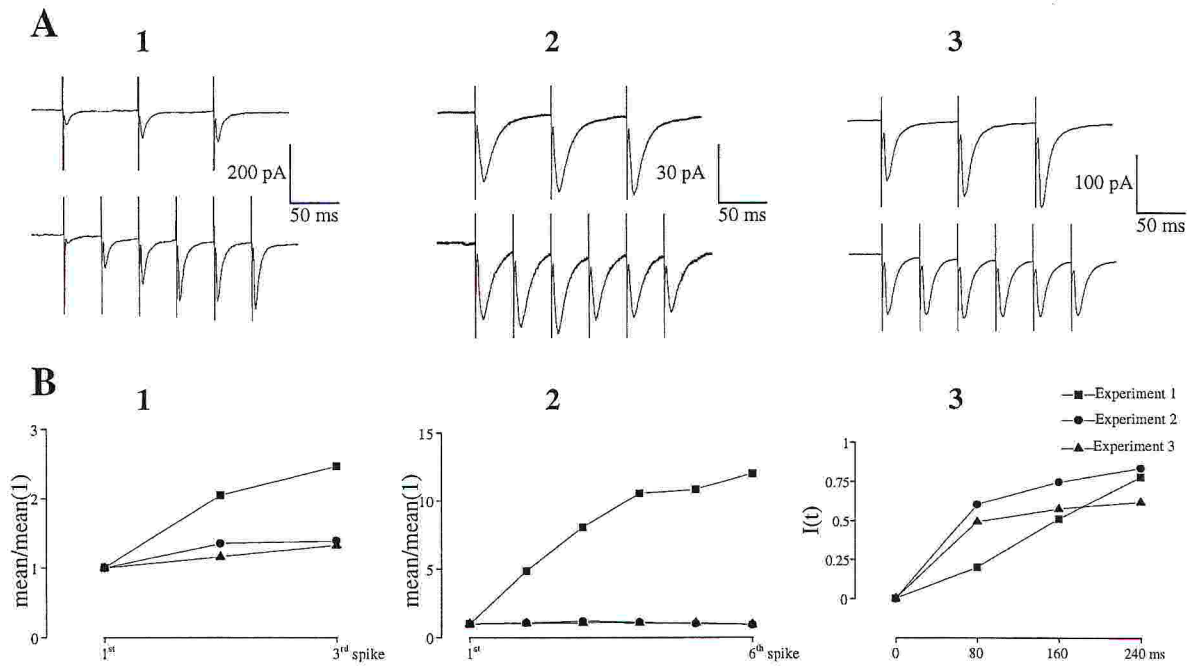
Figure 4.10 Information transmitted by synaptic signals. A. Averages of 100 recordings with trains of 3 pulses of stimulation at 12.5 and with trains of 6 pulses of stimulation at 25 Hz in three different experiments. B. 1 and 2. mean/mean(1st) of EPSCs for the stimulation at 12.5 Hz (1) and for the stimulation at 25 Hz (2). 3. Information transmitted by the synapse (equation 4.15) in the three different experiments.
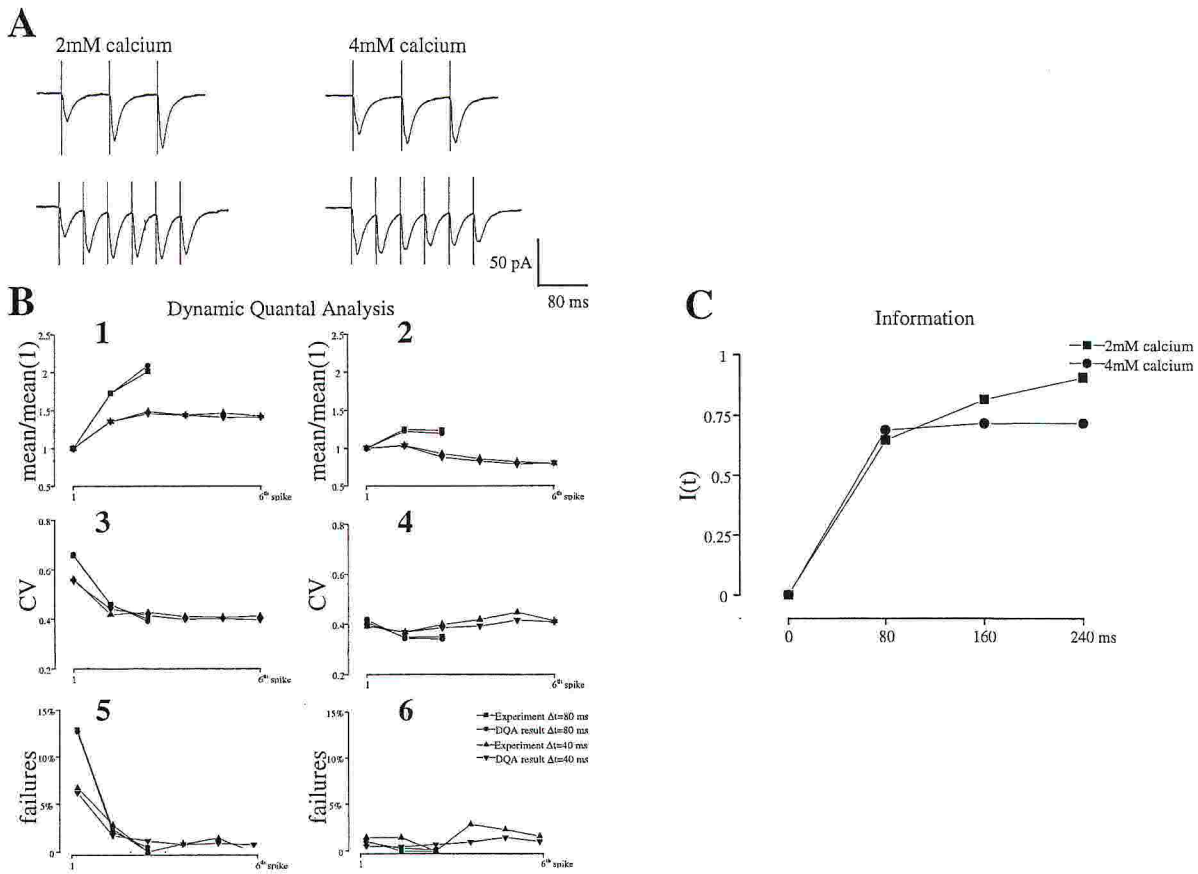
Figure 4.11 Variability of synaptic responses at different extracellular calcium concentrations. A. Averages of 100 recordings with trains of 3 pulses of stimulation at 12.5 and with trains of 6 pulses of stimulation at 25 Hz in the presence of 2 mM (left column) and 4 mM extracellular calcium concentration. B. Comparison of the statistics (mean/mean(1st) (1-2), CV (3-4) and percentage of failures (5-6)) of the synaptic responses obtained by performing the DQA. (Left and right columns correspond to data obtained in the presence of 2mM and 4mM extracellular calcium concentration respectively). C. Information transmitted by the synapse (equation 4.15) in the two different physiological conditions relative to the two frequencies of stimulation.

5 DISCUSSION

Synaptic activity in the hippocampus is highly stochastic (Allen and Stevens, 1994). In comparison to other excitatory synaptic systems in the CNS such as the giant Calyx synapse in the brainstem (von Gerdorff et al., 1997) or the climbing fiber in the cerebellum (Silver et al., 1998), the variability of synaptic responses within different recordings quantified by the CV is considerably high. While in *almost deterministic* synaptic systems the CV can be smaller than 0.01 at the first response, CV can be higher than 1 in hippocampal synaptic responses reflecting a much smaller number of quanta available for release (typically N<10 in the hippocampus and N>100 in the Calyx of held or in the climbing fiber).

It follows that an approach to analyse and characterise synaptic responses in unreliable systems such as the hippocampus must differ at least in two major respects from the case of reliable synapses. On the one hand, whereas the dynamic process leading to facilitation or depression (short-term plasticity) can be treated with discrete or continuos dynamical systems in deterministic synapses, since fluctuations from the mean responses can be neglected, a detailed analysis of synaptic responses in unreliable systems must be performed by using the framework of stochastic process theory. In this respect, the significance of the parameters of deterministic models can be still related to probabilistic parameters such as the release probability or the number of available or released quanta (Tsodyks and Markram, 1997). On the other hand, for highly stochastic synaptic systems it is a major problem to determine how synaptic signals can be integrated both in space and in time. In this respect, a characterisation of the variability of synaptic responses can help to understand how and at which time (and possibly space) scale unreliable synaptic signals can become reliable and can transmit information (Lisman, 1997; Zador, 1998).

In the present study, a simple analysis of the mean synaptic responses was found to give useful information on the dynamics of neurotransmitter release underlying facilitation and depression of EPSCs evoked by presynaptic action potentials in CA3 hippocampal pyramidal neurons. Furthermore, with more accurate analysis, it was shown that a dynamical approach, in which the evolution of repetitive synaptic transmission is interpreted in terms of stochastic chains rather

than by using independent statistical distributions, is necessary to account for the correlation within responses in a train (see chapter 4).

5.1 Short-term plasticity and neurotransmitter release dynamics

5.1.1 The dynamic behaviour of synapses reflects presynaptic changes

In the present experiments it has been shown that, following activation of afferent fibers with trains of stimuli, EPSC patterns are highly variable. A discrete dynamical system derived as the average of the stochastic process, in which both the release probability and the number of synaptic vesicles available for exocytosis change, has been proposed. The comparison between the experimental results and this model indicates that short-term changes of presynaptic conditions can account for this variability.

The correlation between the probability of release and the behaviour of synaptic transmission generated by more than one action potential has been studied in the rat neocortex and hippocampus (Thomson et al., 1995; Debanne et al., 1996). While in the neocortex pairs of monosynaptically coupled cells were used to analyse EPSPs or EPSCs activated by single presynaptic fibers, in the hippocampus a minimal extracellular focal stimulation has been applied in the vicinity of the recording cell in order to obtain synaptic responses. In comparison with pair recordings, with this technique it is impossible to guarantee that only one presynaptic fiber is stimulated. Nevertheless, in voltage clamp recordings, possible postsynaptic voltage-dependent changes of synaptic efficacy can be eliminated.

In the neocortex, synapses between pyramidal neurons are strongly depressing while synapses from pyramidal neurons to inhibitory interneurons are facilitating (Thomson et al., 1993). In pyramid-pyramid connections in the neocortex, with a train of more than 10 presynaptic action potentials, the first mean EPSPs (3-6) are dominated by depression and the following ones fluctuates around a stationary value depending on the firing frequency. The strength of depression, dependent on initial release probability, can be modulated by long-term synaptic plasticity, obtained by pairing presynaptic trains with postsynaptic depolarisation (Markram and Tsodyks, 1996).

In comparison to the neocortex (Thomson et al., 1993; Thomson and Deuchars, 1994; Thomson et al., 1995), synaptic responses in the hippocampus are highly unreliable (Allen and Stevens, 1994). There is also evidence that mechanisms underlying paired-pulse facilitation and depression at single pyramid-pyramid connections are presynaptically mediated and dependent on the amplitude of the first EPSP or EPSC (Deuchars and Thomson, 1996; Debanne et al., 1996; Dobrunz and Stevens, 1997). In keeping with this, synapses with different release probabilities have been found in hippocampal pyramidal neurons in culture (Rosenmund et al., 1993; Murthy et al., 1997) and in slices (Hessler et al., 1993). In the experiments shown in this study, the high variability of EPSC patterns, present in both mossy fibers and associative commisural fibers, could be ascribed to presynaptic mechanisms. In synapses in which the release elicited by the first action potential occurs with a low probability, the synapse will be generally potentiated by the increased probability of release with the following spikes. In contrast, in synapses in which the first action potential produces the release of a larger number of quanta, the number of vesicles available for release at the following spikes will be decreased; this depletion will compensate and eventually overcome the effect of the increased probability resulting in a depression of the synaptic efficacy (Dobrunz and Stevens, 1997). This conclusion confirms the hypothesis that the balance between the effect of residual calcium accumulation and the depletion of vesicles account for the synaptic response to a burst of action potentials in CA3 hippocampal pyramidal neurons (Miles and Wong, 1986), although other mechanisms besides vesicle depletion may contribute to synaptic depression (Zucker, 1989). In this respect, however, in the case of AMPA-mediated glutamatergic activity in which there is evidence that receptor saturation does not occur (Forti et al., 1997) and in which deactivation and desensitisation are very fast (Clements, 1997), the observation that the kinetics of single or mean currents does not change within the train (see figure 3.4) is in favour to the hypothesis that there are no relevant postsynaptic contributions to this form of short-term plasticity.

Synaptic depletion is generally occurring in any synapse and can be considered a general mechanism partially accounting for synaptic depression. Therefore, changes in the stationary synaptic responses to short trains of presynaptic action potentials such as those induced by a temperature variation in GABAergic hippocampal synapses (see chapter 4) can be at least partially ascribed to changes in the dynamics of the neurotransmitter release machinery.

A simple model accounting for the evolution of mean synaptic responses has been, at this stage, proposed. In this model, after a few stimulations of the presynaptic terminal, the probability of release will not increase any more because the accumulation of residual calcium saturates the probability function; this condition will determine an equilibrium between the mechanisms of exocytosis and reavailability of synaptic vesicles that eventually will result in a steady state value of the mean number of available vesicles. Therefore, the stationary EPSC value depends on the frequency of stimulation (exocytosis time course) and on the time course of reavailability of synaptic vesicles. In the comparison between experimental data and the model, the reavailability function used to mimic EPSC patterns obtained experimentally was the sum of two exponential functions, one with a time constant of the order of tens of milliseconds and the other with a time constant of the order of hundreds of milliseconds. Ultrafast mechanisms of vesicles endocytosis have been reported in several systems such as neuroendocrine cells (Artalejo et al., 1995). Experimental evidences suggest that these mechanisms may speed up the recovery from depression, especially in the presence of elevated levels of residual calcium (Dittman and Regehr, 1998). Furthermore, mechanism of flickering of fusion pores responsible for a "kiss and run" type of secretion (Breckengridge and Almers, 1987; Alvarez de Toledo et al., 1993; Fesce et al., 1994) may also be a candidate for the fastest dynamics of release. Finally, fast recovery from depression may be due to releasing sites or quanta that are transiently refractory independent of endocytosis (Dobrunz et al., 1997) and previous activation of the terminal may drive the site into an exocytosis-competent state through mechanisms such as vesicle docking and priming (Schweizer et al., 1995). In general, several biophysical mechanisms can keep hippocampal synapses "efficient" by recovering in a short time scale releasable vesicles. A simple analysis of mean synaptic responses suggests that reavailability in hippocampal glutamatergic synapses is faster in comparison to other systems such as neocortical glutamatergic synapses.

5.1.2 The analysis of transmitter release dynamics can be used to investigate changes in synaptic function

The analysis of postsynaptic response fluctuations evoked by stimulation of presynaptic fibers has been used to study the mechanisms of expression of long-term plasticity (Bekkers and Stevens, 1990; Manabe et al., 1993; Oliet et al., 1994, Stricker et al., 1996). This method is

called *Quantal Analysis* (reviewed by Voronin, 1994) and one of its particularly effective variants is the *Coefficient of Variation Method* (Faber and Korn, 1991; Kullmann, 1994b).

QA has been mainly applied to analyse currents or potentials evoked by a single or at most two presynaptic spikes. A more detailed analysis of the stochastic process of release induced by several action potentials can be an alternative and possibly more powerful way to investigate changes in synaptic function. The comparison between experimental data and the model proposed in chapter 3 shows that this kind of analysis is able to indicate the possible underlying changes in the probability of release and in the time course of reavailability of synaptic vesicles by using a relatively small (30-40) number of recordings.

5.2 Analysis and interpretation of synaptic variability

Short-term plasticity can be simply divided in facilitating or depressing behaviours. These behaviours may be understood in terms of changes in the release probability and in the number of available quanta (synaptic depletion) (Miles and Wong, 1986). At this level, the statistics of synaptic responses can be modelled either with simple binomial distributions by changing p and N at each action potential or with simple (but correlated) binomial chains. The typical behaviours in the CV and in the number of failures associated to both facilitating and depressing synaptic responses can indicate whether short-term synaptic plasticity can be associated to the release process, as proposed by several methods derived from the quantal theory (Kullmann, 1989; Faber and Korn, 1991; Kullmann, 1994). In this respect, it must be pointed out that the variability of synaptic responses is generally also affected by the experimental noise as well as by the stochastic process of receptor activation which can determine a CV for the quantal size (Kullmann, 1992).

At the level of cumulative responses, individual (uncorrelated) binomial distributions fail to be a good description of synaptic activity. At least in some cases, the simple technique of reshuffling is an efficient way to discriminate different models in terms of their correlation trend. Furthermore, this level of characterisation in terms of cumulative responses, allows the investigation on how synaptic signals can be integrated in time; in particular, a calculation of the

information transmitted by synaptic responses can be obtained from experiments with different frequencies of presynaptic firing.

5.2.1 The dynamic quantal approach

The necessity for a *dynamic approach* to the problem of synaptic transmission has been suggested by several lines of experimental evidence, in particular by the frequency dependent behaviour of synaptic responses in the neocortex (Markram and Tsodyks, 1996), in the brainstem Calyx synapse (von Gersdorff et al., 1997) and in the hippocampus. An interesting stimulus-dependent mobilisation model, aimed at characterising the frequency dependent changes of quantal parameters at the lobster neuromuscular junction (Worden et al., 1997), has recently been found efficient in predicting synaptic depression at the Calyx of Held (Neher et al., 1998).

A simple model proposed by Tsodyks and Markram (1997) can account for the time course of mean synaptic responses in the CNS (Tsodyks and Markram, 1997; Markram et al., 1998). Tsodyks and Markram do not consider the variability of synaptic responses around their mean, but in terms of mean responses their formulation is equivalent to that described in this thesis, once their "fraction of restored resources" R_j is identified with N_j/N and their "utilisation" u_j with p_j. Two minor differences are that (i) since their formulation is not in terms of explicit quanta, but only of continuous variables, the restored resources are not discretized (this makes no practical difference as long as only means are considered); and (ii) their model for the evolution of u_j (p_j) follows a different equation from the Dodge-Rahamimoff, although also used without reference to specific biophysical mechanisms (Markram et al., 1998).

The dynamic quantal approach used here not only relates synaptic transmission to biophysical mechanisms such as the restoring of available quanta (resources), but also accounts for the statistics of cumulative synaptic responses, i.e. for the correlation which is an intrinsic property of synaptic dynamics. It has been found that repetitive synaptic responses (particularly in facilitating behaviours) are almost always positively correlated. This property can be accounted for by setting the change in the release probability dependent on the previous release events, i.e. by imposing that the changes in p_j may be themselves dependent on the number of quanta actually released: in the simplified scheme that is proposed here, the change in the release probability occurs only when the previous release event is not a failure. The important

ingredient is the additional element of stochasticity, that is, the variability in the time course of the release probability. More accurate descriptions of such variability may be used as well as the introduction of additional elements of stochasticity, for example in the reavailability process. Furthermore, a third level of approximation (model 3) may account for changes also in the quantal size q. The postsynaptic filters applied to computer simulations (section 4.2) may give an idea of the effects of changes in q to the statistics of synaptic responses. In general, changes in q may lead to a discrepancy between the time course of the CV and that of the percentage of failures (Figure 4.9 third column). This has been never observed in experimental data in the hippocampus.

A possible source of positive correlation among successive synaptic responses could be the presence of failures of propagation of action potentials in the terminal, or failures in stimulation, which in our case cannot be fully controlled. In this situation, not only the release probability, but the whole release process would be conditional on this type of failure, and a constant baseline percentage of failures at each action potential would be observed. Since during trains of 6 stimulating pulses the percentage of failures can decrease from more than 70% to less than 10% in strongly facilitating synapses (data not shown), the hypothesis that positive contributions to correlations arise only from failures in stimulation seems to be unrealistic.

5.2.2 Reliability in synaptic signals

The characterisation of stochastic synaptic transmission is extremely relevant to the study of neural network activity (Liaw and Berger, 1996). In synapses in which a large number of quanta are released at each action potential, fluctuations of synaptic signals from the *mean value* are relatively small and can be, to a first approximation, neglected. In this case, once short-term synaptic plasticity is accounted for as activity-dependent changes of mean synaptic responses, the network activity can be considered deterministic at the level of single connections. This can be the case of several synapses in the CNS such as the Calyx of Held in the auditory brainstem or the climbing fiber in the cerebellum. In the CA3 region of the hippocampus, a lower variability of synaptic responses can be also observed in GABAergic synaptic activity (see chapter 4). In this respect, since presynaptic action potentials can almost always generate postsynaptic responses in GABAergic synapses, it might be argued that in CA3 pyramidal

neurons these synapses are "more powerful" in transmitting information with single synaptic events than glutamatergic synapses (Miles and Wong, 1994).

In synapses with a low number of quanta available for release, the marked *unreliability* (Allen and Stevens, 1994) of synaptic responses, although possibly exaggerated by the recording conditions (Hardingham and Larkman, 1998), does not allow the approximation of *deterministic synapses*. Still, synaptic signals can be integrated both in space (the activity of several presynaptic neurons) and in time (integration of synaptic signals during a burst of action potentials) and the problem of understanding the space and time scales of neural codes, which could be taken to be the space and time scales at which the activity becomes deterministic, is particularly relevant.

The consequences of different dynamic behaviours of synapses in terms of synaptic function and neural codes have been discussed in the neocortex (Tsodyks and Markram, 1997). In this system, as excitatory connections to pyramidal cells and to interneurons exhibit different features, it has been proposed that modulations of synaptic properties generated by synaptic plasticity can regulate the temporal codes expressed by neocortical circuits. Markram and Tsodyks showed that the time window of transient synaptic responses determines the interval in which simultaneous synaptic inputs can summate to generate a *transient* postsynaptic response, i.e. the time window of neuronal codes. Nevertheless, Markram and Tsodyks did not directly approach the problem of the variability of synaptic responses, which deals with the question on how reliable information can arise from unreliable synaptic signals. In the cortex, the highly reliable mechanism of spike generation (with a precision of the order of ms) is in contrast with the higher unreliability of synaptic signals. Thus, as suggested by a recent theoretical analysis proposed by Zador (1998), the density of synchronous connections can provide a form of signal (space) integration that can maintain a reliable transmission with unreliable synapses, but only if the fine structure of trains carries information, providing for the necessity of time integration as well.

The statistical analysis of synaptic responses evoked by trains of action potentials can be useful to investigate the time integration of synaptic signals. In particular, information quantities such as the one defined in equation 4.15 are indicative of the capability of a system to discriminate within different inputs (Rolls and Treves, 1998). In this work an amount of transmitted information has been measured in hippocampal synaptic responses by using two frequencies of

stimulation. The information transmitted by the cumulative synaptic responses was slower in facilitating behaviours, but could reach higher values at the end of the train. This indicates that the time scale for signal integration is longer in facilitating synapses, in which case bursts of action potentials could indeed be said to make unreliable synapses reliable, as proposed by Lisman (1997). Since short-term plasticity is not an invariant property of synapses, the information that can be transmitted by synaptic signals can change in time course in the same synapses, as the experiments with different $[Ca]_o$ have demonstrated. This evidence suggests how long term changes of synaptic efficacy may affect the coding expressed by neuronal networks. Indeed, phenomena such as LTP and LTD may result not simply in a modulation of synaptic strength, but also of the mechanisms of integration of synaptic signals by neuronal networks, i.e. of the time and space scales over which functional brain circuits may transmit reliable information. In this respect, it must be pointed out that constant frequency firing has been used here to investigate temporal synaptic integration properties of hippocampal excitatory synapses, but transmission of information is determined by more realistic bursts of action potentials in which spikes do not occur at constant time interval. LTP and LTD associated to an increase or a decrease of the initial release probability can diminish or augment the time window for neuronal coding, i.e. the number of spikes that can reliably transmit information through the neuronal network.

6 APPENDIX

In this chapter, a high space-time resolution imaging system, for recording calcium fluorescence, based on a commercial CCD camera, is described. The time-course of $[Ca^{2+}]_i$ gradients generated by action potentials was measured in hippocampal CA1-CA3 pyramidal cells within brain slices. Image sequences were captured at 93 to 400 frames/sec, revealing frequency dependent anisotropy of fluorescence increase in soma and proximal dendrites of principal cells during trains of evoked action potentials. Synchronisation of image acquisition with voltage and current recordings permitted to characterise the timing of transmembrane potential variation, Ca^{2+} current and Ca^{2+} diffusion providing striking 2D visualisations of $[Ca^{2+}]_i$ gradients at the limit of the relaxation time for the dye-Ca^{2+} binding reaction. Numerical simulations on a model cell were used to gain a better understanding of the relationship between $[Ca^{2+}]_i$ and fluorescence measurements, as well as to provide indirect estimates for the endogenous buffering power in the soma. In summary, it is shown at which time scale fast transients of calcium fluorescence signals evoked by action potentials can be recorded and how these signals must be interpreted. This system has been also used to detect calcium signals generated by the depolarising action of GABA in the developing hippocampus and the role of temperature, using AM-ester calcium dyes.

6.1 Imaging neuronal calcium fluorescence at high spatio-temporal resolution

6.1.1 Methods

A modular upright microscope was equipped with a 40× or a 63× water-immersion objective and an epi-fluorescence illuminator incorporating two dichroic filter-cubes. These were used in combination with XF23 and XF41 excitation/emission interference filter sets (Omega Optical) for Calcium Green-1 and Calcium Crimson fluorescence, respectively. Excitation light from a 75 W stabilised Xenon arc source was coupled to the microscope via a liquid light guide gated by a rapid shutter. Light was attenuated with a diaphragm to avoid phototoxicity and excessive

bleaching. Fluorescence was measured using a fast modified CCD camera (CA-D1 128T, DALSA) with a maximum of 15 MHz readout rate and 12 bit/pixel precision. In particular, the CCD sensor's output was digitised at 12 bit/pixel by customised electronics permitting image acquisition rates up to 735 frames/s. Each image was formed by an array of 128×128 pixels, corresponding to a spatial resolution of 0.78 µm/pixel. Distances in the specimen plane were calibrated once for all by placing a 10 µm-pitch graticule under the objective.

Slices were prepared as described in the methods section of chapter 3. Electrical recordings were made from CA3 and CA1 pyramidal neurons in the slice using patch pipettes pulled from 2 mm o/d borosilicate glass. Pipettes had a resistance of 4-6 MΩ when filled with intracellular solution containing (in mM): 123 K-gluconate, 12 KCl, 4 $MgCl_2$, 10 HEPES, 4 Na_2ATP, 0.3 Na_2GTP, 10 Phosphocreatine, adjusted to pH 7.2 with KOH. Impermeant potassium salts of calcium-sensitive fluorescent dyes Calcium Green-1 (470-500 nm excitation, 520-560 nm emission, dissociation constant K_d=190 nM) and Calcium Crimson (540-580 nm excitation, 595-625 nm emission, K_d=185 nM) were dissolved in intracellular solutions in the concentration range 35-150 µM and loaded into cells by establishing whole-cell recording conditions (Eilers et al., 1995) using a standard EPC-7 patch-clamp amplifier. In some experiments, action-potential waveforms were constructed from current-clamp recordings obtained from a different cell in the same slice (Spruston et al., 1995), and played-back to the imaged neuron in voltage clamp. For these recordings, potassium channels were blocked by replacing K-gluconate and KCl with 135 CsCl in the intracellular solution whereas sodium channels were blocked by addition of 1 µM TTX to the superfusate.

The frame-enable signal from the CCD camera was also sampled, allowing for off-line determination of current, voltage and image acquisition timing. The control signals required to trigger the optical section of the set-up were generated by the same software and interface. Image sequences were acquired at 93-400 frames/s, digitised at 12 bit/pixel and stored in real time to the RAM of a Pentium PC using a high-performance frame-grabber (IC-PCI/AM-DIG16, Imaging Technology) controlled by macros written in Optimas 5.0 language, or by customised software written in Visual C++.

The camera operated in an efficient frame-transfer mode, whereby pixel data were shifted from the light-exposed to the masked region of the CCD sensor in less than 4% of the inter-frame

interval (Figure 6.1). This avoided image blurring and maximised photo-charge integration time. Accepted images were saved on a UW-SCSI hard drive and analysed using routines developed from Matlab 5.1 Image Processing Toolbox. For each image pixel, fluorescence signals were computed as ratios

$$\frac{\Delta F(t)}{F(0)} = \frac{F(t) - F(0)}{F(0)} \qquad (6.1)$$

In this expression, t is time, $F(t)$ is fluorescence following a stimulus that causes calcium elevation within the cell and $F(0)$ is pre-stimulus fluorescence computed by averaging 10-20 images. Both $F(t)$ and $F(0)$ were corrected for mean auto-fluorescence computed from a 20×20 pixel rectangle devoid of obvious cellular structures. Ratio magnitude was encoded by 8 bit pseudo-colour look-up tables to produce false-colour images. The local ratio computation in equation 6.1 is expected to provide correction for time-independent non-uniformity in optical path-length and dye concentration (Neher and Augustine, 1992). This was kept as constant as possible during image acquisition by waiting until dye dialysis had produced stable $F(0)$ values (15-20 min with input resistance ≤ 15 MΩ). Excitation intensity was adjusted to produce photo-bleaching rates $\leq 0.5\%$/s during tens of 1s-long illumination periods. Where indicated, a three-point zero-phase digital filter (Oppenheim and Shaffer, 1989) and a 3×3 two-dimensional median filter (Lim, 1990) were applied to fluorescence traces and images, respectively. To model the dynamics of Ca^{2+} entering the soma of pyramidal cells, the computational scheme proposed by Nowycky and Pinter (1993) was adopted. Briefly, $[Ca^{2+}]_i$ was evaluated as a function of time t and radial distance r in a spherical cell following uniform Ca^{2+} entry across the outer membrane. The sphere volume was averaged subdivided into discrete shells and diffusion-reaction of Ca^{2+} with a mobile exogenous buffer (dye) of absolute concentration $[B_m]$ and an immobile endogenous buffer of concentration $[B_s]$ was described by the following equation:

$$\frac{\partial [Ca^{2+}]_i}{\partial t} = \int_0^{r_o} \delta(r - r_o) \frac{I_{Ca}}{2FV_o} dr$$

$$+ D_{Ca} \left(\frac{\partial^2 [Ca^{2+}]_i}{\partial r^2} + \frac{2}{r} \frac{\partial [Ca^{2+}]_i}{\partial r} \right) \tag{6.2}$$

$$- K_{on}^{B_m} [B_m][Ca^{2+}]_i + K_{off}^{B_m} [B_m Ca]$$

$$- K_{on}^{B_s} [B_s][Ca^{2+}]_i + K_{off}^{B_s} [B_s Ca]$$

Here D_{Ca} is Ca^{2+} diffusion coefficient in the cytoplasm, K_{on}^X is the association rate constant of calcium binding to buffer X (B_m or B_s), K_{off}^X is the dissociation rate of calcium from the (X Ca) complex[1], I_{Ca} is the transmembrane calcium current, F is Faraday's constant, V_o is the volume of the shell just below the membrane (Yamada et al., 1989), d is Dirac's delta and r_o the cell radius. The first line of the equation's r.h.s. represents a transmembrane source of calcium, the second radial diffusion, the third binding of calcium to dye and the fourth binding of calcium to the endogenous buffer. The reaction-diffusion of B_m as well as of the (B_m Ca) complex was described by two analogous equations without source terms. Finally, two more equations, missing both radial diffusion and source, were used to compute the changes of $[B_s]$ and $[B_s$ Ca]. Table 2 lists the parameters used for numerical computations.

An image of the set-up used for the experiments reported in the appendix is shown in Figure 6.2.

6.1.2 Imaging rapid calcium concentration gradients

Identified cells having proximal and apical dendrites in the horizontal plane of focus were patch-clamped under direct visual control with pipettes containing cell-impermeant Calcium Green-1 (75 μM). The maximal changes in fluorescence $\Delta F(t) / F(0)$ observed in the present set of experiments amounted to less than 30% and were typically less than 10%, whereas test applications of 25 mM K^+ and 150 μM NMDA to the bath caused $\Delta F(t) / F(0)$ to increase by more that 100%, indicating that the dye was not binding Ca^{2+} near saturation. In other control experiments, $\Delta F(t) / F(0)$ signals following an action-potential were reduced below detection threshold by adding to the superfusate broad spectrum blockers of voltage activated calcium channels Ni^{2+} (50 μM) and Cd^{2+} (200 μM).

---

[1] The dissociation constant K_D^X for the reaction $X + Ca^{2+} \leftrightarrow$ (X Ca) equals K_{off}^X / K_{on}^X
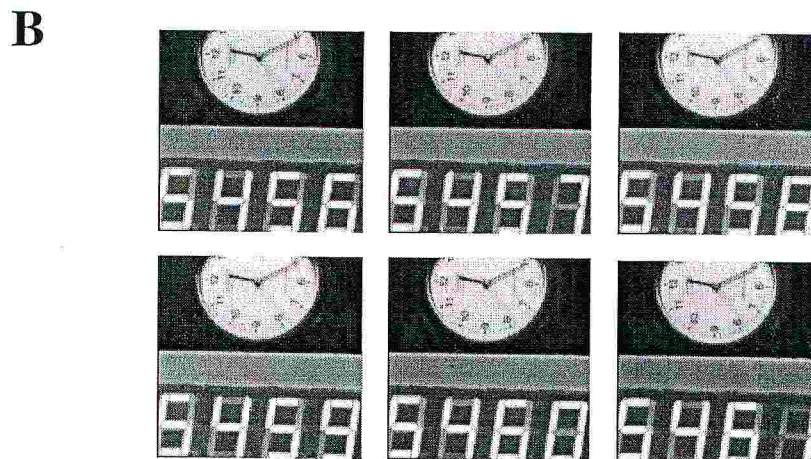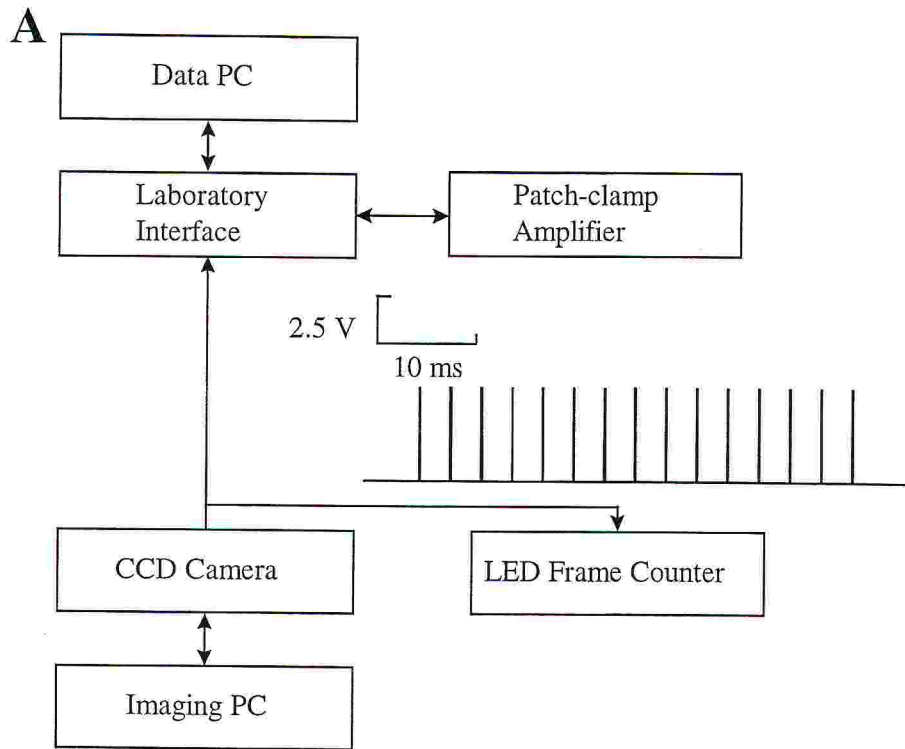
Figure 6.1 System description. A. Block-diagram representation of the major electronic components of the system. The comb-like waveform in the middle of the panel is a segment of the frame-enable signal (FVAL) from the CCD camera, sampled by the laboratory interface. Each upward swing of the signal marks the beginning of a new frame integration period. B. Six consecutive images, captured at the maximum frame rate allowed by the CCD camera (400 frames/sec), are shown. Images were generated by focusing the camera onto a LED counter clocked by the FVAL pulses, each pulse incrementing the counter by one digital unit. Images show no lag in response, indicating that the effective speed of the CCD camera is that of the FVAL clock.
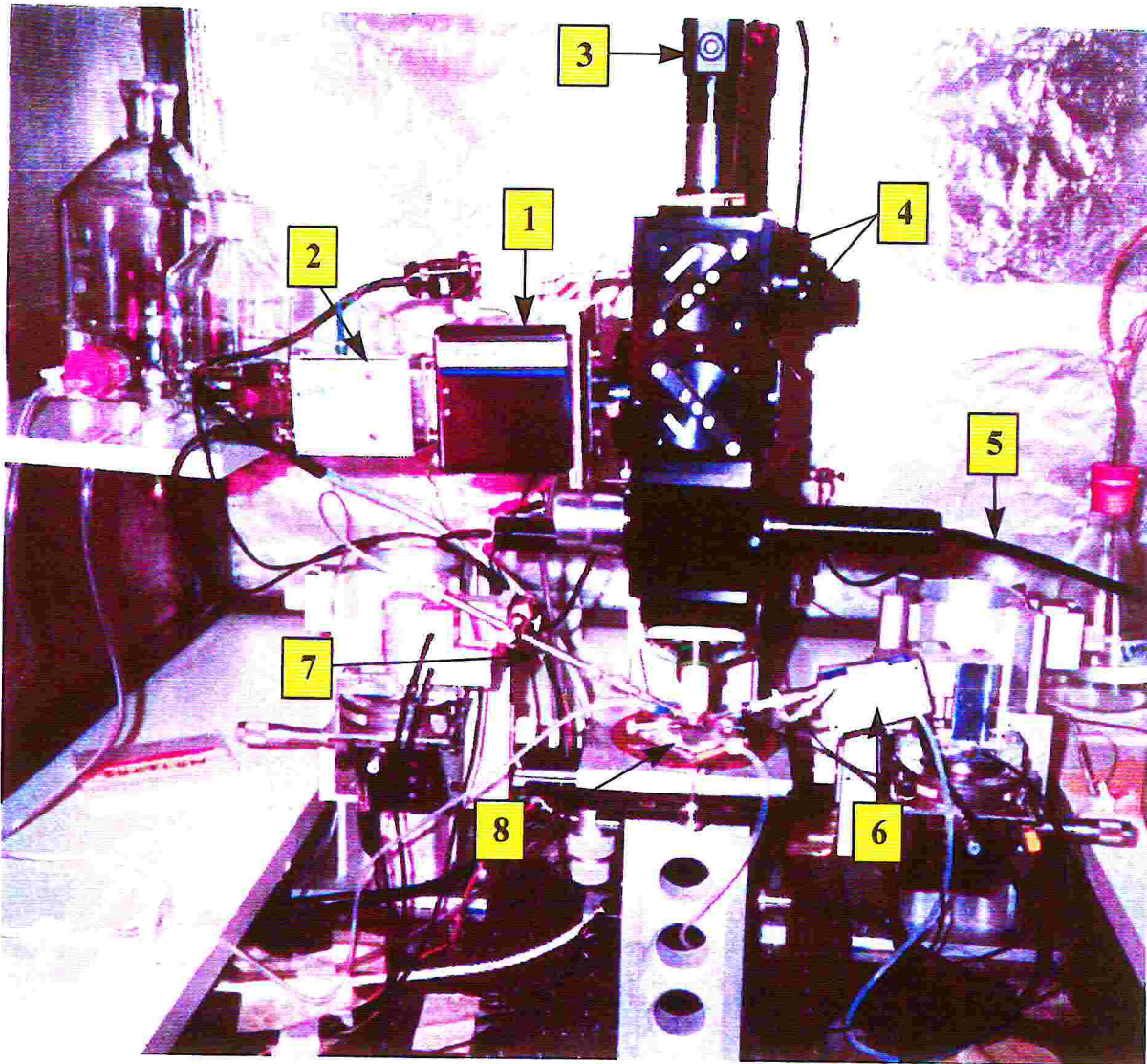
Figure 6.2 Image of the set-up used for the experiment reported in the appendix. 1. DALSA CA-D1 fast CCD camera used for calcium fluorescence measurements. 2. Circuitry developed for the control of the CCD acquisition and for its synchronisation with the electrophysiological recordings. 3. Slow CCD used for IR visualisation of the brain slices. 4. Dichroic filter cubes. 5. liquid light guide used for excitation. 6. Headstage of the patch clamp amplifier. 7. Holder used either for electrical stimulation or for fast application of drugs. 8. Recording chamber.

TABLE 2. Parameters used for numerical computations

Symbol	Definition	Value	Comment
Geometry			
r_o cell radius		7.5 μm	used by Nowycky & Pinter, 1993
dr shell thickness		0.25 μm	intracellular space discretized in 30 concentric shells
Calcium			
I_{Ca} Ca current		400 pA	peak value; waveform as shown in Figure 6.6
$[Ca^{2+}]_i$ Initial Ca concentration		0.05 μM	Helmchen, Imoto & Sakmann, 1996.
D_{Ca} Diffusion constant for free calcium in cytoplasm		220 μm²s⁻¹	Allbritton, Meyer & Stryer, 1992
Fixed buffer			
$[B_s]$ Total concentration		530 μM	similar to Nowycky & Pinter, 1993.
K_D^{Bs} dissociation constant		3800 μM	conc and affinity selected so that κ ≈ 120.
K_{on}^{Bs} forward binding rate		570 μM⁻¹s⁻¹	equal to dye's,
			see also Klingauf & Neher, 1997
Mobile buffer (Dye)			
$[B_m]$ Total concentration		75 μM	used in most experiments
K_D^{Bm} dissociation constant		0.190 μM	CG-1, Molecular Probes estimate
K_{on}^{Bm} forward binding rate		570 μM⁻¹s⁻¹	Eberhard & Erne, 1991
D_{Bm} Diffusion constant		200 μm²s⁻¹	used by Nowycky & Pinter, 1993

In contrast, contribution to Ca^{2+} influx from NMDA receptors (Garaschuk et al., 1996) was probably too small to be measured under the present recording conditions, as block by CPP (20 μM) did not produce appreciable changes in $\Delta F(t) / F(0)$.

The peak amplitude of $\Delta F(t) / F(0)$ transients following a single action potential was a monotonically decreasing function of Calcium Green-1 concentration in the range 35-150 μM (Figure 6.3 A) (Borst et al., 1995; Helmchen et al., 1996; Helmchen et al., 1997). At 75 μM, resting fluorescence $F(0)$ was twofold higher for Calcium Crimson than for Calcium Green-1 (Figure 6.3 C, solid bars). This is probably due to a combination of different dye affinities and compartmentalisation, as well as sensor quantum efficiency (Figure 6.3 B) at the different wavelengths used. Peak values of $\Delta F(t) / F(0)$ transients for Calcium Green-1 and Calcium Crimson differed by a factor of 3 or more (Figure 6.3 C, empty bars), which is only partially accounted for by the twofold difference in denominator values. Fluorescence signals following single action potentials were measured from cell somas with typical S/N $\geq$ 6 for Calcium Green-1 and $\geq$ 4 for Calcium Crimson (single-pixel values for data collected at 200 frames/s using dye concentration of 75 μM in the pipette).

Figure 6.4 shows one representative data set from experiments in which Ca^{2+}-dependent changes in dye fluorescence were measured at full-frame resolution (128x128 pixels) with a temporal resolution of 10.8 ms from large CA3 pyramidal cells. Successive action potentials elicited by somatic injection of current pulses produced distinguishable contributions to Ca^{2+} entry. Individual contributions were resolved down to about 20 ms inter-spike intervals at the cell periphery (Figure 6.4 B, green trace). By contrast, $\Delta F(t) / F(0)$ increased in a markedly more continuous fashion near the cell centre (Figure 6.4 B, red trace). Thus substantial $[Ca^{2+}]_i$ gradients developed rapidly within the cell cytoplasm, with instantaneous magnitude depending strongly on the cell firing frequency.

These recordings were also characterised by conspicuous delays between fluorescence and voltage peaking. As shown in Figure 6.4 C (first frame), no fluorescence changes could be detected during the course of an action potential. The delayed $\Delta F(t) / F(0)$ signal reached a maximum near the cell boundary only 19.8±7.3 ms (n=6 cells) after the peak of an action potential, generating a characteristic annular pattern of fluorescence (Figure 6.4 C, second and

third frame). The annular front relaxed towards the cell centre in 178 ± 45 ms as diffusion caused progressive re-equilibration of cytoplasmatic Ca^{2+} (Figure 6.4 D and 6.4 E).
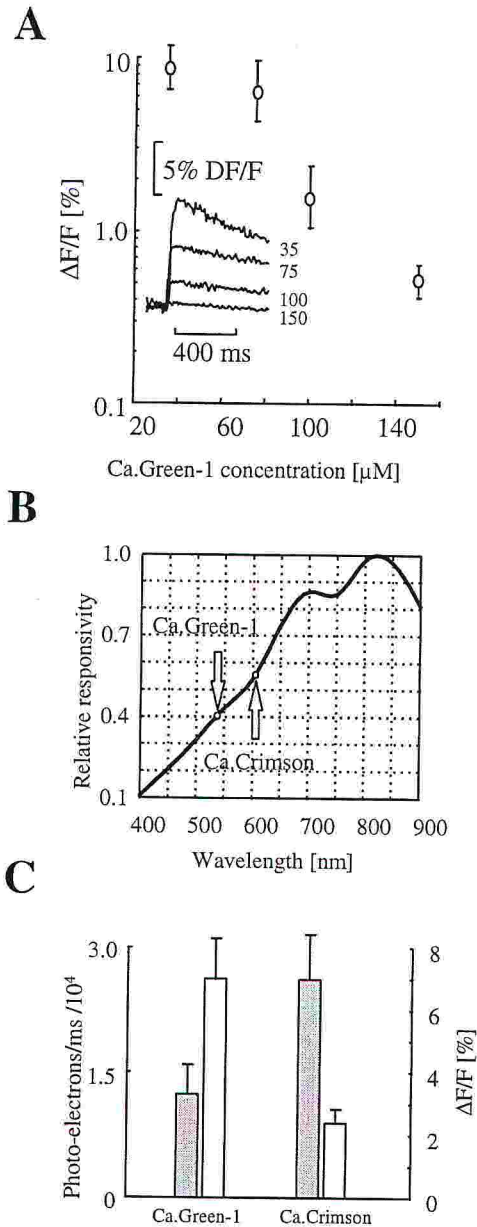
Figure 6.3 Dye response characterisation. A. Fluorescence peak response of Calcium Green-1 to a single action-potential, plotted against dye concentration. Inset: 4 unfiltered sample responses from different cells at shown dye concentrations (µM). B. Relative spectral responsivity of the DALSA CA-D1 CCD sensor. Arrows correspond to dye maximal emission wavelength C. Mean neuronal stationary fluorescence measured at the single pixel level (solid bars, left axis) and single action-potential evoked fluorescence peak response (hollow bars, right axis) for Calcium Green-1 and Calcium Crimson. Dyes were loaded into CA1-CA3 pyramidal cells at 75 µM pipette concentration. Data in (A) and (C) are mean ± S.D. (n=5 cells).
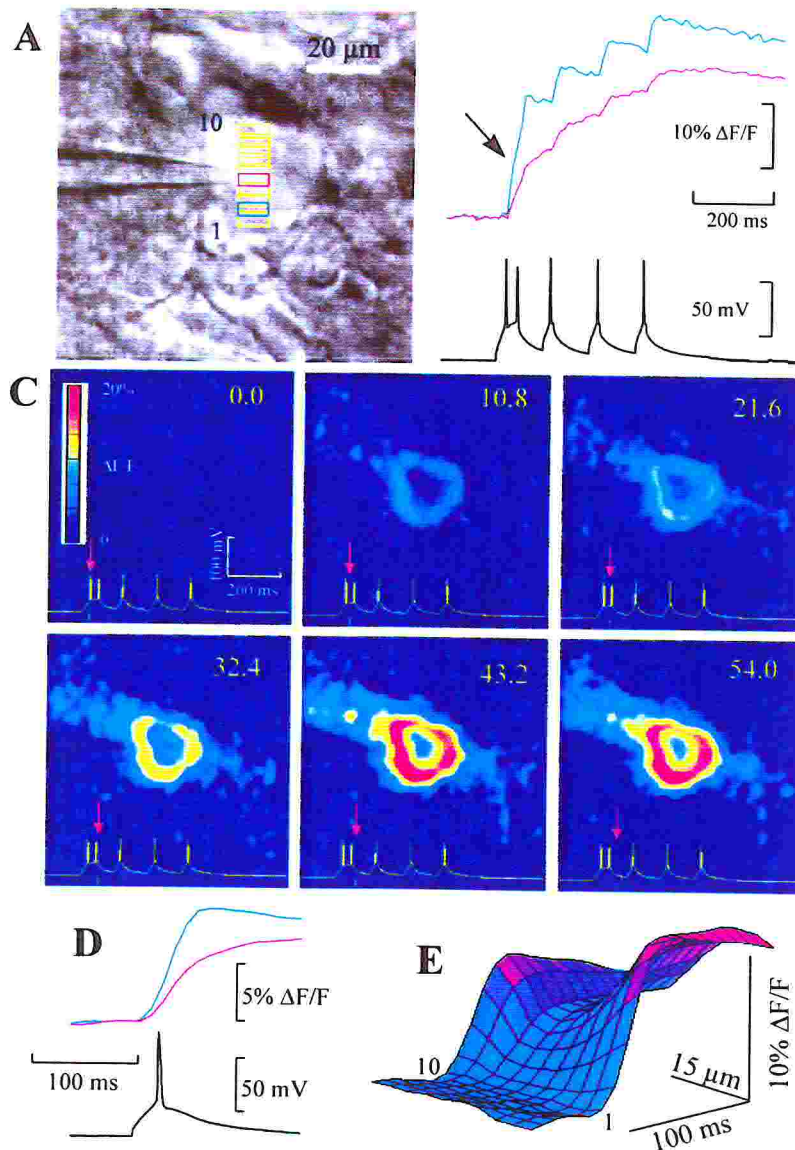
Figure 6.4 Fast $[Ca^{2+}]_i$ gradients. A. Infra-red transmitted-light image of a CA3 pyramidal neuron with a superimposed array of 10 partially overlapping regions of interest (ROIs). B. Simultaneous recordings of transmembrane voltage (bottom trace) and unfiltered means of fluorescence change from the red (middle trace) and green (upper trace) ROIs in A. Potential was measured in response to somatic injection of four 30 ms 200 pA pulses. The first pulse evoked two action potentials in rapid succession (26 ms inter-spike interval). Contribution to calcium entry from each of these two action potentials is clearly identifiable as a slope change in the $\Delta F(t)/F(0)$ rise time course measured at the cell boundary (arrow). Inter-frame interval was 10.8 ms. C. Six selected false-colour images from the sequence collected during the recordings in B. D. Bottom: single action potential evoked by a 30 ms 200 pA somatic current-pulse injection in the same cell. Top: corresponding fluorescence changes measured from the red and green ROIs in (A). ROI and trace colours are matched. E. Space-time 3D plot: receding axis is distance along the cell profile, from ROI 1 to 10, abscissa is time, surface height gives local fluorescence change (also encoded as surface colour).

90

Somatic fluorescence returned to baseline levels a few seconds after the last action potential (time constant 1.2 ± 0.3 s, as measured by mono-exponential fits following a single action-potential, with 75 μM Calcium Green-1 in the pipette), as a consequence of cell buffering and extrusion.

6.1.3 Timing of calcium entry

It has been suggested that, in the squid axon, most of the Ca^{2+} enters during the repolarisation phase of the action potential (Llinas et al., 1981). Thus, a series of experiments was undertaken using faster frame rates (5.4 ms inter-frame interval) commanding membrane potential to follow the waveform of simulated action potentials (Doerr et al., 1989) (Figure 6.5 A, top trace) after establishing pharmacological conditions that permitted the selective detection of Ca^{2+} currents. The fast inward currents elicited under these conditions (Figure 6.5 A, bottom trace) were reduced by more than 90% by superfusion with nominally zero extracellular Ca^{2+}. The simplest explanation is that simulated action potentials elicited essentially Ca^{2+} tail currents generated by the sudden increase in driving force following membrane repolarisation, whereas little or no current flowed during the brief depolarisation phase even though the channels were opened (Johnston and Wu, 1995). Current integration revealed that Ca^{2+} influx following an action potential was rather large ($5.7 \pm 2.1 \times 10^{-17}$ mol, n=3 cells). Similar results have been obtained in DRG cells from chick embryos (McCobb and Beam, 1991) as well as in a calyx type synapse in the rat medial nucleus of the trapezoid body (Borst and Sackmann, 1996). However, it should be pointed out that a substantial fraction of the whole-cell Ca^{2+} current originated likely from unclamped regions of the membrane which did not experience the commanded action-potential waveform. Therefore, the timing of the currents reported here is probably not entirely reliable as these should be understood as attenuated and distorted versions of the real Ca^{2+} currents flowing during a natural action potential.

6.1.4 Frequency-dependent calcium responses

Action potentials are known to actively invade the apical dendritic tree of CA1 pyramidal neurons (Jaffe et al., 1992; Andreasen and Lambert, 1995; Stuart et al., 1997) in a frequency-dependent manner (Callaway and Ross, 1995; Tsubokawa and Ross, 1996). In this set of experiments, repetitive action potentials were elicited in CA1 neurons by trains of brief somatic

current pulses. For stimulation frequencies up to 40 Hz, one action potential was usually evoked by each pulse.

In general, only a fraction of the apical dendrite (up to 90-100 μm from the soma) was clearly distinguishable with sufficient signal/noise (S/N). However, fluorescence signals displayed striking differences even in such relatively limited portions of the imaged cells, as shown in Figure 6.6. In particular $\Delta F(t)/F(0)$ relative maxima formed 40-60 μm from the soma, irrespective of action potential frequency. In the soma, $\Delta F(t)/F(0)$ increased linearly with the number of action potentials, whereas in the proximal dendrite (up to 60 μm from the soma) $\Delta F(t)/F(0)$ increment was comparatively attenuated. Finally, beyond the first noticeable dendritic branching, fluorescence failed to rise after the first few action potentials in a train. Differences in these three distinct patterns of $\Delta F(t)/F(0)$ dynamics were particularly evident at the highest stimulation frequency used (40 Hz; see Figure 6.6 E) in accord with previous experimental and theoretical investigations (Jaffe et al., 1994). A likely explanation for the compartmentalisation of the $\Delta F(t)/F(0)$ rise is the anisotropic distribution of Ca^{2+} channels (Christie et al., 1995) whereas failure of action potential invasion may account for the $\Delta F(t)/F(0)$ behaviour at dendritic branch points (Spruston, et al., 1995).

6.1.5 Modelling somatic [Ca^{2+}]$_i$ dynamics

The results in Figures 6.4 to 6.6 indicate that Ca^{2+} imaging can be performed in brain slices with high spatial resolution under conditions whereby the ultimate temporal limitation is set by the kinetic properties of the fluorescent indicator used. Specifically, the time-course of fluorescence transients at stimulus onset was influenced by dye relaxation time τ, which is given by the expression (Kao and Tsien, 1988)

$$\frac{1}{\tau} = K_{on}[Ca^{2+}]_i + K_{off}. \tag{6.3}$$

K_{on} and K_{off} are, respectively, thermodynamic association and dissociation constants for the binding of calcium to dye. Following an action potential, [Ca^{2+}]$_i$ is likely to rise locally to ≈300 nM (Helmchen et al., 1996). Thus, using published figures for the rate constants (Eberhard and Erne, 1991), values for τ of ≈ 3.2 ms and ≈ 2.5 ms can be estimated, at room temperature, for Calcium Green-1 and Calcium Crimson, respectively.
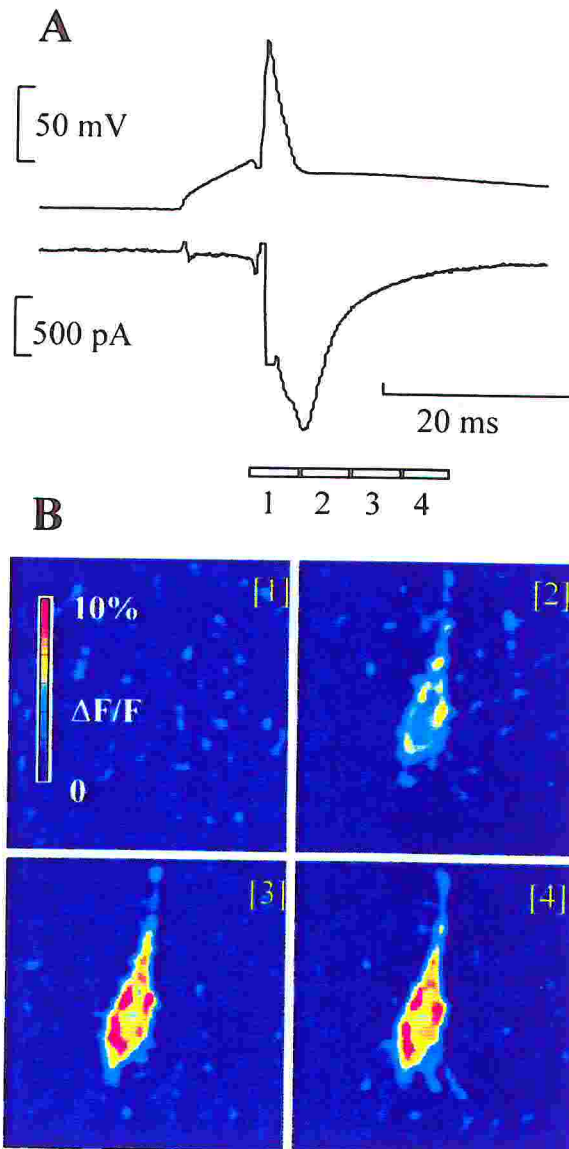
Figure 6.5 Calcium entry and calcium current. A. Patch-clamp recordings from a CA1 pyramidal neuron loaded with 75 μM Calcium Green-1 in a CsCl-based intracellular solution and in the presence of 1 μM extracellular TTX. Top: simulated action-potential applied under voltage-clamp. The voltage wave-form was obtained from a different cell in the same slice under current-clamp using a K-gluconate based intracellular solution (and no TTX). Bottom: current trace representing the difference between the recordings obtained in 2 mM and nominally zero extracellular calcium. B. Four false-colour consecutive images taken at 5.4 ms intervals during the voltage-clamp recording in A. Photo-charge integration intervals are marked by boxes at the bottom of A; box separation lines indicate the short frame-shift periods during which CCD integration was disabled.
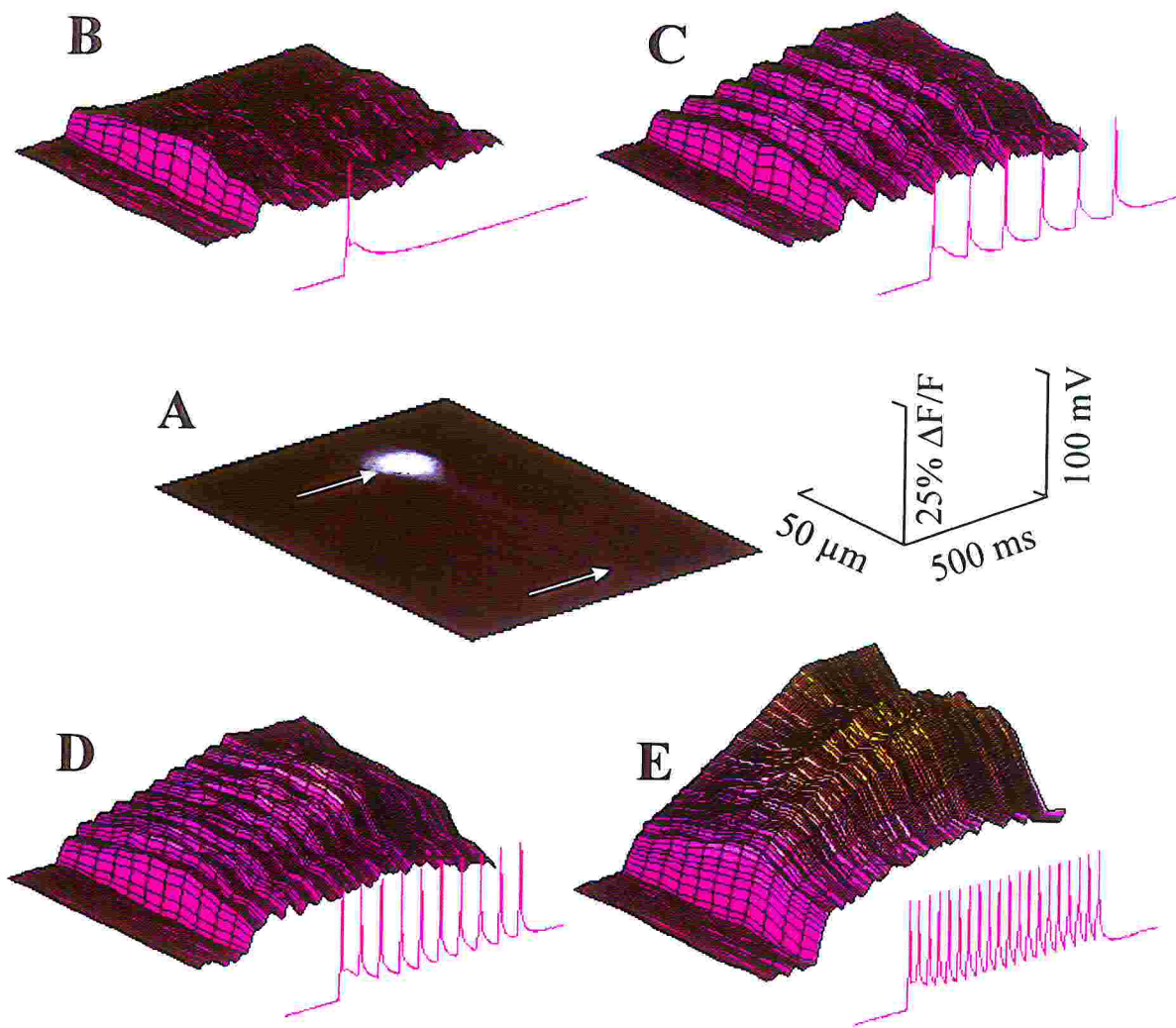
Figure 6.6 Time-resolved spatial distribution of calcium entry during evoked action potential activity. A. Fluorescence image of a CA1 hippocampal pyramidal neuron loaded with 75 μM Calcium Crimson. B. Solid line: membrane potential vs. time. A single action potential was evoked by intra-somatic current pulse injection (450 pA, 10 ms) via the loading pipette in whole-cell current-clamp. Space-time 3D plot: receding axis is distance along the cell profile, measured between the positions marked by arrows in (A); abscissa is time (same as voltage record); surface height represents mean relative fluorescence changes (also encoded as surface colour) measured from 1 ROI partially covering the soma width and 11 partially overlapping ROIs stretched across the proximal dendrite (ROIs not shown). Data refers to a sequence of 180 frames captured at 5.0 ms inter-frame interval. C. Same as B, for repetitive current pulse injection (450 pA, 10 ms) at inter-pulse intervals of 100 ms. D. 50 ms. E. 25 ms.

Fluorescent dyes are not expected to track accurately $[Ca^{2+}]_i$ changes that take place on a time scale faster than 3-4 $\tau \approx 10$ ms (Kao and Tsien, 1988), in good agreement with the results shown in Figures 6.4 and 6.5. In order to achieve a better understanding of $[Ca^{2+}]_i$ transients in the soma of pyramidal cells, a simple model of reaction-diffusion in a spherical cell was utilised (Sala and Hernández-Cruz, 1990). The model included Ca^{2+} and a fast high-affinity mobile buffer (dye) of concentration $[B_m]$ as diffusing species. Binding of Ca^{2+} to dye occurred in the presence of a low affinity immobile buffer of concentration $[B_s]$, which competed for Ca^{2+}. To keep the model as simple as possible, Ca^{2+} leakage and extrusion were not included. Model parameters were selected from the experimental and theoretical literature (see Table 3), with the exception of the dissociation constant K_D^{Bs} of $[B_s]$ which was adjusted by trial-and-error to produce responses in reasonable agreement with experimental data. Figure 6.7 shows model responses to brief injection of a Ca^{2+} current (Figure 6.7 A) peaking ≈ 5 ms after the maximum of the action potential, taken as t=0, and decaying in ≈ 10 ms (see Figure 6.5 A). The largest current value, 400 pA, was selected in agreement with experimental results, considering that about 20% of the total current entered from the soma. The time course of $[Ca^{2+}]_i$ at different depths below the cells surface (0.25, 1.5, 3.0, 4.5 and 6.0 μm) is shown in Figure 6.7 B. In the outermost shell $[Ca^{2+}]_i$ reached peak values ≈ 300 nM few ms after the current peak but rose at a considerably slower rate progressing towards the cell centre. As clearly evident in Figure 6.7 C, the distribution of the dye-calcium complex at the same depths represents a delayed and distorted version of $[Ca^{2+}]_i$. To compare model predictions to experimental results, contribution from out-of-focus fluorescence (Hiraoka et al., 1990) was taken into account by adding a weighted average of signals from peripheral shells to inner shells (Figure 6.7 D). Finally, model output was averaged over 5 ms intervals to simulate photo-charge integration by the CCD sensor (Figure 6.7 E, dashed lines).

The combination of model values for total $[B_s]$ and K_D^{Bs} corresponded to an incremental Ca^{2+}-binding ratio (Neher and Augustine, 1992)

$$\kappa = \frac{\Delta[B_s Ca]}{\Delta[Ca^{2+}]_i} = \frac{[B_s]\ K_D^{B_s}}{([Ca^{2+}]_{rest} + K_D^{B_s})\ ([Ca^{2+}]_{peak} + K_D^{B_s})} \qquad (6.4)$$

of about 120 (mean value, averaged over all discrete shells in which the intracellular space was subdivided). For comparison, values of κ in the range 64 to 186 were estimated experimentally in the proximal apical dendrites of hippocampal CA1 neurons (Helmchen et al., 1996).

TABLE 3. Dye rate constants (from Eberhard and Erne, 1991).

T	Calcium Green		Calcium Crimson	
°C	K_{off}	K_{on}	K_{off}	K_{on}
	s^{-1}	$\mu M^{-1} s^{-1}$	s^{-1}	$\mu M^{-1} s^{-1}$
20.5	139	570	187	710

6.1.6 Discussion

Intracellular Ca^{2+} was visualised by loading cells with fluorescent dyes selective for this ion and measuring fluorescent transients using a fast CCD camera.

Fast Ca^{2+} imaging (i.e. faster than standard video-rate) of $[Ca^{2+}]_i$ gradients has been performed either with confocal microscopy operating in the line-scan mode (Hernández-Cruz et al., 1990), or with cooled CCD devices (Lasser-Ross et al., 1991). A substantial effort was devoted to obtain simultaneously high spatial and temporal resolution of fluorescence signal detection. This was achieved by assembling a range of different optical and electronic components optimised for high-speed detection of fluorescence emissions from long-wavelength Ca^{2+}-selective probes. The core of the optical detection section was based on a low-cost commercial CCD sensor, originally designed for industrial applications, whose output was digitised by a specialised A/D board. This allowed image capture at rates up to of 735 frames/s, with the possibility of acquiring over 3500 full-frame images in sequence with 12 bit/pixel accuracy.
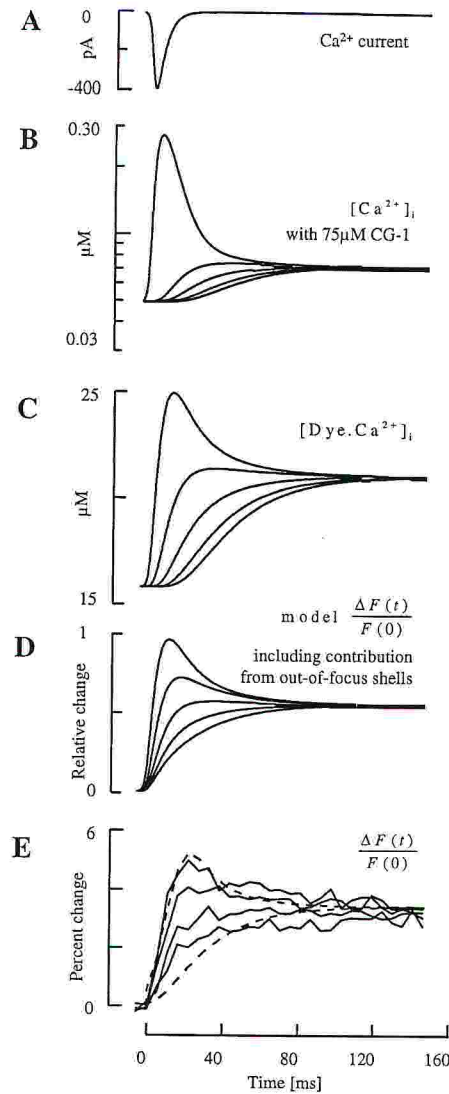
Figure 6.7 Modelling Calcium entry into the soma. A. Time waveform of the Ca^{2+} current I_{Ca} used in the source term of Eq. 6.2. B. $[Ca^{2+}]_i$ time course at various depths within the cell: 0.25, 1.5, 3.0, 4.5 and 6 μm from the surface, top to bottom. C. Time course of $[B_mCa^{2+}]_i$ at the same depths as in B. D. Relative change in model fluorescence signals associated with $[B_mCa^{2+}]_i$ distribution. Signals from inner shells included a weighted average of out-of-focus contributions from more peripheral shells. E. Solid lines: sample fluorescence responses following a single action potentials in a CA3 pyramidal cell loaded with 75 μm Calcium Green-1. Unfiltered traces were generated by averaging real fluorescence images captured at 5.4 ms intervals from 2 μm × 2 μm contiguous regions covering the space from surface to centre of the cell. Dashed lines represent a scaled version of the uppermost and lowermost trace in D, averaged over 5.4 ms periods to simulate CCD photo-charge integration during image acquisition.

Such high rates and sensitivity result from the good quantum efficiency of the sensor (40%) and the extremely high speed at which frames were transferred from the unmasked to masked regions of the CCD. The system utilised was capable of capturing hundreds of images in sequence with minimal 1.36 ms inter-frame interval at full-frame resolution (128×128 pixels) with 12bit/pixel precision. Data presented in this thesis were acquired at inter-frame intervals between 10.8 and 5.0 ms. Because of the short integration times used, photon shot-noise $N_{Ph}{}^{*}$ proved to be the dominant factor in these experiments, which made CCD cooling unnecessary above about 90 frames/s. The relative performances of two single-wavelength dyes, Calcium Green-1 and Calcium Crimson, were evaluated in terms of stationary and time-dependent fluorescence signals. Despite the smaller $\Delta F(t)$ signals produced, Calcium Crimson allowed fluorescence transient measurements at higher frame rates than Calcium Green-1 whose lower resting fluorescence (see Figure 6.3) made it difficult to estimate reliably $F(0)$ above 200 frames/s. At the high rates utilised, the limiting factor proved to be the dye relaxation time τ (see equation 6.3) so that frequencies higher than 200 frames/s would seem unnecessary for measuring $[Ca^{2+}]_i$ transients at room temperature. In fact, $\Delta F(t)/F(0)$ responses elicited by single action-potentials were detected at the maximum camera rate of 400 frames/s without appreciable differences (data not shown). However, given the relatively steep dependence on temperature the $\Delta F(t)/F(0)$ rise time course (Markram et al., 1995), faster acquisition rates are probably required around physiological temperature.

High frame-rate imaging permitted the 2D visualisation of the substantial $[Ca^{2+}]_i$ gradients that developed rapidly within the cell cytoplasm following action potentials (see Figures.6.4 C and 6.5 B), with local and instantaneous magnitude depending strongly on the cell firing frequency (see Figures 6.4 B and 6.6). However, it is important to realise that fast imaging of Ca^{2+} poses also a number of problems when trying to derive a quantitative estimate $[Ca^{2+}]_i$ from $\Delta F(t)/F(0)$, that is to say from the concentration of intracellular dye-bound calcium $[B_mCa^{2+}]_i$. The common assumption is that ion and dye are locally in equilibrium so that $[Ca^{2+}]_i$ can be derived from the mass-action law. This is reasonable when $[B_mCa^{2+}]_i$ gradients are

---

* The overall noise associated with the acquisition of an image by a CCD device is $N_T = (N_R^2 + N_D^2 + N_{Ph}^2)^{1/2}$. Here N_R and N_D are the readout noise and the dark-charge noise of the CCD, respectively, whereas N_{Ph} is the photon shot-noise associated with the fluorescence signal.

imaged by integrating fluorescence signals over intervals significantly longer than τ (Neher and Augustine, 1992), but not for the short exposure times used in the present experiments. Numerical simulations on an extremely simplified spherical cell model showed that diffusion patterns for $[Ca^{2+}]_i$ can differ substantially from those reported by $\Delta F(t)/F(0)$ (compare Figures 6.7 B and 6.7 D). For fixed incremental Ca^{2+}-binding ratio around 120, $[B_m Ca^{2+}]_i$ distributions agreed with measured fluorescence gradients only for $D_{Bm} \approx D_{ca}$, indicating that the presence of a rapidly diffusing dye may substantially alter the time course of the "unperturbed" somatic $[Ca^{2+}]_i$ gradients. The problem cannot be solved simply by lowering the dye concentration as rapid $[Ca^{2+}]_i$ elevations would just saturate the dye faster, particularly near the cell membrane, producing a non-linear fluorescence response. For these reasons, $\Delta F(t)/F(0)$ should be understood to represent, at best, a low-pass filtered version of the free Ca^{2+} transients (Nowycky and Pinter, 1993). It appears that the challenge for the future would be to perform quantitative analysis of rapid $[Ca^{2+}]_i$ gradients using fluorescence data in the context of realistic reaction-diffusion schemes, taking into account the details of cell geometry and channel distribution.

6.2 Temperature dependence of GABAergic activity in the neonatal rat hippocampus

A peculiar characteristic of the hippocampus of neonatal rats is the presence of spontaneous network-driven oscillatory events, the so-called giant depolarising potentials (GDPs). These events that can be recorded in slices (Ben Ari et al., 1989) as well as in the intact hippocampal formation (Khalilov et al., 1997; Leinekugel et al., 1998) consist in large depolarisations with superimposed fast action potentials followed by an afterhyperpolarisation. GDPs are generated by the interplay between GABA acting on $GABA_A$ receptors (Ben Ari et al., 1989) and glutamate acting mainly on AMPA type ionotropic receptors (Gaiarsa et al., 1991; Bolea et al., 1998). As in many other brain structures (Wu et al., 1992; Serafini et al., 1995; Chen et al., 1996; Kaneda et al.,1996; Owens et al., 1996), in early postnatal life GABA depolarises and excites neuronal membranes by an outward flux of chloride (Cherubini et al., 1991).

This highly correlated neuronal activity is thought to promote functional maturation of precursor networks (Goodman and Shatz, 1993). This could be achieved via an elevation of $[Ca^{2+}]_i$ following calcium entry through voltage-activated calcium channels (Leinekugel et al., 1995). Thus, calcium fluctuations occurring simultaneously in groups of neighbouring cells and strictly correlated with GDPs can be detected by optical recordings with Ca^{2+}-sensitive dyes in the CA1 (Garaschuk et al., 1998) and in the CA3 (Leinekugel et al., 1997) area of the hippocampus. Interestingly, early network oscillations and associated calcium bursts can be blocked when the temperature is reduced from 32-35°C to 20-24°C (Garaschuk et al., 1998). The final part of this thesis work was aimed at investigating the effects of changing temperature on GDPs generation and on GABAergic synaptic transmission in the CA3 hippocampal area of newborn rats, by using electrophysiology and the high space-time resolution calcium imaging previously described.

6.2.1 Methods

Neonatal Wistar rats (P3-P6) were used. During the experiments, slices were superfused at 3ml/min either at room temperature (24 °C) or at 32 °C.

Temperature was changed by heating the final part of the perfusion inflow tube with a resistance and was controlled by a thermocouple placed in the bath. Changes in temperature were obtained in a few minutes.

Electrical recordings were made from CA3 pyramidal neurons in the slice using patch pipettes having a resistance of 3-5 MΩ when filled with intracellular solution containing (in mM): 140 KCl, 1 MgCl$_2$, 5 HEPES, 1 EGTA, 10 sucrose, 2 Na$_2$ATP (pH 7.2 adjusted with KOH).

Spontaneous miniature GABAergic currents were recorded in TTX (1 μM), to block voltage-gated sodium channels and kynurenic acid (1 mM) to block ionotropic glutamate receptors.

Drugs were dissolved in the external solution and applied in the bath via a three way tap system by changing the superfusion solution to one which differed only in its content.

Monosynaptic GABAergic responses and GDPs were evoked in CA3 pyramidal cells by extracellular electrical stimulation, (as described in chapters 3 and 4), in the presence of kynurenic acid (1 mM) to block ionotropic glutamate receptors and in the presence of a low (10 nM) concentration of TTX, to reduce spontaneous events. Monosynaptic GABAergic currents were evoked by trains of six voltage pulses (4-10 V amplitude and 40 μs duration at 80-160 ms

interpulse interval, every 20 s). GDPs were evoked by short (4-8) trains of pulses (10-20 V amplitude and 40 μs duration at 10 ms interpulse interval).

GABA (0.5 mM) was applied via a patch electrode (having a resistance of about 2 MΩ) connected to a pneumatic picopump triggered by the computer. The pipette was positioned close (20-60 μm) to the soma of the patched cell (the duration of the application ranged between 5 to 40 ms).

In the imaging experiments, slices were incubated for 2-3 hours at 32 °C with a solution containing 10-20 μM of the calcium sensitive probe fluo-3 (AM-ester) before being transferred to the recording chamber. Fluo-3 was dissolved in dimethylsulphoxide (DMSO) at the final concentration of 10 mM, so that the final DMSO concentration in the incubating bath never exceeded 0.2 %.

6.2.2 Temperature dependence of GDPs

Stable whole cell recordings (in current clamp configuration) lasting more than 30 min were obtained at 32 °C from CA3 hippocampal pyramidal cells in slices from P3-P6 old rats that exhibited spontaneous GDPs (n=23). These events consisted of large (30-50 mV) depolarising potentials lasting 400-700 ms, which triggered action potentials, followed by an afterhyperpolarisation. GDPs were completely abolished by bicuculline (10 μM) and/or by kynurenic acid (1 mM) indicating that they originated from the interplay between GABA and glutamate (Bolea et al., 1998). Bicuculline also blocked spontaneous ongoing synaptic activity, suggesting that at early stages of development, GABA-mediated synaptic responses represent the main excitatory postsynaptic currents that are active at resting membrane potential (Hosokawa et al., 1994).

When the temperature was decreased from 32 °C to 24 °C, GDPs disappeared while spontaneous action potential-dependent GABA-mediated synaptic responses were still present. However, as shown in the example of Figure 6.8, these occurred at lower frequency and, in comparison with the events recorded at 32 °C, had slower kinetics. In particular, in six neurons in which more than 100 events were recorded at 32 °C and 24 °C, no significant changes in peak amplitude were detected (at -70 mV peak amplitude was 5.6 ± 1.1 mV at 24 °C and 6.6 ± 1.1 mV at 32 °C, mean ± SEM) whereas a decrease in frequency and an increase in half width were

observed: the frequency was 3.16 ± 0.21 Hz and 1.56 ± 0.15 Hz while the half width was 39.6 ± 3.9 ms and 63.5 ± 1.6 ms at 32 °C and 24 °C (mean $\pm$ SEM), respectively.

6.2.3 Temperature dependence of GABA-induced calcium transients

The disappearance of spontaneous GDPs at 24 °C indicates that temperature has striking effects at the network level. Therefore, in a subset of cells in the CA3 area of the hippocampus, the excitability of the network, at different temperatures, was investigated by monitoring calcium entry following evoked GDPs or direct application of GABA.

Calcium transients associated to spontaneous GDPs have been detected in hippocampal slices loaded with AM-ester calcium dyes (Garashuk et al. 1998). In this thesis, calcium transients, associated to GDPs evoked by repetitive stimulation of the stratum radiatum in the presence of kynurenic acid (1 mM) were studied in four slices at 24 °C and 32 °C (see the schematic drawing of Figure 6.9 A). As illustrated in the representative example of Figure 6.9, at both temperatures, evoked GDPs were associated to calcium signals that occurred with appreciable delays within the set of loaded neurons, indicating a propagation of firing activity. Calcium transient were not recorded in the patched neuron because of the cell dialysis. In comparison to 24 °C, at 32 °C evoked GDPs had a smaller amplitude. Moreover associated changes in fluorescence ($\Delta F/F$) in the surrounding cells were smaller and had a more rapid onset (Figure 6.9 B). Figure 6.9 C shows seven false colour images selected from the frame sequences recorded simultaneously with the evoked GDPs (arrows in Figure 6.9 B) at 24 °C and 32 °C. Interestingly, in this particular experiment, at both temperatures, a propagation of the signal from the region closer to the stimulating electrode (b) towards the CA1 hippocampal area was observed. Evoked GDPs as well as calcium signals were prevented by bicuculline (10 μM, data not shown).

Similar results were obtained in three slices when GABA was locally applied (in the presence of kynurenic acid, 1 mM) by a pressure pipette positioned close the patched cell (Figure 6.10 A). Pressure application of GABA at a holding potential of -70 mV, produced at both temperature an inward current that was associated to an increase in fluorescence in neighbouring cells. At 32 °C, GABA-induced currents had a faster kinetics and, as in the case of the evoked GDPs, they were associated with a calcium signal that was faster and lower in amplitude. In this particular

case, at 32 °C the signal propagated towards cells located in the stratum radiatum (possibly interneurons) with a delay of hundreds of ms (Figure 6.10 B and C). At 32 °C, the spread of the signal towards stratum radiatum was also observed in one of the four slices in which calcium transients were induced by GDPs. Temperature-dependent changes in calcium signals could be observed in the same slice by cooling down and warming up the slice repetitively (up to four times).
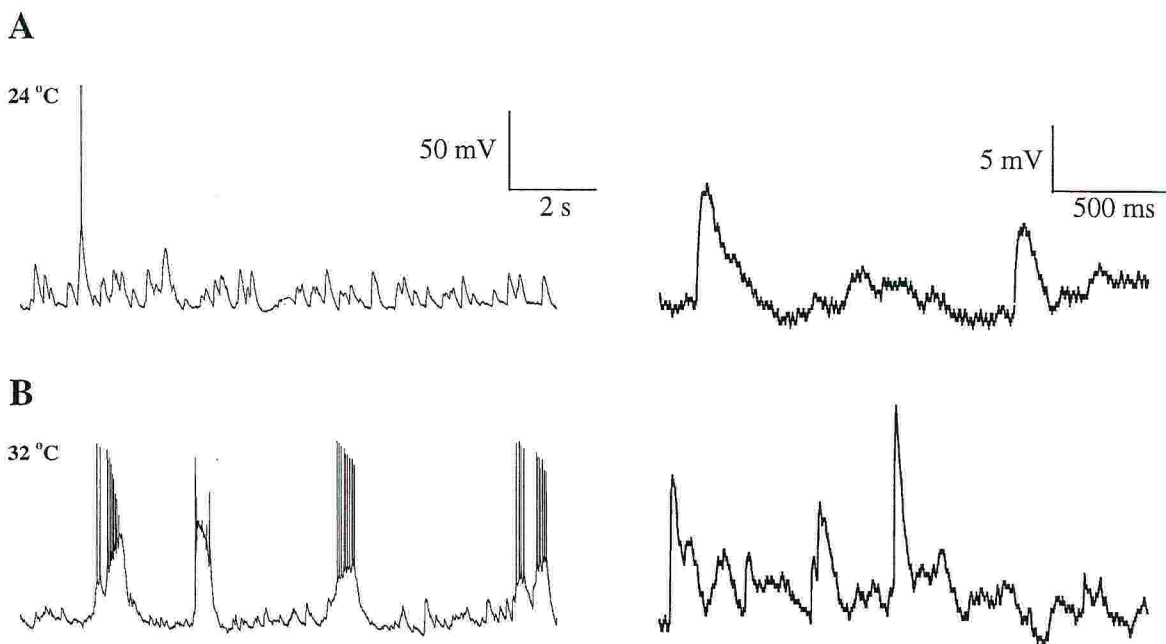

Figure 6.8 Spontaneous GDPs occur only at 32 °C. A. Traces recorded in current clamp mode from a CA3 pyramidal cell at P5, showing spontaneous ongoing synaptic activity at 24 °C at two different time scales. B. Same as A but at 32 °C. Notice that GDPs can be observed only at 32 °C.
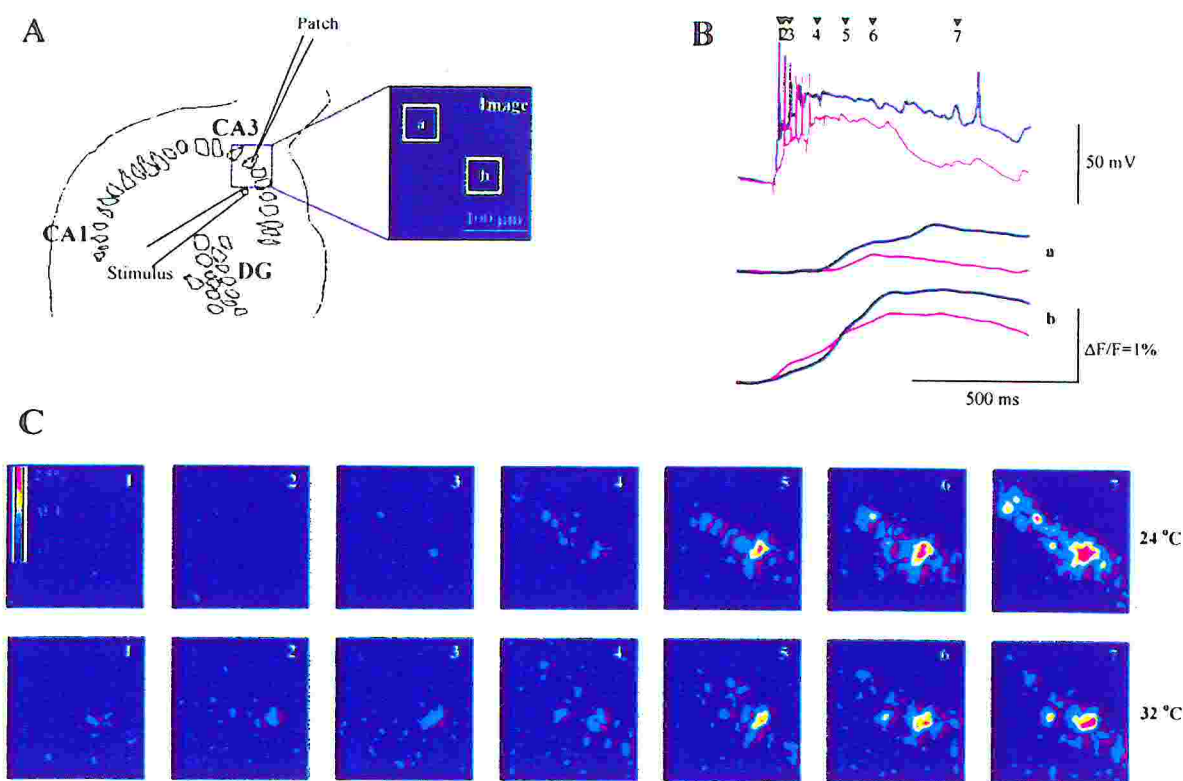
Figure 6.9 Calcium signals induced by evoked GDPs. A. Scheme illustrating the experimental protocol. The blue region indicates the area of the slice in which calcium fluorescence was imaged. GDPs were evoked by electrical stimulation with a pipette positioned in the stratum radiatum (stimulus) and recorded with a patch pipette (patch) from a CA3 pyramidal neuron. B. Upper traces: GDPs evoked at 24 °C (blue trace) and at 32 °C (red trace). Middle and bottom traces: correspondent calcium transients averaged in the small regions a and b indicated in A. C. False colour images selected from the frame sequences recorded simultaneously with the currents reported in B. The timing of each image is indicated by the arrows drawn in B. Upper and bottom rows belong to sequences taken at 24 °C and 32 °C respectively. The colour scale is reported in the first image.

These results confirm the depolarising action of GABA early in development and indicate that the firing activity evoked either by electrical stimulation or GABA application can propagate. Moreover, the present data suggest that, at more physiological temperature (32 °C), evoked GDPs can spread faster and involve a larger number of neurons. This is in the presence of kynurenic acid that prevents the occurrence of spontaneous GDPs.
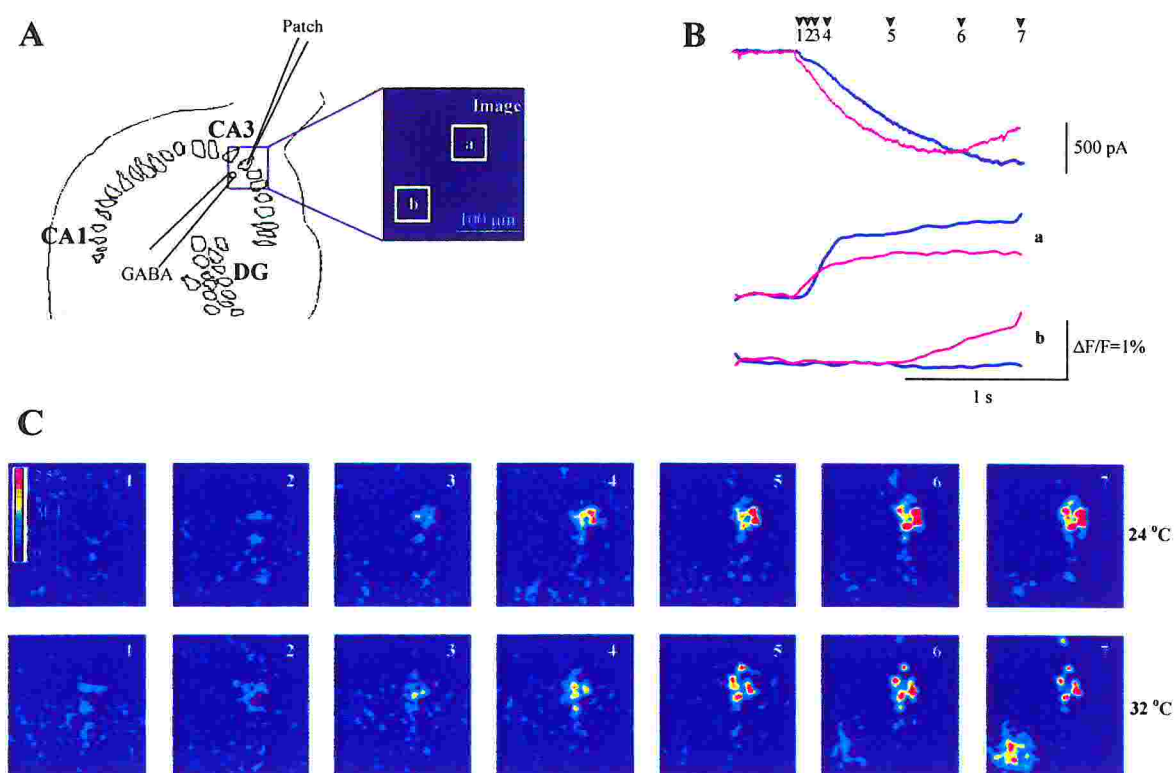
104

Figure 6.10 Calcium signals induced by brief applications of GABA. A. Scheme illustrating the experimental protocol. The blue region indicates the area of the slice in which calcium fluorescence was imaged. Currents evoked by brief (16 ms) applications of GABA were recorded from a CA3 pyramidal neuron at P4. B. Upper traces: current induced by GABA application at 24 °C (blue trace) and at 32 °C (red trace). Middle and bottom traces: correspondent calcium transients averaged in the small regions a and b indicated in A. C. False colour images selected from the frame sequences recorded simultaneously with the currents reported in B. The timing of each image is indicated by the arrows drawn in B. Upper and bottom rows belong to sequences taken at 24 °C and 32 °C respectively. The colour scale is reported in the first image.

6.2.4 Temperature dependence of miniature GABAergic currents

To investigate the mechanisms underlying the above mentioned effects on the network activity, experiments were performed on miniature and evoked monosynaptic GABAergic currents at 24 °C and 32 °C. Spontaneous miniature GABAergic currents were recorded at a holding potential of -70 mV from five CA3 pyramidal cells at 24 °C and 32 °C (more than hundred events for

105

each experimental condition) in the presence of kynurenic acid (1 mM) and tetrodotoxin (TTX, 1 µM). These currents were reversibly abolished by bicuculline (10 µM) implying that they resulted from the activation of $GABA_A$ receptors. At 24 °C, miniature GABAergic currents occurred at low frequency (< 1 Hz). The representative recording of Figure 6.11 A illustrates spontaneous miniature events recorded from the same neuron at 24 °C and 32 °C. The figure clearly shows that the frequency (but not the amplitude) of miniature events is strongly temperature-dependent (Figure 6.11 B and C) as demonstrated by the shift to the left of the cumulative inter-event interval distribution at 32 °C (p=0.0001, Kolmogorov-Smirnov test). Furthermore, at this temperature, the kinetics of miniature synaptic currents was faster (Figure 6.11 D). Unlike the frequency, amplitude distributions were skewed towards the higher values in both experimental conditions, and consisted of an initial peak followed by a tail of larger amplitude events (Figure 6.12 A).

On average, in five cells, rising the temperature from 24 °C to 32 °C, produced an increase in frequency of miniature currents (from 0.56 ± 0.2 Hz to 1.55 ±0.2 Hz, mean ± SEM, Figure 6.12 B) without a significant change in their amplitude (36 ± 9.2 pA and 47 ± 2 pA at 24 °C and 32 °C, mean ± SEM, respectively). Taken together these data strongly suggest that GABA release is temperature-dependent. The other striking effect of temperature was on the kinetics of synaptic events. A decrease of the mean rise and decay time (from 1.3 ± 0.15 ms to 0.9 ± 0.11 ms and from 14.8 ± 2.9 to 7.5 ± 2.4, mean ± SEM, respectively, Figure 6.12 B) was observed, when the temperature was raised from 24 °C to 32 °C. Thus, raising the temperature has both pre and postsynaptic effects: on one hand it enhances GABA release on the other hand it speeds up the kinetics of $GABA_A$ receptors.

The postsynaptic effect has been further assessed by the experiments in which GABA was applied directly onto the principal cell by brief pressure pulses of different duration (in the presence of TTX, 1 µM). Also in this case, rising the temperature from 24 °C to 32 °C speeded up the kinetics of GABA-induced currents (Figure 6.13). In the experiments in which GABA was applied for 10 ms (n=4), the rising and decaying phases of GABA-induced currents were fitted with the exponential function $\alpha \cdot e^{-t/\tau}$. Thus, the time constant τ of the rising and the decaying phases (τ_{rise} and τ_{decay}) were: τ_{rise} = 0.63 ± 0.17 s and τ_{decay} = 1.36 ± 0.38 s at 24 °C and τ_{rise} = 0.31 ± 0.12 s and τ_{decay} = 0.74 ± 0.22 s at 32 °C, respectively (mean ± SD).
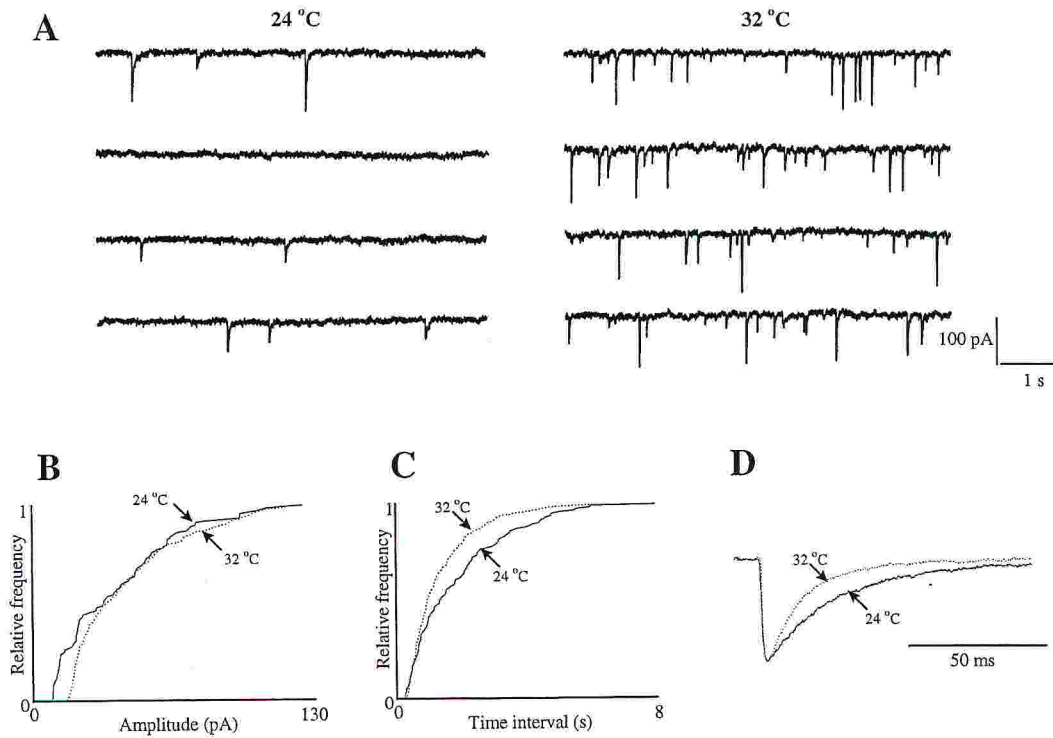
Figure 6.11 Spontaneous miniature currents are temperature-dependent. A. Four consecutive traces showing spontaneous currents recorded at -70 mV in the presence of 1 μM TTX at 24 °C (left) and at 32 °C (right). B and C. Cumulative distribution of the miniature current amplitudes (B) and of the interevent intervals (B) of the experiment shown in A, evaluated with 140 events at 24 °C and with 321 events at 32 °C. D. Normalised and superimposed currents obtained at both temperatures from the experiment shown in A.
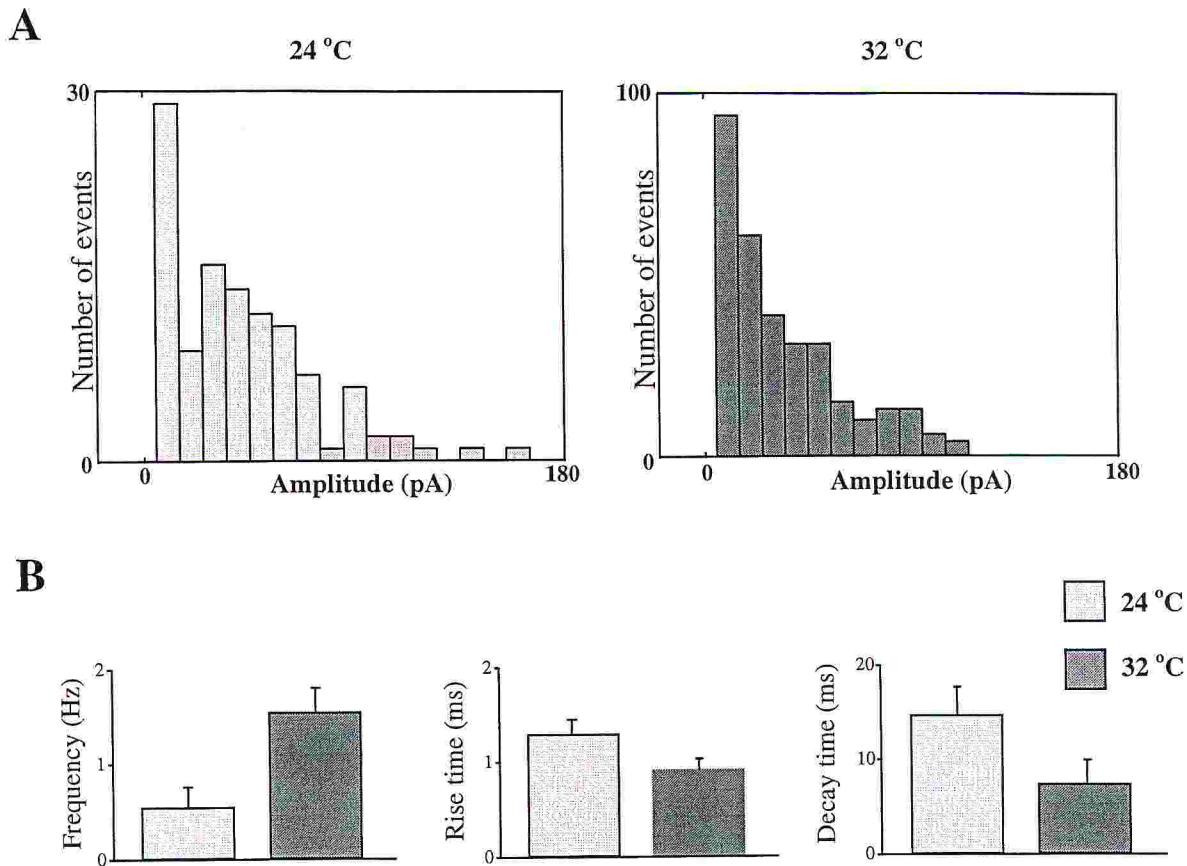
Figure 6.12 Temperature-dependent effects on miniature currents. A. Amplitude distribution histogram of miniature currents shown in Figure 6.11 (10 pA bin). Notice that the amplitude distribution is similar at 24 °C and at 32 °C. B. Temperature-dependent changes in frequency, rise time and decay time of miniature currents. Each column represents the mean ± SEM (n=5 experiments) of frequency, rise time and decay time obtained at 24 °C (light column) and 32 °C (dark column). Differences between data obtained at the two different temperatures are highly significant (see text).

6.2.5 Temperature dependence of GABA-mediated synaptic depression

As already mentioned, the increase in frequency of miniature events observed when the temperature was raised from 24 °C to 32 °C has clearly a presynaptic site of origin. In order to test whether modifications of the dynamics of the release machinery could be responsible for this phenomenon, in another set of experiments the effects of temperature on synaptic responses evoked by brief trains of stimulation was investigated.
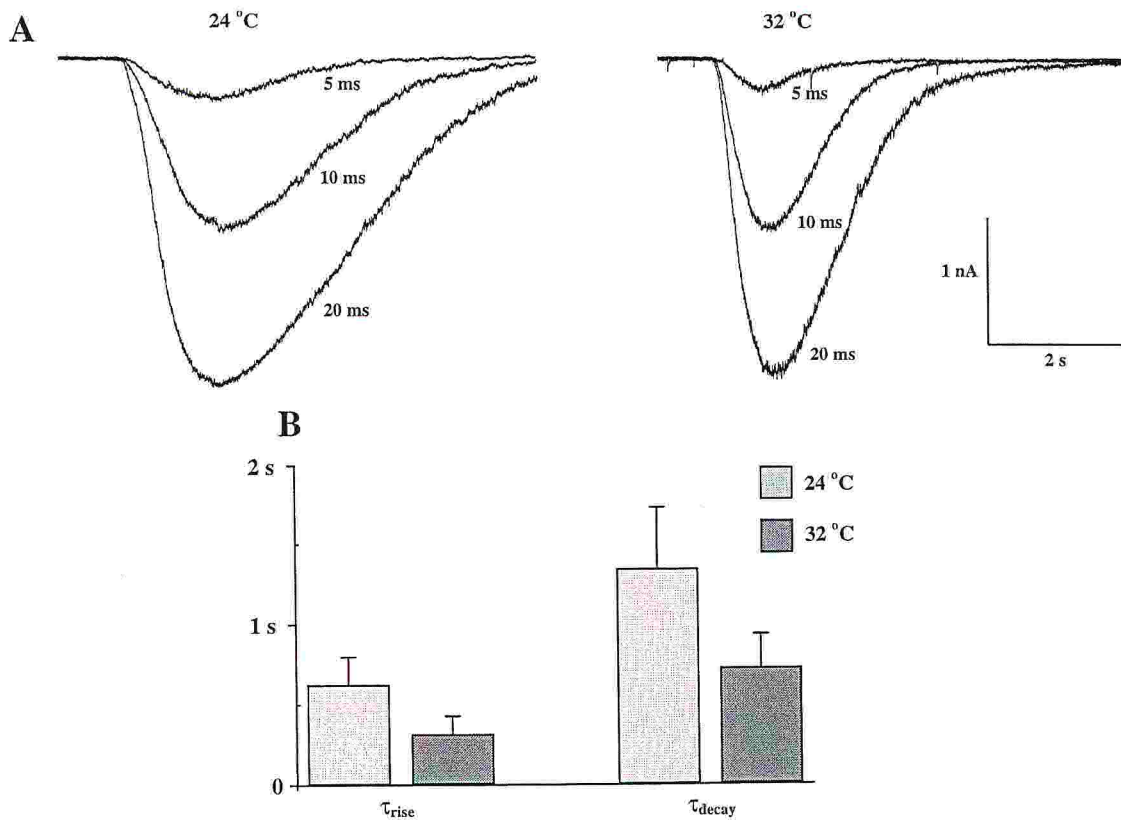
Figure 6.13 Temperature dependence of currents evoked by local application of GABA. A. Currents evoked by pressure application 0.5 mM GABA lasting for 5, 10 and 20 ms duration at 24° (left) and at 32° (right). B. Temperature-dependent changes of the rise (τ_{rise}) and decay (τ_{decay}) time constants obtained, in four different cells, by interpolating with an exponential function ($f=\alpha \cdot e^{-t/\tau}$) the rising and decaying phase of the currents evoked by application 0.5 mM GABA (10 ms duration) at two different temperatures. Each column represents the mean ± SD at 24 °C (light column) and 32 °C (dark column).

Presynaptic fibers were stimulated with brief trains of six pulses at 6.25 and 12.5 Hz both at 24 °C and 32 °C. A decrease in the amplitude of the nth synaptic current with respect to the first one was always observed. Usually, after the third response, the synaptic currents reached a stationary value. This is clearly illustrated in the representative example of Figure 6.14 A where synaptic currents evoked by 6 pulses of stimulation at 80 ms inter pulse interval are shown superimposed at 24 °C and 32 °C. In the same Figure, the average of 50 recordings are shown. The first response was characterised by a high reliability while the following ones showed a certain degree of variability from trial to trial. Accordingly, an increase in the CV from the first to the

last pulse (Figure 6.14 C) was observed. Moreover, the number of failures was extremely rare or absent.
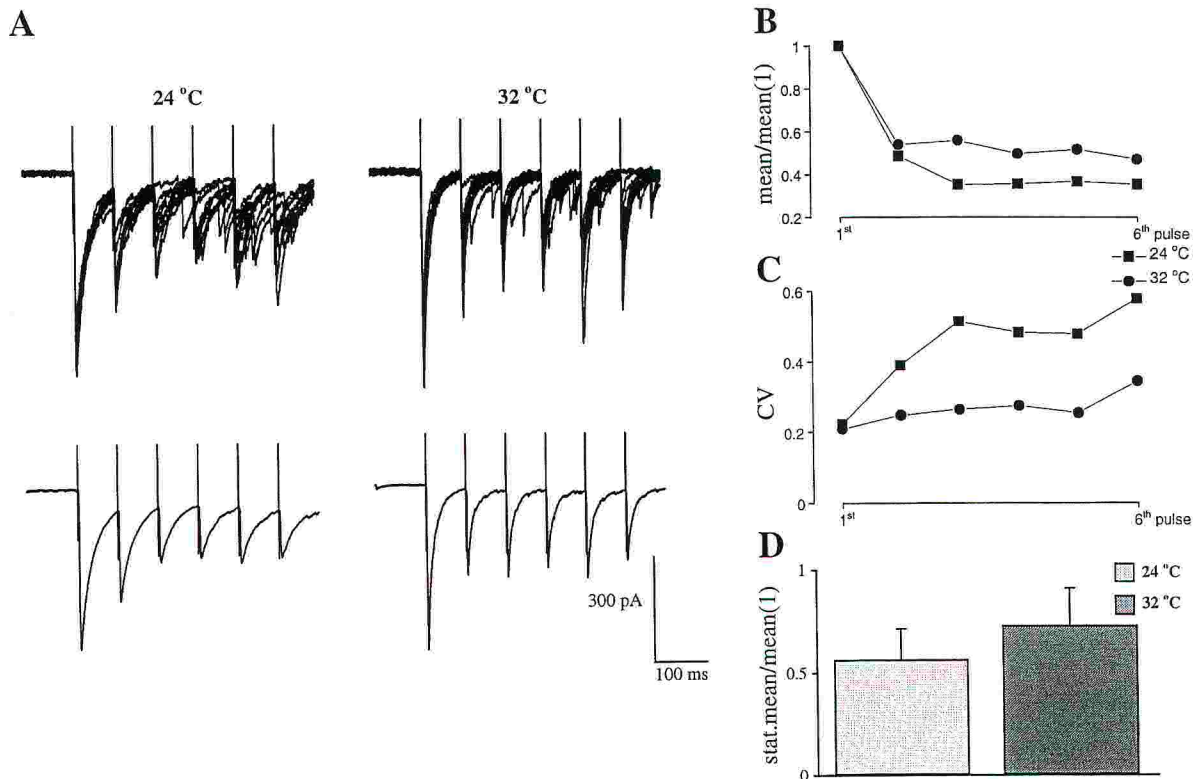
Figure 6.14 Temperature-dependent depression of GABA-mediated synaptic currents evoked by low-frequency stimulation A. Top: 8 consecutive recordings of currents evoked by 6 pulses of stimulation at 80 ms interpulse interval at 24 °C (left) and at 32 °C (right) are superimposed. Bottom: Averages of 50 recordings at the two different temperatures including those shown on the top. B and C. Time course of the mean current amplitudes normalised to the first ones (B) and of the CVs (C) relative to the experiment reported in A. Squares and circles represents data recorded at 24 °C and 32 °C respectively. D. Temperature-dependent changes of GABA-mediated synaptic depression. Each column represents the mean ± SD (n=4 experiments) of the ratio between the stationary mean current amplitude (obtained by averaging the 4th, 5th and 6th mean current amplitudes) and the first one at 24 °C (light column) and 32 °C (dark column).

When the temperature was raised from 24 °C to 32 °C, the depression of synaptic responses was attenuated (Figure 6.14). This effect was associated to a decrease in the CV. This was found in

all cells tested (n=4, Figure 6.14 D). The degree of depression was expressed as the ratio between the mean peak amplitude of the last three responses (those at the stationary value) and the first one. This ratio was 0.57 ± 0.15 and 0.73 ± 0.18 at 24 °C and 32 °C, respectively (mean $\pm$ SD). Similar results were obtained when the stimulation frequency was 6.25 Hz (Figure 4.7) indicating that the effects of temperature do not depend much on the frequency of stimulation.

6.2.5 Discussion

The results described in this section provide evidence that network activity in the developing hippocampus is strongly temperature-dependent and that GDPs induction relies on the increased excitability of the system due to an enhancement of GABA release.

In the neonatal hippocampus, calcium signals associated to GDPs depend on calcium entry through voltage-activated calcium channels following membrane depolarisation by GABA or $GABA_A$ agonists (Leinekugel et al., 1995) and/or through NMDA receptors whose magnesium block would be relieved by GABA depolarisation (Leinekugel et al., 1997; Garaschuk et al., 1998).

With the high spatio-temporal resolution of the imaging system described in this thesis it was possible to monitor the onset and propagation of calcium signals generated by evoked GDPs or by direct application of GABA at 10 ms time resolution. In fact, although it has been demonstrated that glutamate plays a role in the induction of spontaneous GDPs, GDPs could still be elicited by electrical stimulation and could propagate when ionotropic glutamate receptors were blocked by kynurenic acid (Bolea et al., 1998). In both cases, (evoked GDPs or GABA application), it is clear that the calcium signal firstly originates in one or few neurons and only subsequently (in hundreds of ms) spreads and invades clusters of neighbouring cells. Propagation of detectable calcium signals is probably underestimated because of the limited number of dye-loaded cells. Moreover, the present results suggest that, at higher temperature, GDP- or GABA-triggered calcium transients are faster and involve propagation to a larger number of cells. This phenomenon may be due to the more pronounced excitability of the network.

In terms of dynamical systems, the transition from a low firing non oscillating to an oscillating bursting behaviour such as that observed in the present experiments, represents a structural bifurcation (Rinzel and Ermentrout, 1989). Similar transitions in network dynamics have been

observed in a number of different preparations in distinct experimental conditions. For instance, synchronous bursting activity can be triggered in cultured cortical neurons by lowering the extracellular magnesium concentration (Canepari et al., 1997) or in the spinal cord preparation by applying a solution containing strychnine and bicuculline (Bracci et al., 1996). These results can be explained, in the first case, by the relieve of the magnesium block of NMDA receptors and by an increase in transmitter release, while in the second case, by the pharmacological block of inhibition. The interpretation of the temperature-dependent transition between different patterns of activity in the developing hippocampus appears to be more complex. The analysis of spontaneous and evoked GABAergic synaptic currents reported here suggest that the structural transition towards an oscillating behaviour is due to a temperature-dependent enhancement of GABA release.

The data reported in this section support the hypothesis that rising the temperature has both pre and postsynaptic effects on miniature GABA-mediated synaptic currents: it increases the frequency and speeds up their kinetics. An increase of transmitter release at physiological temperature has been well characterised at the neuromuscular junction (Barrett et al., 1978) and more recently, at excitatory synapses in rat visual cortex (Hardingham and Larkman, 1998). In particular, using pair recordings from interconnected pyramidal cells, Hardingham and Larkman (1998) have found that synaptic connections become more reliable at higher temperatures, increasing the mean number of transmitter quanta released per presynaptic action potential. In the experiments reported in this section, the rise in frequency of miniature events may depend on the increased release probability as well as on the increase in the number of releasing sites. However this seems unlikely due to the similar amplitude distribution observed in the majority of the cases at different temperatures. In line with the data on excitatory transmission in the visual cortex (Hardingham and Larkman, 1998), rising the temperature did not change the mean amplitude of miniature events suggesting that the quantal size was not modified. The change in the kinetics of synaptic currents, also demonstrated by the similar modifications of GABA-evoked currents, can be explained by changes in the kinetics of GABA receptor channels.

Temperature had striking effects also on GABA-mediated synaptic responses evoked by low frequency stimulation of presynaptic fibers. In contrast to hippocampal glutamatergic synapses (Allen and Stevens, 1994), GABAergic ones were more reliable and the occurrence of failures was very low, indicating, in agreement with other studies (Miles 1990; Edwards et al., 1990;

Lambert and Wilson, 1993) a low quantal variance. Moreover, in comparison with glutamatergic responses, where different patterns of activity (depression, facilitation or both) can be recorded (see chapters 3 and 4), an attenuation of synaptic currents (low-frequency synaptic depression) was routinely observed (Pearce et al., 1995). This low-frequency depression was temperature-dependent, being reduced at 32 °C. Since the number of available quanta is progressively decreased during the presynaptic train of action potentials, the stationary synaptic response that is reached after few synaptic events can be at least partially affected by the rate of recovery from synaptic depletion (Dittman and Regehr, 1998). In keeping with this hypothesis, the evidence that the variability of synaptic responses within the train is higher at the lowest temperature suggests that the rate of recovery of available quanta is faster at 32 °C. These results, together with those on the frequency of miniature GABAergic currents, suggest that GABAergic vesicular release is more efficient at 32 °C because the machinery of release is faster. However, the possibility that desensitisation of GABA receptors may contribute to the low-frequency synaptic depression (Jones and Westbrook, 1995) cannot be excluded. In this respect, recovery from desensitisation would be faster at higher temperature.

The experiments reported in this thesis lead to the conclusion that rising the temperature increases the efficiency of GABA release and therefore enhances network excitability. In addition, the speed-up of the kinetics of postsynaptic signals may contribute to this enhancement by reducing the shunting effects associated to the anionic conductance (Chen et al., 1996).

6.3 Future perspectives

A common feature of biophysical events is the presence of macroscopic deterministic dynamical processes generated by averaging or integrating microscopic stochastic events. The typical example is the integration of a large number of stochastic openings of voltage-gated ionic channels leading to the deterministic generation of an action potential. According to the quantal theory of neurotransmitter release, something similar may occur in the phenomenon of synaptic transmission, where stochastic release of single transmitter quanta may be subject to an integration operated by synapses or neural networks. This operation may appear trivial (or

similar to the case of single channel signal integration) in synapses characterised by a large number of releasing sites (> 100) such as the auditory brainstem Calyx of Held (von Gersdorff et al., 1997), or the cerebellar climbing fiber (Silver et al., 1998). The problem of understanding signal integration seems much more complicated in other central synapses, especially in synapses characterised by a small number of releasing sites (< 10) such as the glutamatergic hippocampal synapses. This problem, which is fully discussed in this thesis, is a fundamental ingredient to understand neuronal networks activity and function. In order to investigate space and time integration of synaptic signal, appropriate statistical frameworks such as that presented in this thesis must be coupled to experimental techniques that enable to record nervous activity from several neurons. In this respect, optical techniques offer many advantages, especially if coupled with traditional electrophysiological techniques. In particular, they offer the possibility to detect nervous signals at a high space-time resolution (CCD imaging). At present, optical techniques are intrinsically limited by the *nature* and the *quality* of optical signals, which are often indirect measurements of physiological activity, as in the case of calcium imaging (see section 6.1), and have typically a worse S/N in comparison to recordings with microelectrodes. Nevertheless, the use of optical techniques appears to be necessary in the future to investigate nervous activity in different compartments of a single neuron or in many neurons simultaneously.

7 REFERENCES

ALLEN, C. AND STEVENS, C. F. An evaluation of causes for unreliability of synaptic transmission. *Proc. Natl. Acad. Sci. USA* 91: 10380-10383, 1994.

ALVAREZ DE TOLEDO, G., FERNÁNDEZ-CHACÓN, R. AND FERNÁNDEZ, J. M. Release of secretory products during transient vesicle fusion. *Nature Lond.* 363: 554-558, 1993.

ANDREASEN M. AND LAMBERT J. D. C. Regenerative properties of pyramidal cell dendrites in area CA1 of the rat hippocampus. *J. Physiol. Lond.* 483.2: 421-441, 1995.

ARTALEJO, C. R., HENLEY, J. R., NcNIVEN, M. A. AND PALFREY, H. C. Rapid endocytosis coupled to exocytosis in adrenal chromaffin cells involves Ca^{2+}, GTP and dynamin, but not clathrin. *Proc. Natl. Acad. Sci. USA* 92: 8328-8332, 1995.

ASHER, P. AND NOVAK, L. The role of divalent cations in the N-methyl-D-aspartate-activated channels of mouse central neurons in culture. *J. Physiol. Lond.* 399: 247-266, 1988.

BARRETT, E. F., BARRETT, J. N., BOTZ, D., CHANG, D. B. AND MAHAFFEY, D. Temperature-sensitive aspects of evoked and spontaneous transmitter release at the frog neuromuscular junction. *J. Physiol. Lond.* 279: 253-273, 1978.

BARRETT, E. F. AND STEVENS C. F. Quantal independence and uniformity of presynaptic release at the frog neuromuscular junction. *J. Physiol. Lond.* 227: 665-689, 1972.

BASHIR, Z. I. AND COLLINGRIDGE, G. L. Synaptic plasticity: long-term potentiation in the hippocampus. *Curr. Op. in Neurobiol.* 2: 328-335, 1992.

BAXTER, D. A., BITTNER, G. D. AND BROWN, T. H. Quantal mechanisms of long-term synaptic potentiations. *Proc. Natl. Acad. Sci.* USA 82: 5978-5982, 1985.

BATTISTIN, T. AND CHERUBINI, E. Developmental shift from long-term depression to long-term potentiation at the mossy fibre synapses in the rat hippocampus. *Eur. J. Neurosci.* 6: 1750-1755, 1994.

BEAR, M. F. AND MALENKA, R. C. Synaptic plasticity: LTP and LTD. *Curr. Op. in Neurobiol.* 4: 389-399, 1994.

BEKKERS, J. M. AND STEVENS, C. F. Presynaptic mechanism for long-term potentiation in the hippocampus. *Nature Lond.* 346:724-729, 1990.

BEN ARI, Y., CHERUBINI, E., CORRADETTI, R. AND GAIARSA, J. L. Giant synaptic potentials in immature rat CA3 hippocampal neurons. *J. Physiol. Lond.* 416: 303-325, 1989.

BENNETT, M. R. AND FLORIN, T. A statistical analysis of the release of acetylcholine at newly formed synapses in striated muscle. *J. Physiol.* 238: 93-107, !974.

BETS, W. J. Depression of transmitter release at the neuromuscular junction. *J. Physiol. Lond.* 206: 629-644, 1970.

BLISS, T. V. P. AND COLLINGRIDGE, G. L. A synaptic model of memory: long-term potentiation in the hippocampus. *Nature Lond.* 361: 31-39, 1993

BLISS, T. V. P. AND LØMO, T. Long-lasting potentiation of synaptic transmission in the dentate of the anesthetized rabbit following stimulation of the perforant path. *J. Physiol. Lond.* 232: 331-356, 1973.

BOLEA, S., AVIGNONE, E., SANCHEZ-ANDRES, J. V., BERRETTA, N. AND CHERUBINI, E. Non-NMDA receptor activation is essential for generating giant depolarizing potentials (GDPs) in neonatal rat hippocampal slices. *J. Physiol. Lond.* 509: P69, 1998.

BORST, J. G. G., HELMCHEN, F. AND SAKMANN, B. Presynaptic and postsynaptic whole-cell recordings in the medial nucleus of the trapezoid body of the rat. *J. Physiol. Lond.* 489: 825-840, 1995.

BORST, J. G. G. AND SAKMANN, B. Calcium influx and transmitter release in a fast CNS synapse. *Nature Lond.* 383: 431-434, 1996.

BRACCI, E., BALLERINI, L. AND NISTRI, A. Spontaneous rhythmic burst induced by pharmacological block of inhibition in lumbar motoneurons of the neonatal rat spinal cord. *J. Neurophysiol.* 75: 640-647, 1996.

BRECKENRIDGE, L. J. AND ALMERS, W. Currents through the fusion pore that forms during exocytosis of a secretory vesicle. *Nature Lond.* 328: 814-817, 1987.

BROWN T. H. AND ZADOR A. M. Hippocampus. In *The Synaptic Organization of the Brain* (ed. by Gordon M. Shepherd), Oxford University Press, Oxford-New York, 1990.

BURNASHEV, N., SCHOEPFER, R. AND MONYER, H. Control by asparagine residues of calcium permeability and magnesium blockade in the NMDA receptor. *Science* 257: 1415-1419, 1992.

CALLAWAY, J. C. AND ROSS, W. N. Frequency-dependent propagation of sodium action-potentials in dendrites of hippocampal CA1 pyramidal neurons. *J. Neurophysiol.* 74: 1395-1403, 1995.

CANEPARI, M., BOVE, M., MAEDA, E., CAPPELLO, M. AND KAWANA, A. Experimental analysis of neuronal dynamics in cultured cortical networks and transitions between different patterns of activity. *Biol. Cybern.* 77: 153-162, 1997.

CHARPAK S. AND GÄHWILER, B. H. Glutamate mediates a slow synaptic response in hippocampal slice cultures. *Proc. R. Soc. Lond. B Biol. Sci.* 243: 221-226, 1991.

CHEN, G., TROMBLEY, P. AND VAN DEN POL, A. N. Excitatory actions of GABA in developing hypothalamic neurons. *J. Physiol. Lond.* 494: 451-464, 1996.

CHERUBINI, E., GAIARSA J. L. AND BEN ARI, Y. GABA: an excitatory transmitter in early postnatal life. *TINS* 14: 515-519, 1991.

CHRISTIE, B. R., ELIOT, L. S., ITO, K., MIYAKAWA, H. AND JOHNSTON, D. Different Ca^{2+} channels in soma and dendrites of hippocampal pyramidal neurons mediate spike-induced Ca^{2+} influx. *J. Neurophysiol.* 73: 2553-2557, 1995.

CLEMENTS, J. D. Transmitter timecourse in the synaptic cleft: its role in central synaptic function. *TINS* 19: 163-171, 1996.

CREAGER, R., DUNWIDDIE, T. AND LYNCH, G. Paired pulse and frequency facilitation in the CA1 region of the in vitro rat hippocampus. *J. Physiol. Lond.* 299: 409-424, 1980.

DEBANNE, D., GUÉRINEAU, N. C., GÄHWILER, B. H. AND THOMPSON S. M. Paired-pulse facilitation and depression at unitary synapses in rat hippocampus: quantal fluctuation affects subsequent release. *J. Physiol Lond.* 491: 163-176, 1996.

DEL CASTILLO, J. AND KATZ, B. Quantal component of the end plate potential. *J. Physiol Lond.* 124: 560-573, 1954a.

DEL CASTILLO, J. AND KATZ, B. Statistical factors involved in neuromuscolar facilitation and depression. *J. Physiol Lond.* 124: 574-585, 1954b.

DEUCHARS, J. AND THOMSON, A. M. CA1 pyramid-pyramid connections in rat hippocampus *in vitro*: dual intracellular recordings with biocytin filling. *Neuroscience* 74: 1009-1018, 1996.

DITTMAN, J. S. AND REGEHR, W. G. Calcium dependence and recovery kinetics of presynaptic depression at the climbing fiber to Purkinje cell synapse. *J. Neurosci.* 18: 6147-6162, 1998.

DOBRUNZ, L. E. HUANG, E. P. AND STEVENS, C. F. Very short-term plasticity in hippocampal synapses. *Proc. Natl. Acad. Sci. USA* 94: 14843-14847, 1997.

DOBRUNZ, L. E. AND STEVENS, C. F. Heterogeneity of release probability, facilitation, and depletion at central synapses. *Neuron* 18: 995-1008, 1997

DODGE, F. A., RAHAMIMOFF, R.. Cooperative action of calcium ions in transmitter release. *J. Physiol. Lond.* 193: 419-432, 1967.

DOERR, T., DENGER, R. AND TRAUTWEIN, W. Calcium currents in single SA nodal cells of the rabbit heart studied with action potential clamp. *Pflügers Arch.* 413: 599-603, 1989.

DOMENICI, M. R., BERETTA, N. AND CHERUBINI, E. Two distinct forms of long-term depression coexist at the mossy fiber-CA3 synapse in the hippocampus during development. *Proc. Natl. Acad. Sci. USA* 95: 8310-8315, 1998.

DUDEK, S. M. AND BEAR, M. F. Homosynaptic long-term depression in area CA1 of hippocampus and the effects of NMDA receptors blockade. *Proc. Natl. Acad. Sci. USA* 89: 4363-4367, 1992.

DUNLAP, K. Two types of γ-aminoburiric receptrors on embryonic sensory neurons. *Br. J. Pharmac.* 74: 579-585, 1981.

EBERHARD, M. AND ERNE, P. Calcium binding to fluorescent calcium indicators: Calcium Green, Calcium Orange and Calcium Crimson. *Biochem. Biophys. Res. Comm.* 180: 209-215, 1991.

EDWARDS, F. A., KONNERTH, A. AND SAKMANN, B. Quantal analysis of inhibitory synaptic transmission in the dentate gyrus of rat hippocampal slices: a patch clamp study. *J. Physiol. Lond.* 430: 213-249, 1990.

EFRON, B. The Jackknife, the bootstrap and other resampling plans. *SIAM Monograph* Vol. 38. CBMS-NSF. SIAM Philadelphia, 1982.

EILERS, J., SCHNEGGENBURGER, R. AND KONNERTH, A. Patch clamp and calcium imaging in brain slices. *In Single Channel Recording.* (Ed. by B. Sakmann and E. Neher), Plenum Press, New York, 213-229, 1995.

ELMQVIST, D. AND QUASTEL, D. M. J. A quantitative study of end-plate potentials in isolated human muscle. *J. Physiol. Lond.* 178: 505-529, 1965.

ERULKAR, S. D. AND RAHAMIMOFF, R. The role of calcium ions in tetanic and post-tetanic increase of miniature end-plate potential frequency. *J. Physiol. Lond.* 278: 501-511, 1978.

FABER, D. S. AND KORN, H. Applicability of the coefficient of variation method for analysing synaptic plasticity. *Biophys. J.* 60:1288-1294, 1991

FATT, P. AND KATZ, B. Spontaneous subthreshold activity at motor nerve endings. *J. Physiol Lond.* 117: 109-128, 1952.

FESCE, R. Stochastic approaches to the study of synaptic function. *Progr. in Neurobiol.* 35: 85-133, 1990.

FESCE, R., GROHOVAZ, F., VALTORTA, F. AND MELDOLESI, J. Neurotransmitter release: fusion or 'kiss-and-run'? *Trends in Cell Biology* 4: 1-4, 1994.

FORTI, L. BOSSI, M., BERGAMASCHI, A., VILLA, A. AND MALGAROLI, A. Loose-patch recordings of single quanta at individual hippocampal synapses. *Nature Lond.* 388: 874-878, 1997.

FOSTER, T. C. AND MCNAUGHTON, B. L. Long-term enhancement of CA1 synaptic transmission is due to quantal size, not to quantal content. *Hippocampus* 1, 79-91, 1991.

FREUND, T. F. AND BUZSAKI, G. Interneurons of the hippocampus. *Hippocampus* 6: 345-470, 1996.

GÄHWILER B. H., CAPOGNA, M., McKINNEY, R. A. AND THOMPSON, S. M. Organotypic slice cultures: a technique has come of age. *TINS* 20: 471-477, 1997.

GAIARSA, J. L., CORRADETTI, R., CHERUBINI, E. AND BEN ARI, Y. Modulation of GABA-mediated synaptic potentials by glutamatergic agonists in neonatal CA3 rat hippocamapl neurons. *Eur. J. Neurosci.* 3: 301-309, 1991.

GARASCHUK, O., HANSE, E. AND KONNERTH, A. Developmental profile and synaptic origin of early network oscillations in the CA1 region of rat neonatal hippocampus. *J. Physiol. Lond.* 507: 219-236, 1998.

GARASCHUK, O., SCHNEGGENBURGER, R., SCHIRRA, C., TEMPIA, F. AND KONNERTH, A. Fractional Ca^{2+} currents through somatic and dendritic glutamate-receptor channels of rat hippocampal CA1 pyramidal neurons. *J. Physiol. Lond.* 491: 757-772, 1996.

GARDNER, D. AND KANDELL, E. R. Physiological and kinetic properties of cholinergic receptors activate by multiaction interneurons in buccal ganglia of Aplysia. *J. Neurophysiol.* 40: 333-348, 1977.

GOODMAN, C. S. AND SHATZ, C. J. Developmental mechanisms that generate precise patterns of neuronal connetivity. *Cell* 72: 77-98, 1993.

HARDINGHAM, N. R. AND LARKMAN, A. U. The reliability of excitatory synaptic transmission in slices of rat visual cortex *in vitro* is temperature dependent. *J. Physiol. Lond.* 507: 249-256, 1998.

HEBB, D. O. Organization of behaviour. *Wiley*, New York, 1949.

HELMCHEN, F. BORST, J. G. G. AND SAKMANN, B. Calcium dynamics associated with a single action potential in a CNS presynaptic terminal. *Biophysical J.* 72: 1458-1471, 1997.

HELMCHEN, F. IMOTO, K. AND SAKMANN, B. Ca^{2+} buffering and action potential-evoked Ca^{2+} signaling in dendrites of pyramidal neurons. *Biophysical J.* 70: 1069-1081, 1996.

HENZE, D. A., CARD, J. P., BARRIONUEVO, G. AND BEN-ARI, Y. Large amplitude miniature excitatory postsynaptic currents in hippocampal CA3 pyramidal neurons are of mossy fiber origin. *J. Neurophysiol.* 77:1075-1086. 1997.

HERNANDEZ-CRUZ, A., SALA, F. AND ADAMS, P. R. Subcellular calcium transients visualized by confocal microscopy in a voltage-clamped vertebrate neuron. *Science* 247: 858-862, 1990.

HESSLER, N. A., SHIRKE, A. M. AND MALINOW, R. The probability of transmitter release at a mammalian central synapse. *Nature Lond.* 366:569-572, 1993.

HIRAOKA, Y., SEDAT, J. W. AND AGARD, D. A. Determination of three-dimensional imaging properties of a light microscope system. *Biophysical J.* 57: 325-333, 1990.

HODGKIN, A. L. AND HUXLEY, A. F. A quantitative description of membrane current and its application to conduction and excitation in nerve. *J. Physiol. Lond.* 117: 500-544, 1952.

HOSOKAWA, Y., SCIANCALEPORE, M., STRATTA, F., MARTINA, M. AND CHERUBINI, E.. Developmental changes in spontaneous GABA$_A$-mediated synaptic events in rat hippocampal CA3 neurons. *Eur. J. Neurosci.* 6: 805-813, 1994.

JAFFE, D. B. AND JOHNSTON, D. The induction of long-term potentiation at hippocampal mossy fibers follows a hebbian rule. *J. Neurophysiol.* 64: 948-960, 1990.

JAFFE, D. B., ROSS, W. N., LISMAN, J. E., LASSER-ROSS, N., MIYAKAWA, H. AND JOHNSTON, D. A model for dendritic Ca^{2+} accumulation in hippocampal pyramidal neurons based on fluorescence imaging measurements. *J. Neurophysiol.* 71: 1065-1077, 1994.

JAFFE, D. B., JOHNSTON D., LASSER-ROSS, N., LISMAN, J. E., MIYAKAWA, H. AND ROSS, W. N. The spread of Na^+ spikes determines the pattern of dendritic Ca^{2+} entry into hippocampal neurons. *Nature Lond.* 357: 244-246, 1992.

JOHNSTON, D. AND WU, S. M. Foundations of Cellular Neurophysiology. *MIT Press*, Cambridge, MA., 334-338, 1995.

JONAS, P., MAJOR, G. AND SAKMANN, B. Quantal components of unitary EPSCs at the mossy fibre synapse on CA3 pyramidal cells of rat hippocampus. *J. Physiol Lond.* 472: 615-663, 1993.

JONES, M. V. AND WESTBROOK G. L. The impact of receptor desensitization on fast synaptic transmission. *TINS* 19: 96-101, 1996.

KAMIYA, H., SHINOZAKI, H. AND YAMAMOTO, C. Activation of metabotrobic glutamate receptors type 2/3 suppresses transmission at rat hippocampal mossy fiber synapses. *J. Physiol. Lond.* 493:447-455. 1996.

KAMIYA, H. AND ZÜCKER, R. S. Residual Ca^{2+} and short-term synaptic plasticity. *Nature Lond.* 371: 603-606, 1994.

KANEDA, M., FARRANT, M. AND CULL-CANDY, S .G. Whole-cell and single channel currents activated by GABA and glycine in granule cells of the rat cerebellum. *J. Physiol. Lond.* 485: 419-43, 1996.

KAO, J. P. AND TSIEN, R. Y. Ca^{2+} binding kinetics of fura-2 and azo-1 from temperature-jump relaxation measurement. *Biophysical J.* 53: 635-639, 1988.

KAPUR, A., YECKEL, M. F., GRAY, R. AND JOHNSTON, D. L-type calcium channels are required for one form of hippocampal mossy fiber LTP. *J. Neurophysiol.* 79: 2181-2190, 1998.

KATZ, B. AND MILEDI, R. The role of calcium in neuromuscular facilitation *J. Physiol Lond.* 195: 481-492, 1968.

KENDALL, M. AND STUART, A. The advanced theory of statistics (4th ed.). Vol.2. *Charles Griffin and co., London, UK,* 1979.

KHALILOV, I., ESCLAPEZ, M., MEDINA, I., AGGOUN, D., LAMSA, K., LEINEKUGEL, X., KHAZIPOV, R. AND BEN ARI, Y. A novel in vitro preparation: the intact hippocampal formation. *Neuron* 19: 743-749, 1997.

KHIROUG, L., SOKOLOVA, E., GINIATULLIN, R., AFZALOV, R. AND NISTRI, A. Recovery from desensitization of neuronal nicotinic acetylcholine receptors of rat chromaffin cells is modulated by intracellular calcium through distinct second messengers. *J. Neurosci.* 18: 2458-2466, 1998.

KORN H. AND FABER, D. S. Quantal analysis and synaptic efficacy in the CNS. *TINS* 14: 439-445, 1991.

KULLMANN, D. M. Applications of the expectation-maximization algorithm to quantal analysis of postsynaptic potentials. *J. Neurosci. Methods* 30: 231-245, 1989.

KULLMANN, D. M. Quantal variability of excitatory transmission in the hippocampus. *Proc. R. Soc. Lond. B Biol. Sci.* 253: 107-116, 1992.

KULLMANN, D. M. Quantal analysis using maximum entropy noise deconvolution. *J. Neurosci. Methods* 44: 47-57, 1994a.

KULLMANN, D. M. Amplitude fluctuations of dual-component EPSCs in hippocampal pyramidal cells: implications for Long-Term Potentiation. *Neuron* 12: 1111-1120, 1994b.

LACAILLE, J.-C. Postsynaptic potentials mediated by excitatory and inhibitory amino acids in interneurons of Stratum Pyramidale of the CA1 region of rat hippocampal slices in vitro. *J. Neurophysiol.* 66: 1441-1454, 1991.

LAMBERT, N. A. AND WILSON, W. A. Heterogeneity in presynaptic regulation of GABA release from hippocampal inhibitory neurons. *Neuron* 11: 1057-1067.

LARKMAN, A. U., HANNAY, T., STRATFORD, K. J. AND JACK, J. J. B. Presynaptic release probability influences the locus of long-term potentiation. *Nature Lond.* 360: 70-73, 1992.

LARKMAN, A. U., JACK, J. J. B. AND STRATFORD, K. J. Quantal analysis of excitatory synapses in rat hippocampal CA1 in vitro during low-frequency depression. *J. Physiol. Lond.* 505: 457-471, 1997.

LASSER-ROSS, N., MIYAKAWA, H., LEV-RAM, W., YOUNG S. R. AND ROSS, W. N. High time resolution fluorescence imaging with a CCD camera. *J. Neurosci. Meth.* 36: 253-261, 1991.

LEINEKUGEL, X., KHALILOV, I., BEN ARI, Y. AND KHAZIPOV, R. Giant Depolarizing Potentials: the septal pole of the hippocampus paces the activity of the developing intact septohippocampal complex *in vitro*. *J. Neurosci.* 18, 6349-6357, 1998.

LEINEKUGEL, X., MEDINA, I., KHALILOV, I., BEN ARI, Y., AND KHAZIPOV, R. Ca^{2+} oscillations mediated by the synergistic excitatory actions of $GABA_A$ and NMDA receptors in the neonatal hippocampus. *Neuron* 18: 243-255, 1997.

LEINEKUGEL, X., TSEEB, V., BEN ARI, Y., AND BREGESTOVSKI, P. Synaptic $GABA_A$ activation induces Ca^{++} rise in pyramidal cells and interneurones from rat neonatl hippocampal slice. *J. Physiol. Lond.* 487: 319-329, 1995.

LIAW, J.-S. AND BERGER, T. W. Dynamic synapse: a new concept of neural representation and computation. *Hippocampus* 6:591-600, 1996.

LIM, J. S. Two Dimensional Signal and Image Processing. *Prentice Hall, Englewood Cliffs*, NJ. 469-476, 1990.

LISMAN, J. E. Bursts as a unit of neural information: making unreliable synapses reliable. *TINS* 20: 38-43, 1997.

LLINAS, R., STEINBERG, I.Z. AND WALTON, K. Presynaptic calcium currents in squid giant synapse. *Biophysical J.* 33: 289-322, 1981.

LORENTE DE NO, R. Studies on the structure of the cerebral cortex. II. Continuation of the study of the ammonic system. *J. Psychol. Neurol.* 46: 113-177, 1934.

LYNCH, G. S., DUNWIDDIE, T. AND GRIBKOFF, V. Heterosynaptic depression: a postsynaptic correlate of long term potentiation. *Nature Lond.* 266: 737-739, 1977.

MAC DONALD, R. L. AND OLSEN, R. W. $GABA_A$ receptor channels. *Annu. Rev. Neurosci.*, 17: 569-602, 1994.

MAGLEBY, K. L. AND ZENGEL, J. E. A quantitative description of stimulation-induced changes in transmitter release at the frog neuromuscular junction. *J. Gen. Physiol.* 80:613-638 1982.

MALLART, A. AND MARTIN, A. R. An analysis of facilitation of transmitter release at the neuromuscular junction of the frog. *J. Physiol. Lond.* 193: 679-694, 1967.

MALINOW, R. AND TSIEN, R. W. Presynaptic enhancement shown by whole cell recordings of long-term potentiation in hippocampal slices. *Nature Lond.* 346: 177-180, 1990.

MANABE, T., WILLIE, D. J. A., PERKEL, D. J. AND NICOLL, R. A. Modulation of synaptic transmission and Long-Term Potentiation: effects on paired pulse facilitation and EPSC variance in the CA1 region of the hippocampus. *J. Neurophysiol.* 70: 1451-1458, 1993.

MARKRAM, H., HELM. P. J. AND SAKMANN B. Dendritic calcium transients evoked by single back-propagating action potentials in rat neocortical pyramidal neurons. *J. Physiol. Lond.* 485.1: 1-20, 1995.

MARKRAM, H. AND TSODYKS, M. V. Redistribution of synaptic efficacy between neocortical pyramidal neurons. *Nature Lond.* 382: 807-810, 1996.

MARKRAM, H.. WANG, Y., AND TSODYKS, M. V. Differential signalling via the same axon of neocortical pyramidal neurons. *Proc. Natl. Acad. Sci. USA* 95: 5323-5328, 1998.

MELKONIAN, D. S. Transient analysis of a chemical synaptic transmission. *Biol. Cybern.* 68:341-350, 1993.

METROPOLIS, N., ROSENBLUTH, A., ROSENBLUTH, M., TELLER, A. AND TELLER, E. Equation of state calculations by fast computing machines. *J. Chem. Phys.* 21:1087. 1953.

MCCOBB, D. P. AND BEAM, K. G. Action potential waveform voltage-clamp commands reveal striking differences in calcium entry via low and high voltage-activated calcium channels. *Neuron* 7: 119-127, 1991.

MCNAUGHTON, B. L. Long term synaptic enhancement and short term potentiation in rat fascia dentata act through different mechanisms. *J. Physiol. Lond.* 324: 249-262, 1982.

MILES, R. Variation in strength of inhibitory synapses in the CA3 region of guinea-pig hippocampus in vitro. *J. Physiol. Lond.* 431: 659-676, 1990.

MILES, R. AND WONG, R. K. S. Unitary inhibitory synaptic potentials in the guinea-pig hippocampus in vitro. *J. Physiol. Lond.* 356: 97-113, 1984.

MILES, R. AND WONG, R. K. S. Excitatory interactions between CA3 neurons in the guinea pig hippocampus. *J. Physiol. Lond.* 373: 397-418, 1986.

MOZRZYMAS, J. W. AND CHERUBINI, E. Changes in intracellular calcium concentration affect desensitization of $GABA_A$ receptors in acutely dissociated P2-P6 rat hippocampal neurons. *J. Neurophysiol.* 79: 1321-1328, 1998.

MURTHY, V. N., SEJNOWSKI, T. J. AND STEVENS C. F. Heterogeneous release properties of visualized individual hippocampal synapses. *Neuron* 18: 599-612, 1997.

NEHER, E. AND AUGUSTINE, G.J. Calcium gradients and buffers in bovine chromaffin cells. *J. Physiol.* 450: 273-301, 1992.

NEHER, E., VON GERSDORFF, H., SCHNEGGENBURGER, R. AND WEIS, S. Presynaptic depression at the Calyx of Held. (Abstr.) *Eur. J. Neurosci.* 10, Suppl. 10: 76.01, 1998.

NEWBARRY, N. R. AND NICOLL, R. A. Direct hyperpolarizing action of baclofen on hippocampal pyramidal cells. *Nature Lond.* 308: 450-452, 1984.

NICHOLS, J. G., MARTIN, A. R. AND WALLACE, B. G. From neuron to brain (third edition). *Sinauer Associates, inc.*, Sunderland, USA, 1992.

NICOLL, R. A. AND MALENKA, R. C. Contrasting properties of two forms of long-term potentiation in the hippocampus. *Nature Lond.* 377: 115-119, 1995.

NOWYCKY, M. C. AND PINTER, M. J. Time courses of calcium and calcium-bound buffers following calcium influx in a model cell. *Biophysical J.* 64: 77-91, 1993.

OLIET, S. H. R., MALENKA, R. C. AND NICOLL, R. A. Bidirectional control of quantal size by synaptic activity in the hippocampus. *Science* 271: 1294-1297, 1994.

OLIET, S. H. R., MALENKA, R. C. AND NICOLL, R. A. Two distinct forms of long-term depression coexist in CA1 hippocampal pyramidal cells. *Neuron* 18: 969-982, 1997.

OPPENHEIM, A. V. AND SHAFFER, R. W. Discrete-Time Signal Processing. *Prentice Hall, Englewood, Cliffs*, NJ. 311-312, 1989.

OWENS, D. F., BOYCE, L. H., DAVIS, M. B. E. AND KRIEGSTEIN, A. R. Excitatory GABA responses in embryonic and neonatal cortical slices demonstrated by gramicidin perforated-patch recordings and calcium imaging. *J. Neurosci.* 16: 6414-6423, 1996.

PEARCE, R. A. Physiological evidence for two distinct types of $GABA_A$ responses in rat hippocampus. *Neuron* 10: 189-200, 1993.

PEARCE, R. A., GRUNDER, S. D. AND FAUCHER, L. D. Different mechanisms for use-dependent depression of two $GABA_A$-mediated IPSCs in rat hippocampus. *J. Physiol. Lond.* 484: 425-435, 1995.

PIN, J. AND BOCKAERT, J. Get receptive to metabotropic glutamate receptors. *Curr. Op. in Neurobiol.* 5: 342-349, 1995.

PRESS, W. H., FLANNERY, B. P., TEUKOLSKY, S. A., AND VETTERLING, W. T. Numerical recipes. *Cambridge University Press, Cambridge, UK,* 1989.

QUASTEL, D. M. J. The binomial model in fluctuation analysis of quantal neurotransmitter release. *Biophys. J.* 72:728-753, 1997.

RAMON Y CAJAL, S. Histologie du systeme nerveux de l'homme et des vertebres. Vol.2 *Maloine*, Paris, 1911.

RANDALL, A. D. AND COLLINGRIDGE, G. L. Amino acid receptor-mediated synaptic currents in the CA1 region of hippocampus. *In Ion Channel, vol.3 eds. Narashi, T., Plenum Press, New York*, 1992.

REDMAN, S. Quantal analysis of synaptic potentials in neurons of central nervous system. *Physiol. Rev.* 70:165-198, 1990.

RINZEL, J. AND ERMENTROUT, G. B. Analysis of neuronal excitability and oscillations. *In Methods in neuronal modelling*, (ed. by C. Koch and I . Segev), MIT press, Cambridge, USA, 135-169, 1989.

ROLLS, E. T. AND TREVES, A. Neural networks and brain function. *Oxford Univ. Press*, Oxford, 1998.

ROSENMUND, C., CLEMENTS, J. D. AND WESTBROOK, G. L. Nonuniform probability of glutamate release at a hippocampal synapse. *Science* 262: 754-757, 1993.

SALA, F. AND HERNÁNDEZ-CRUZ, A. Calcium diffusion modeling in a spherical neuron - relevance of buffering properties. *Biophysical J.* 57: 313-324, 1990.

SALIN, P. A., SCANZIANI, M., MALENKA, R.C. AND NICOLL, R. A. Distinct short-term plasticity at two excitatory synapses in the hippocampus. *Proc. Natl. Acad. Sci. USA* 93: 13304-13309, 1996.

SCHWEIZER, F. E., BETZ, H. AND AUGUSTINE, G. J. From vesicle docking to endocytosis: intermediate reactions of exocytosis. *Neuron* 14: 689-696, 1995

SCIANCALEPORE, M., STRATTA, N., FISHER, N. D. AND CHERUBINI E. Activation of metabotrobic glutamate receptors increase the frequency of spontaneous GABAergic currents through protein Kinase A in neonatal rat hippocampal neurons. *J. Neurophysiol.* 74: 1118-1122, 1995.

SERAFINI, R., VALEYEV, A. Y., BARKER, J. L. AND POULTER, M. O. Depolarizing GABA-activated Cl⁻ channels in embryonic rat spinal and olfactory bulb cells. *J. Physiol. Lond.* 488: 371-386, 1995.

SHEPHERD, G. M. Neurobiology (third edition). *Oxford University Press*, New York Oxford, 1994.

SHIGEMOTO, R., KINOSHITA, A., WADA, E., NOMURA, S., OHISHI, H., TAKADA, M., FLOR, P. J., NEKI, A., ABE, T., NAKANISHI, S. AND MIZUNO, N. Differential presynaptic localization of metabotropic glutamate receptors subtypes in the rat hippocampus. *J. Neurosci.* 17: 7503-7522, 1997.

SILVER, R. A., MOMIYIAMA, A. AND CULL-CANDY, S. G. Locus of frequency-dependent depression identified with multiple-probability fluctuation analysis at rat climbing fibre-Purkinje cell synapse. *J. Physiol. Lond.* 510: 881-902, 1998.

SLOMIANKA, L. AND GENESER, F. A. Postnatal development of zinc-containing cells and neuropil in the hippocampal region of the mouse. *Hippocampus* 7:312-340, 1997.

SOMOGYI, P., NUNZI, M. G. AND SMITH, A. D. A new type of specific interneuron in the monkey hippocampus forming synapses exclusively with the axon initial segments of pyramidal cells. *Brain Res.* 259: 137-142, 1983.

SPRUSTON, N., SCHILLER, Y., STUART, G. AND SAKMANN, B. Activity-dependent action potential invasion and calcium influx into hippocampal CA1 dendrites. *Science* 268: 297-300, 1995.

STANTON, P. K. AND SEJNOWSKI, T. J. Associative long-term depression in the hippocampus induced by hebbian covariance. *Nature Lond.* 229: 215-218, 1989.

STRICKER, C., FIELD, A., AND REDMAN, S. J. Changes in quantal parameters of EPSCs in rat CA1 neurones in vitro after the induction of long-term potentiation. *J. Physiol. Lond.* 490: 443-454, 1996.

STRICKER, C., REDMAN, S. J., AND DALEY, D. Statistical models of synaptic transmission: model discrimination and confidence limit. *Biophys. J.* 67:532-547, 1994.

STRICKER, C. AND REDMAN, S. J. Statistical models of synaptic transmission evaluated by the expectation-maximization algorithm. *Biophys. J.* 67:656-670, 1994.

STUART, G., SPRUSTON, N., SAKMANN, B. AND HÄUSSER, M. Action potential initiation and backpropagation in neurons of the mammalian CNS. *TINS* 20: 125-131, 1997.

SÜDHOF, T. C. The synaptic vesicle cycle: a cascade of protein-protein interactions. *Nature Lond.* 375: 645-653, 1995.

TAKAHASHI, T., FORSYTHE, I. D., TSUJIMOTO, T., BARNIES-DAVIES, M. AND ONODERA, K. Presynaptic calcium current modulation by a metabotropic glutamate receptor. *Science* 274: 594-597, 1996.

THOMSON, A. M., DEUCHARS, J AND WEST, D. C. Large, deep layer pyramid-pyramid single axon EPSPs in slices of rat motor cortex display paired pulse and frequency-dependent depression, mediated presynaptically and self-facilitation, mediated postsynaptically. *J. Neurophysiol.* 70: 2354-2369, 1993.

THOMSON, A. M. AND DEUCHARS, J. Temporal and spatial properties of local circuits in neocortex. *TINS* 17: 119-126, 1994.

THOMSON, A. M., WEST, D. C. AND DEUCHARS, J. Properties of single axon excitatory postsynaptic potentials elicited in spiny interneurons by action potentials in pyramidal neurons in slices of rat neocortex. *Neuroscience* 63: 727-738, 1995.

TSODYKS, M. V. AND MARKRAM, H. The neural code between neocortical pyramidal neurons depends on neurotransmitter release probability. *Proc. Natl. Acad. Sci. USA* 94: 719-723, 1997.

TSUBOKAWA, H. AND ROSS, W. N. IPSPs modulate spike backpropagation and associated $[Ca^{2+}]_i$ changes in the dendrites of hippocampal CA1 pyramidal neurons. *J. Neurophysiol.* 76: 2896-2906, 1996.

URBAN, N. N. AND BARRIONUEVO, G. Induction of hebbian and non-hebbian mossy fiber long-term potentiation by distinct patterns of high frequency stimulation. *J. Neurosci.* 16: 4293-4299, 1996.

VAN DER KLOOT, W. AND MOLGÓ, J. Quantal Acetylcholine release at the vertebrate neuromuscular junction. *Physiol. Rev.* 74: 899-991, 1994.

VERE-JONES, D. Simple stochastic models for the release of quanta of transmitter from a nerve terminal. *Aust. J. Statist.* 8: 53- 63.,1966.

VON GERSDORFF, H., SCHNEGGENBURGER, R. WEIS, S. AND NEHER, E. Presynaptic depression at a Calyx synapse: the small contribution of metabotropic glutamate receptors. *J. Neurosci.* 17: 8137-8146, 1997.

VORONIN, L. L. Quantal analysis of hippocampal Long-Term Potentiation. *Rev. in the Neurosci.* 5: 141-170, 1994.

VORONIN, L. L. AND KHUNT, U. Long-Term Potentiation affects facilitation ratio of EPSPs recorded from CA1 pyramidal cells in the guinea pig hippocampal slice. *Neurosci. Res. Commun.* 6: 149-155, 1990.

WEISSKOPF, M. G., CASTILLO, P. E., ZALUTSKY, R. A. AND NICOLL, R. A. Mediation of hippocampal mossy fiber long-term potentiation by cyclic AMP. *Science* 265: 1878-1882, 1994.

WORDEN, M. K., BYKHOVSKAIA, M. AND HACKETT, J. T. Facilitation at the lobster neuromuscular junction: a stimulus-dependent mobilization model. *J. Neurophysiol.* 78: 417-428, 1997.

WU, W., ZISKIND-CONHAIM, L. AND SWEET, M. A. Early development of glycine- and GABA-mediated synapses in rat spinal cord. *J. Neurosci.* 12: 3935-3945, 1992.

YAMADA, W. M., KOCH, C. AND ADAMS, P. R. Multiple channels and calcium dynamics. *In Methods in Neuronal Modeling* (ed. by C. Koch and I. Segev), The MIT Press, Cambridge, MA., 109-115, 1989.

ZADOR, A. Impact on synaptic unreliability on the information transmitted by spiking neurons. . *J. Neurophysiol.* 79: 1219-1229, 1998.

ZALUTSKY, R. A. AND NICOLL, R. A. Comparison of two forms of long-term potentiation in single hippocampal neurons. *Science* 248: 1619-1624, 1990.

ZUCKER, R. S. Changes in the statistics of transmitter release during facilitation. *J. Physiol. Lond.* 229: 787-810, 1973.

ZUCKER, R. S. Short-term synaptic plasticity. *Ann. Rev. Neurosci.* 12: 13-31, 1989.